OIL TRANSMISSION PIPELINES CONDITION MONITORING USING WAVELET ANALYSIS AND ULTRASONIC TECHNIQUES

Waheed Sami AbuShanab

PhD - 2013

OIL TRANSMISSION PIPELINES CONDITION MONITORING USING WAVELET ANALYSIS AND ULTRASONIC TECHNIQUES

Waheed Sami AbuShanab

A thesis submitted in partial fulfilment of the requirements of the Manchester Metropolitan University for the degree of Doctor of Philosophy

Faculty of Science and Engineering
The School of Engineering
2013

ABSTRACT

Proper and sensitive monitoring capability to determine the condition of pipelines is desirable to predict leakage and other failure modes, such as flaws and cracks. Currently methods used for detecting pipeline damage rely on visual inspection or localized measurements and thus, can only be used for the detection of damage that is on or near the surface of the structure.

This thesis offers reliable, inexpensive and non-destructive technique, based on ultrasonic measurements, to detect faults within Carbon steel pipes and to evaluate the severity of these faults. The proposed technique allows inspections in areas where conventionally used inspection techniques are costly and/or difficult to apply. This work started by developing 3D Finite Elements Modelling (FEM) to describe the dynamic behaviour of ultrasonic wave propagations into the pipe's structure and to identify the resonance modes. Consequently, the effects of quantified seeded faults, a 1-mm diameter hole of different depths in the pipe wall, on these resonance modes were examined using the developed model.

An experimental test rig was designed and implemented for verifying the outcomes of the finite element model. Conventional analysis techniques were applied to detect and evaluate the severity of those quantified faults. However, those signal processing methods were found ineffective for such analysis. Therefore, a more capable signal processing technique, using continuous wavelet techniques (CWT), was developed.

The energy contents of certain frequency bands of the CWT were found to be in good agreement with the model predicted responses and show important information on pipe's defects. The developed technique is found to be sensitive for minor pipe structural related deficiencies and offers a reliable and inexpensive tool for pipeline integrity management programs.

ACKNOWLEDGMENTS

I wish to express sincere appreciation to my supervisor, Dr. Alhussien Albarbar, for his assistance and valuable support in the preparation of this thesis. In addition, I offer special thanks to whose familiarity with the needs and ideas of the early phase of this research program was most helpful. Also, offer great thanks to my wife for her unlimited corporation.

I am very grateful to the members of the faculty for their valuable input and feedback as well as their technical support during the research.

Also, I wish to present my full respect along with my great thanks and gratitude to my parents who have supported and stood by me faithfully.

DECLARATION

No portion of the work referred in this thesis has been submitted in support of an application for another degree or qualification at this, or any other university, or institute of learning

Date: _____

Signed:_____

TABLE OF CONTENTS

ABSTRACT ..... **III**

ACKNOWLEDGMENTS ..... **IV**

DECLARATION ..... **V**

TABLE OF CONTENTS ..... **VI**

LIST OF FIGURES ..... **X**

LIST OF TABLES ..... **XIII**

LIST OF PUBLICATIONS ..... **XIV**

NOMENCLATURE ..... **XV**

INTRODUCTION AND BACKGROUND **1**

1.1 INTRODUCTION 2

1.2 PIPELINE INTEGRITY MANAGEMENT PLAN 3

1.3 CURRENT MONITORING METHODS 4

1.3.1 ULTRASONIC METHODS 5

1.3.1.1 AUTOMATED AND ONLINE ULTRASONIC TESTING 6

1.3.1.2 LONG-RANGE, GUIDED WAVE TESTING 7

1.3.2 ELECTROMAGNETIC METHODS 9

1.3.2.1 ELECTROMAGNETIC ACOUSTIC TRANSDUCERS 9

1.3.2.2 EDDY CURRENTS 10

1.3.2.3 MAGNETIC FLUX LEAKAGE 11

1.3.3 RADIOGRAPHIC METHODS 12

1.3.4 THERMOGRAPHIC METHODS 13

1.3.5 DYNAMIC METHODS 14

1.4 SIGNIFICANT OF THE THESIS 16

1.5 ACADEMIC AIM 17

1.6 OBJECTIVES 17

1.7 METHODOLOGY 17

1.8 THESIS OUTLINE 18

LITERATURE REVIEW **20**

2.1 INTRODUCTION 21

2.2 ACOUSTIC EMISSION WAVE PROPAGATION AND TRANSDUCTION 22

2.3 WAVE MODES 23

2.4 ATTENUATION 30

2.5 Source Location 33
2.5.1 linear Source Location 33
2.5.2 2D Source Location 35
2.5.3 Location Methods in Practical Situations 36
2.5.4 Transduction 38
2.6 Signal Processing 38
2.6.1 Ultrasonic Signal Energy 43
2.6.2 Wave Arrival Time Estimation 45
2.7 Ultrasonic Fault Diagnosis and Monitoring 48
2.7.1 Pipe and Pipeline System Condition Monitoring 52
2.8 Summary of Literature Review 54
FINITE ELEMENT MODELLING AND SIMULATION 56
3.1 Introduction 57
3.2 Dynamic Models and Analogies 57
3.3 Finite Element ModelLing 58
3.4 The Structural Element and The Structural System 59
3.5 Assemblies and Analysis Of A Structure 61
3.6 The Boundary Condition 63
3.7 Surfaces 64
3.8 Specifying a Frequency Range For The Acoustic Modes 65
3.9 Displacement Normalization 66
3.10 Acoustic Analysis 66
3.11 Interpreting the Extracted Modes in A Coupled Structural-Acoustic Natural Frequency Analysis 68
3.12 Selection of Software and Development of the Modeling System 70
3.13 Geometry, Material Properties, and Boundary Conditions 71
3.14 Model Dynamic Analysis Using Abaqus Cae. 74
3.14.1 Acoustic Equations 74
3.14.2 Frequency-Domain Solution Using Projections onto Model Spaces 75
3.15 Acoustic Output Quantities 77
3.16 Results Visualization 77
THE EXPERIMENTS SETUP AND PROCUDURE 81
4.1 Introduction 82
4.2 Apparatus And Procedure 82
4.2.1 Ultrasound Sensors 84

4.2.2 PRE-AMPLIFIERS 85
4.3 PULSE GENERATOR 86
4.4 DATA ACQUISITION SYSTEM 87
4.5 SAMPLING TECHNIQUES 88
4.6 DISPLAY TECHNIQUES 89
4.7 DOT AND VECTOR DISPLAYS 91
4.8 SAMPLING RATE 92
4.9 PROBES AND PROBING TECHNIQUES 93
4.10 EXPERIMENTAL PROCEDURES 94

ULTRASONIC CONVENTIONAL TECHNIQUES 95

5.1 INTRODUCTION 96
5.2 FOURIER SERIES 97
5.3 FOURIER TRANSFORM 99
5.4 PROPERTIES OF FOURIER TRANSFORMS 101
5.5.1 LINEARITY 101
5.5.2 TIME SHIFTING AND TIME SCALING 101
5.5.3 FREQUENCY SHIFTING AND FREQUENCY SCALING 102
5.5.4 MOMENTS 102
5.5.5 CONVOLUTION 103
5.6 BASIC FOURIER TRANSFORMS ANALYSIS 104
5.7 THE LIFTING SCHEME 106
5.8 FIXED-POINT ARITHMETIC IMPLEMENTATION 107
5.9 DIGITAL COMPUTER FOURIER ANALYSIS 109
5.10 THE FOURIER INTEGRAL 109
5.11 FFT RESULTS DISCUSSIONS 110

WAVELET TECHNIQUES 113

6.1 INTRODUCTION 114
6.2 TRANSFORMS 116
6.3 FOURIER TRANSFORM 116
6.4 SHORT TIME FOURIER TRANSFORM (STFT) 117
6.5 WAVELET TRANSFORM 119
6.6 VISUALIZATION 122
6.7 THE CONTINUOUS WAVELET TRANSFORM (CWT) 124
6.8 FOURIER TRANSFORM VS. WAVELETS - A COMPARISON EXPERIMENT 125
6.9 COMPUTATION 127

6.10 RECONSTRUCTION 129
6.11 CONTINUOUS WAVELET TRANSFORM RESULTS AND DISCUSSION 131
6.12 SUMMARY OF EXPERIMENTS 132

CONTRIBUTION TO KNOWLEDGE, ACHIEVEMENTS, CONCLUSIONS AND SUGGESTED FUTURE WORK 134

7.1 REVIEW OF THE OBJECTIVES AND ACHIEVEMENTS 135
7.2 CONCLUSIONS 137
7.3 SUGGESTED FUTURE WORK 139
7.3.1 FUTURE WORK RELATED TO DIFFERENT MODELING SYSTEMS 139
7.3.2 FUTURE WORK RELATED TO DIFFERENT TYPES OF DEFECTS 139
7.3.3 FUTURE WORK WITH DIFFERENT MATERIALS 140

REFERENCES 141

APPENDIX A: ULTRASONIC WAVE PROPAGATION SIMULATION WITHIN ABAQUS CAE .. 152

APPENDIX B: MAT LAB CWT CODE 166

APPENDIX C: AIR ULTRASONIC CERAMIC TRANSDUCERS 169

PUBLISHED PAPERS 170

PAPER 1 170
PAPER 2 175

LIST OF FIGURES

FIGURE 1-1: LEAK DETECTION METHODS 2

FIGURE 1-2: A-SCANS RESULTANT 6

FIGURE 1-3: BASIC STRACTURE OF PIEZOELECTRIC AND EMAT [144] 9

FIGURE 1-4: EDDY CURRENT TECHNOLOGY 10

FIGURE 1-5: MAGNETIC FLUX LEAKAGE 11

FIGURE 1-6: RADIOGRAPHIC METHOD 12

FIGURE 1-7: THERMOGRAMS OF STEEL PIPELINE EMBEDDED WITH VARIOUS FAULTS [145] 13

FIGURE 2-8: SCHEMATIC REPRESENTATION OF AE MONITORING 22

FIGURE 2-9: THE MAIN ULTRASONIC (AE) WAVES IN INFINITE AND SEMI-INFINITE MEDIA 24

FIGURE 2-10: REFLECTION, REFRACTION AND MODE CONVERSION OF WAVE CAST BOUNDARY 29

FIGURE 2-11: LINEAR SOURCE LOCATION 34

FIGURE 2-12: SOURCE LOCATION IN TWO DIMENSIONS 35

FIGURE 2-13: SCHEMATIC DIAGRAM OF ZONE LOCATION METHOD (ADAPTED FROM [97]) WHERE (A) OUTPUT OF SENSOR 2 IS THE HIGHEST, AND (B) OUTPUT OF SENSOR 2 IS HIGHEST AND SENSOR 3 IS SECOND HIGHEST 37

FIGURE 2-14: SCHEMATIC REPRESENTATION OF DIFFERENT ULTRASONIC SIGNAL TYPES [10] (A) IS BURST TYPE AND (B) IS CONTINUOUS TYPE 39

FIGURE 2-15: RESOLUTION IN (A) THE STFT AND (B) THE WT 41

FIGURE 2-16: WAVELET ANALYSIS TREE 42

FIGURE 2-17: CUMULATIVE AE COUNTS FATIGUE CYCLES [143]. 51

FIGURE 3-18: A TYPICAL STRUCTURE BUILT UP FROM INTERCONNECTED ELEMENTS. 59

FIGURE 3-19: ABAQUS BASIC PIPE MODEL SIMULATION 71

FIGURE 3-20: BASIC MODEL LOAD CONDITIONS 73

FIGURE 3-21: ABAQUS LOAD DEMONSTRATION 73

FIGURE 3-22: HEALTHY PIPE DISPLACEMENT RESULTANT 78
FIGURE 3-23 : 50% HOLE DEPTH PIPE DISPLACEMENT RESULTANT 78
FIGURE 3-24: HEALTHY PIPE AMPLITUDE RESULTANT 79
FIGURE 3-25: 50% HOLE DEPTH PIPE AMPLITUDE RESULTANT 79
FIGURE 3-26: HEALTHY PIPE VELOCITY RESULTANT 80
FIGURE 3-27: 50% HOLE DEPTH PIPE VELOCITY RESULTANT 80
FIGURE 4-28: THE EXPERIMENTAL PROCEDURE (A) BLOCK DIAGRAM , (B) PROCEDURE 83
FIGURE 4-29: BLOCK- DIAGRAM AND FLOWCHART OF EXPERIMENTAL PROCEDURE AND SOFTWARE ANALYSIS 83
FIGURE 4- 30: AIR ULTRASONIC CERAMIC TRANSDUCER TYPE 235AC130 84
FIGURE 4-31: EXPERMENTAL RIG 84
FIGURE 4-32: RESISTANCE AND INTEGRATED CIRCUIT 85
FIGURE 4-33: BLOCK CIRCUIT DIAGRAM 85
FIGURE 4-34: REAL TIME SAMPLING 89
FIGURE 4-35: EFFECT OF UNDER-SAMPLING 90
FIGURE 4-36: EFFECT OF ALIASING AND VECTOR DISPLAY: (A) PERCEPTUAL ALIASING; (B) VECTOR DISPLAY 91
FIGURE 5-37: FOURIER TRANSFORM OF A SQUARE PULSE WAVEFORM 104
FIGURE 5-38: TIME DOMAIN SIGNATURES FOR FIVE SETS OF EXPERIMENTAL RESULTS (HEALTHY (A), 1 MM HOLE AT 25% (B) , 50% (C), 75% (D) AND 100% DEPTH (E) 111
FIGURE 5-39: ZOOMED TIME DOMAIN SIGNATURES FOR FIVE SETS OF EXPERIMENTAL RESULTS (HEALTHY (A), 1 MM HOLE AT 25% (B) , 50% (C), 75% (D) AND 100% DEPTH (E) 111
FIGURE 5-40: FREQUENCY DOMAIN SIGNATURES FOR FIVE SETS OF EXPERIMENTAL RESULTS (HEALTHY (A), 1 MM HOLE AT 25% (B) , 50% (C), 75% (D) AND 100% DEPTH (E) 112

FIGURE 6-41: FOURIER TRANSFORM: SIGNAL AND ANALYSIS FUNCTION (SOLID LINE IS SIGNAL, DOTTED LINE IS REAL PART OF THE ANALYSIS FUNCTION) 117

FIGURE 6-42: STFT: SIGNAL AND ANALYSIS FUNCTION FOR Ω = Π 119

FIGURE 6-43 STFT: SIGNAL AND ANALYSIS FUNCTION FOR Ω = 6Π 119

FIGURE 6-45: WAVELET TRANSFORM: SIGNAL AND ANALYSIS FUNCTION A =−: 121

FIGURE 6-46: WAVELET TRANSFORM: SIGNAL AND ANALYSIS FUNCTION A =−: 121

FIGURE 6-47: TOP - STFT OF THE CHIRP-SIGNAL; BELOW - WAVELET TRANSFORM OF THE CHIRP-SIGNAL F (T) = SIN (T2). 123

FIGURE 6-48: ATTACK-SIGNAL 125

FIGURE 6-49: ATTACK-SIGNAL: RECONSTRUCTIONS (SOLID CURVE IS THE ATTACK SIGNAL. DASHED CURVE REPRESENTS RE-CONSTRUCTION FROM FOURIER TRANSFORM. CURVE WITH + SYMBOLS THE WAVELET RECONSTRUCTION) 126

FIGURE 6-50: CWT SIGNATURES FOR FIVE SETS OF EXPERIMENTAL RESULTS (HEALTHY (A), 1 MM HOLE AT 25% (B) , 50% (C), 75% (D) AND 100% DEPTH (E) 132

LIST OF TABLES

TABLE 1: ACOUSTIC IMPEDANCE OF SOME COMMON MATERIALS 29

TABLE 2: SPECIMEN PROPERTIES AND PARAMETERS OF THE MODEL.....72

TABLE 3: COMPUTATIONAL COMPLEXITIES (THE NUMBERS OF REAL MULTIPLIES AND REAL ADDS) OF THE SPLIT-RADIX FFT AND ITS INTEGER VERSIONS (FXPFFT AND INTFFT) WHEN THE COEFFICIENTS ARE QUANTIZED/ ROUNDED OFF TO NC ¼ 10 BITS AT EACH STAGE. [I-6].....108

TABLE 4: NUMBER OF NONTRIVIAL COMPLEX MULTIPLIES. A SET OF COMPLEX MULTIPLY IS THREE REAL MULTIPLIES [33].....109

TABLE 5: SPECIMEN CHARACTERIZATIONS 152

LIST OF PUBLICATIONS

1. Inexpensive Pipelines Health Evaluation Technique Based On Using Resonance Determination; Numerical Simulation and Experimental Testing; Waheed Abushanab; April 2013; Engineering; Scientific Research.

2. Oil Transmission Pipelines condition Monitoring Using Wavelet Analysis and Ultrasonic Techniques; Waheed Abushanab; June 2013; Engineering; Scientific Research.

NOMENCLATURE

Δt	Time difference between hits (s)
A	Wave amplitude (V)
a	Scale parameter
AE	AE signals
ANSI	American National Standard Institute
ao	Flexural mode
Ap	Approximation signal
Di	Detail signal
E	Young's modulus (Pa)
E (x), E1 (x), E2 (x),	AE energy at distance x from the source (V2.s)
E0	Energy of the source (V2.s);
f	Frequency (kHz)
FFT	Fast Fourier Transform
h	Thickness (m)
k1, k2	Attenuation factor (m^{-1})
KI	Stress intensity factor (MN.m-3/2)
MAWP	Maximum allowable working pressure
AE	Acoustic Emission
RMS	Root Mean Square of voltage
ADC	Analogue to Digital Converter
DDC	Direct Digital Synthesis
DSO	Digital Storage Oscilloscope
CRT	Cathode Ray Tube
LCD	Liquid-Crystal Display
DSP	Digital signal Processing
MSB	Most Significant Bit
DFT	Discrete Fourier Transform
M-D DFT	Multidimensional Fourier Transform
MDMT	Minimum Design Metal Temperature
MHz	Mega Hertz
NDT	Non Destructive Techniques

Nf,	Number of rays fired
Nh	Number of rays hitting the sensor
NPS	Normal Pipe Size
Nr	Number of reflections
PSD	Power spectral density
r	Propagation distance (m)
R	Cylinder radius (m)
R2	Correlation factor
Rc	Reflection coefficient
S1	Trigger sensor position
STFT	Short Time Fourier Transform
t ,t1,t2,t3, t4	Arrival time(s)
UTS	Ultimate tensile strength (N/m^2)
v	Poisson's ratio
V, V1, V2, V3	Wave velocities (m/s)
WT	Wavelet Transfer
x	Source-sensor distance (m)
xact	Actual source sensor distance (m)
Z1, Z2	Acoustic impedance (Kg/m^2s)
Z1, z2	Source position
α	Attenuation coefficient (dB/m)
θ, β, γ	Angels (deg)
λ	Wave length (m)
ρ	Density (kg/m^3)
ψ (t)	Wavelet in time domain

CHAPTER I

INTRODUCTION AND BACKGROUND

This chapter demonstrates the need for pipeline condition monitoring and the significant of the research project, the academic aim objectives, the research methodology and the projected timeline. Also, review the advantage and disadvantages of the current common pipeline condition monitoring techniques used by oil companies.

1.1 INTRODUCTION

According to a study performed by the German Energy and Water Association (BDEW) there is a high possibility that pipeline leaks will occur as pipelines age due to corrosion, excessive pressure resulting from operational error and the rapid closing or opening of valves which creates damaging transients [1]. Thus, ground maintenance of the pipeline becomes a great concern of all oil companies to detect any possibility of leakage before it occurs to prevent oil spills, pollution and even ecological disaster. However, inspecting entire pipelines using a specific methodology/tool will not detect all pipeline problems over the entire length because, at the moment, inspection tools are designed to detect specific problems only. On the other hand, inspecting the entire pipeline using a combination of various tools to detect all problems is not cost effective [2].

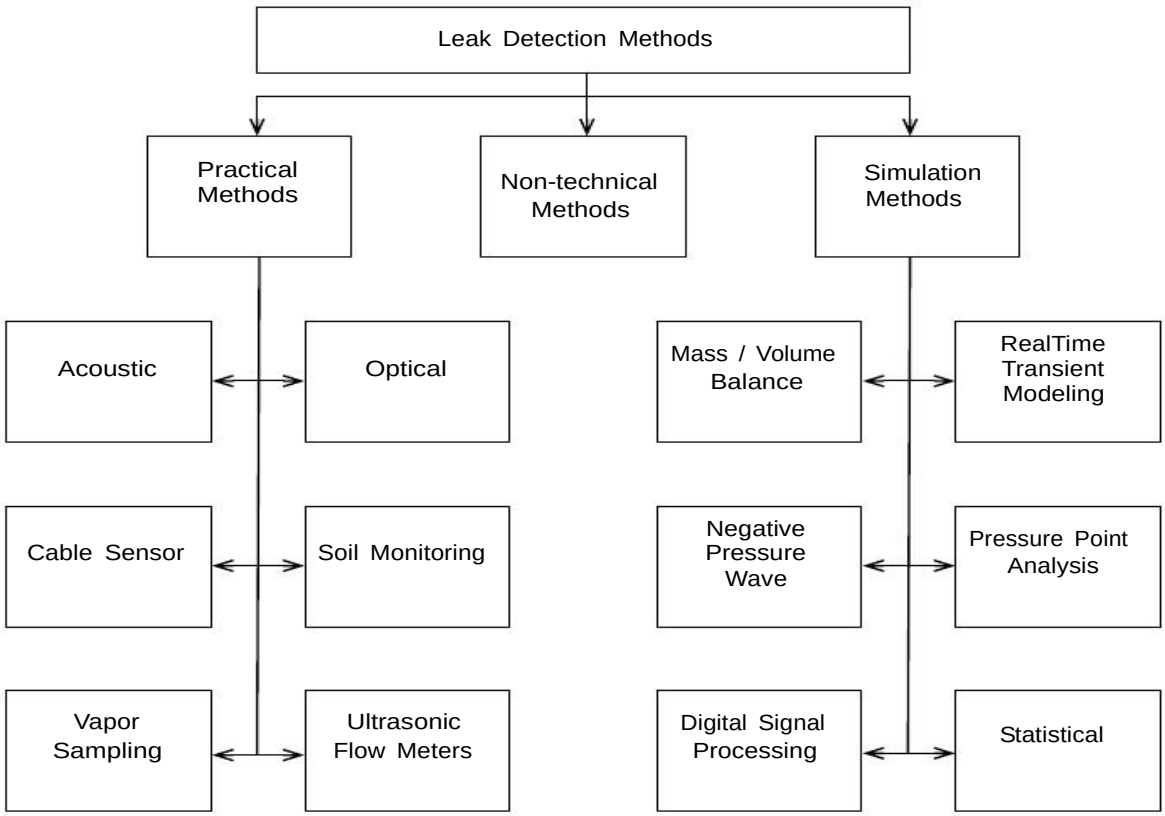

FIGURE 1-1: LEAK DETECTION METHODS

Pipeline condition monitoring normally uses a wide range of leak detection methods as shown in Figure 1-1. None of these methods has been proven reliable and they are currently not widely used [1]. Therefore, a more reliable and quick technique for detecting and locating leaks is currently desirable.

Acoustic analysis can be seen as a promising, accurate and low-cost tool for leak and feature detection in pipelines also, other techniques such as vibration analysis have been developed by groups of researchers in recent years that have been successfully demonstrated under laboratory conditions but are not yet established for use in industrial application [2].

1.2 PIPELINE INTEGRITY MANAGEMENT PLAN

For a successful risk assessment and integrity management program it is important to understand the critical role that the collection of the data plays. A diligent effort must be made to collect all possible data relating to the section of pipeline that collection process. The computerization of data storage has reduces the legwork; however, it has also increased the size of available data files. Greater quantities of data make better analysis, as evaluation of large data can reveal details that otherwise may not be visualized [146].

A pipeline integrity management plan is proposed for the following:

- Pipelines transporting hazardous substances from offshore sources, the consequences of poor integrity management may be catastrophic and could affect the resident workforce on offshore installations and other users of the sea as happened with BP Gulf of Mexico Spill 2010.

- Pipelines are subject to a range of degradation mechanisms, the relative significance of which will depend upon factors such as the fluid(s) being transported (including any contaminants), the external environment, operating parameters, materials of

construction, etc. The progressive deterioration of such as pipelines is referred to as 'ageing'.

- Pipelines can also fail through damage mechanisms which are not age-related, e.g. accidental overpressure, or “dropped object” damage. All potential pipeline threats need to be identified and assessed by operators; otherwise their pipelines may be at risk of failure.

- Knowledge and understanding of pipeline failure mechanisms is constantly evolving. At the same time, improved techniques to allow pipelines to be inspected and monitored for damage and deterioration are being developed.

- Ensuring the integrity of pipelines to secure safety also contributes to ensuring risks to the environments is properly controlled.

1.3 CURRENT MONITORING METHODS

Diagnosis of damage in pipelines requires identifying the location and type of damage and quantification of the degree of damage. Most recent damage detection methods rely on visual inspection or on localized measurements such as acoustic or ultrasound methods, magnetic field methods, radiography, eddy-current methods and thermal field method which requires that the vicinity of the damage area is known before making measurements and that the portion of the structure being inspected is readily accessible [3]. Those methods can detect damage on or near the surface of the structure [4].

Correlation methods using acoustic techniques with two sensors located at different positions along the pipe have been used to identify leakage positions. To get useful information using the correlation method, the acoustic signals should be filtered since these signals have

dispersive characteristics, but the bandwidth of a filter can be difficult to assess in practical situations [5].

1.3.1 ULTRASONIC METHODS

Manual ultrasonic wall thickness testing is the simplest method of detecting metal loss in the pipe wall and is carried out at points of the external surface. This method is based on travel time (time of flight) comparison of longitudinal waves. Thickness gauges are calibrated with standard blocks and then used to test the object of interest. The accuracy of commercially available gauges is typically ±0.5% of the reading. The procedure is very labour intensive, requires removal of pipe insulation or coating, the layout of a grid, and is limited to a point-by-point view of the condition. Here accessibility can be a problem [3].

Ultrasonic NDT methods use waves with frequencies greater than about 2×10^5 Hz, with the maximum typically in the range of 10^6 to 10^7 Hz. Bulk and guided waves are the wave types most commonly used. Guided waves of interest include Rayleigh and Lamb waves. Ultrasonic testing involves the generation of ultrasonic waves and their detection with either a single or a pair of transducers.

The transducer is typically coupled to the solid object of interest through a liquid, gel, or viscous couplant material. Ultrasonic transducers most commonly use piezoelectric materials for detecting and/or generating the signal. Several common testing arrangements are used, including the pulse-echo (A-scan) technique in which a beam is transmitted into the material and reflected back from another surface [6].

This technique often uses a single transducer that acts as both the transmitter and receiver, when the reflecting surface is parallel to the surface of the probe. The resultant A-scans show the initial pulse and the back echo as simple vertical lines (Figure1-2), the time delay between

the two and the speed of the ultrasonic pulse in the material allows distance to the reflecting surface to be calculated.

Cross-sectional views of defects in a specimen are presented in B scans. C-scans show a plan view of the tested surface, indicating the location and size of any holes. D-scans are 2-D presentations of the time of flight values in a top view of the test surface. A P-scan is a projection of a B-scan to give a 3D image [5].

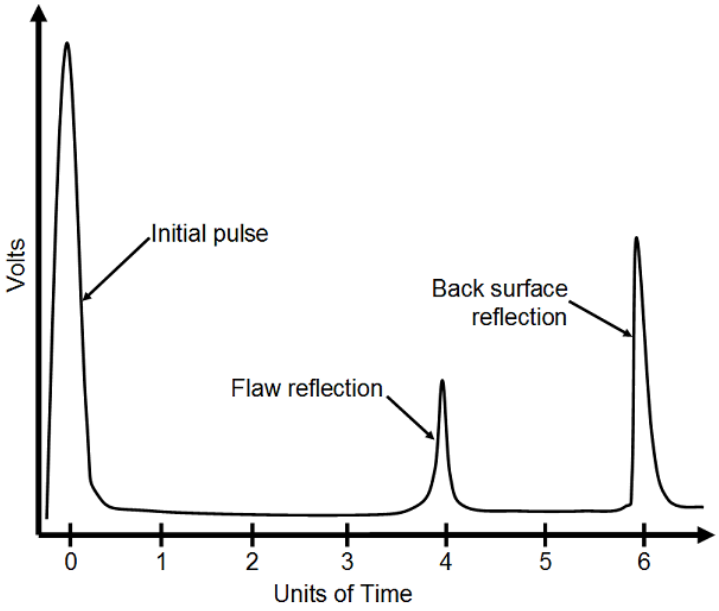

FIGURE 1-2: A-SCANS RESULTANT

1.3.1.1 AUTOMATED AND ONLINE ULTRASONIC TESTING

Instrumentation that can perform automated A-, B-, and C-scans of wall thickness and provide digital information, hard copy, and video images is readily available (General Electric Co.). Numerous other improvements over manual testing are available. It is also possible to permanently install ultrasonic transducers for continuous monitoring in a particular location. On-line inspection (also called in-line 2 inspection) can be achieved using intelligent pigs, which are devices that are inserted into a pipeline and driven through the pipeline by product flow. The instrumentation associated with intelligent pigs allows these devices to conduct a

non-destructive survey of the condition of the pipeline while it is in operation. Data is acquired and downloaded when the pig is retrieved to provide information on the nature and location of defects. Temperature, pressure, and minimum bend radius limitations can be provided by intelligent pigs [4].

On-line inspection with intelligent pigs is becoming an alternative to hydrostatic testing. These tools use different NDT methods, the most common of which are magnetic flux leakage and ultrasonic methods. Quantitative measurements of wall thickness can be made around the entire circumference of the pipe, and it is possible to distinguish external and internal metal loss.

The hole-size thresholds that ultrasonic scanning pigs can detect are typically a diameter greater than 20 mm and a depth greater than 1 mm (USM Go Ultrasonic Flaw Detector). Crouch et al., [6] compared the performance of intelligent pigs mounted with ultrasonic and magnetic flux leakage sensors in a 20-inch (500 mm) gas pipeline fitted with a test spool containing simulated defects, the ultrasonic method was found to be more accurate then intelligent pigs' techniques.

1.3.1.2 LONG-RANGE, GUIDED WAVE TESTING

Lamb waves (also known as plate waves) propagate parallel to the test surface in thin plates and can be used to detect changes in the thickness of the wall of a pipe. Advantages of using guided waves include the ability to perform inspections over long distances, their usefulness is in accessing otherwise inaccessible areas and the test can be performed without the removal of pipe insulation. The use of long-range guided waves for inspecting pipes has been reported by Alleyne and Cawley [7]; Pei et al., [8]; Rose et al., [9]; Lowe et al., [10]; Bray et al., [11]; Alleyne et al., [12]; Wassink et al., [13].

Alleyne et al., developed a guided wave system to test pipes with diameters ranging from 50 mm (2 inch) to 610 mm (24 inch) over a range of 50 m [12]. Three or four rings of dry-coupled, piezoelectric transducers are clamped to the external surface of the pipe to excite low frequency, longitudinal, L (0, 2) mode waves; though it is also possible to use torsion waves. The system can detect hole defects of magnitudes that cause a 5-10% loss of cross-sectional area at a particular axial location. Rose et al., [9] used a multi-element comb transducer that could generate guided waves with different frequencies which excited different modes. This varied the sensitivity to different defect types and sizes.

Both ring and comb type transducer systems have been used to test insulated piping in the chemical processing industry. Guided waves are not affected significantly by the presence of insulation, but liquids in the pipe and pipe coatings can affect the response.

It is not known how the presence of internal corrosion products or scale would affect guided wave reflectivity and whether removal of such materials would be required prior to testing by this method. However, the potential advantages make long-range guided wave testing worthy of investigation that is more detailed. Rose et al. [9] explored this issue "It would be particularly useful if this method could indicate the sizes and locations of defects".

Stalenhoef et al., [14] reported on a technique that used creep and head waves for screening piping of various geometries; this patented technique has been named CHIME (Creeping/Head wave Inspection) and it's sample as two transducers, 1 m apart were placed on the external surface to generate and receive ultrasonic waves.

The presence of defects alters the magnitude of the signal and its arrival time. Signal loss gives an indication of the size of the defect, and full-coverage inspection of the pipe can be achieved. Both uniform, localized holes and corrosion can be detected.

1.3.2 ELECTROMAGNETIC METHODS

1.3.2.1 ELECTROMAGNETIC ACOUSTIC TRANSDUCERS

In order to overcome the temperature limitations of conventional ultrasonic transducers, it is possible to use electromagnetic acoustic transducers (EMATs) to measure the thicknesses of pipes. EMATs produce ultrasonic waves by electromagnetic interaction with an electrical conductor and are used on the external surface of the object to be tested.

The primary advantages of EMATs are that couplant are not required and that elevated temperatures can be withstood. Other advantages include tolerance of rough surfaces and the ability to conduct high-speed scans.

Different wave modes EMATs are available (e.g., Rayleigh, Lamb, vertically polarized shear waves, and horizontally-polarized shear waves). EMATs are more versatile than conventional ultrasonic transducers that use piezoelectric materials because of the additional wave modes that can be generated and received. Figure 1-3 show the basic structure of Piezoelectric based ultrasonic and EMAT technology.

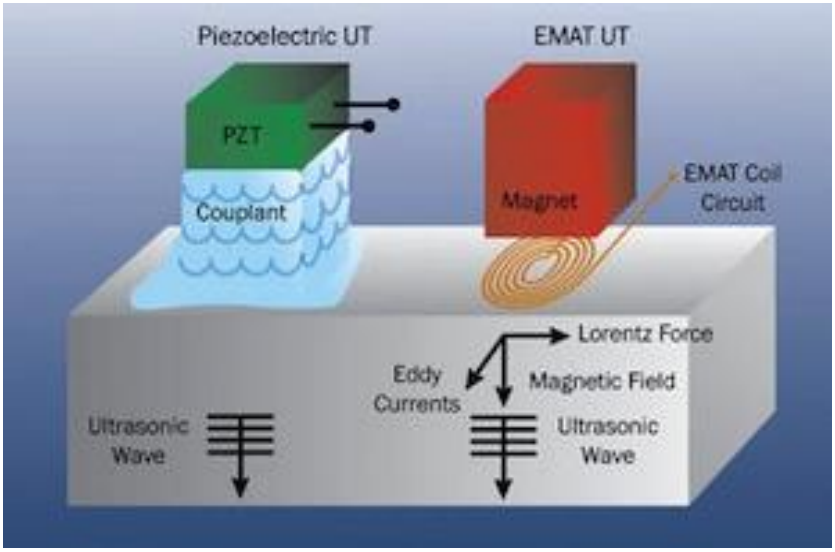

FIGURE 1-3: BASIC STRACTURE OF PIEZOELECTRIC AND EMAT [144]

1.3.2.2 EDDY CURRENTS

Eddy current testing is a common method of locating cracks in piping. The method uses as a source a variable magnetic field such as a coil carrying alternating current with frequencies in the range between 10 Hz to 10 MHz; This induces eddy currents in the object being tested and these are influenced by physical properties of the material (e.g., electrical conductivity and magnetic permeability) as well as its thickness and any discontinuities (e.g., voids and cracks), see Figure 1-4.

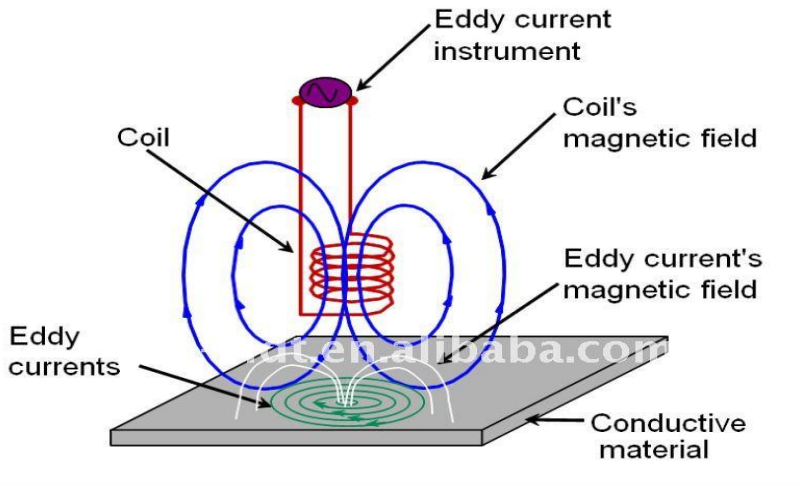

FIGURE 1-4: EDDY CURRENT TECHNOLOGY

Inspection parameters that affect eddy currents include frequency, the size and shape of the generating coil, and the separation between the coil and the object (lift-off). Relevant instrumentation is included in a testing system to detect changes in the magnetic field and compare the response with a reference. A pulsed-eddy-current (PEC) tool can be used to test pipes for damage without the need for the removal of insulation or coatings (Cohn and de Raad, [15]; Stalenhoef et al., [14]; Wassink et al., [13]. In this case, the test probe consists of a transmitter and receiver coil and instrumentation to send step-pulses of current to the transmitter coil. The pulsed magnetic field penetrates the insulation to induce eddy currents in the surface of the object being tested. Diffusion of the eddy currents is dependent on the

properties of the material and its wall thickness. Hence, by comparing the measured arrival time with that of calibration standards, the wall thickness can be determined.

1.3.2.3 MAGNETIC FLUX LEAKAGE

Magnetic flux leakage (MFL) inspection is one of the most common non-destructive techniques used to detect crack-like defects in ferromagnetic materials. In order to improve the accuracy and reliability of crack detection, sensors based on the giant magneto-impedance (GMI) effect are suitable candidates for the magnetic sensors used in MFL detection systems [22]

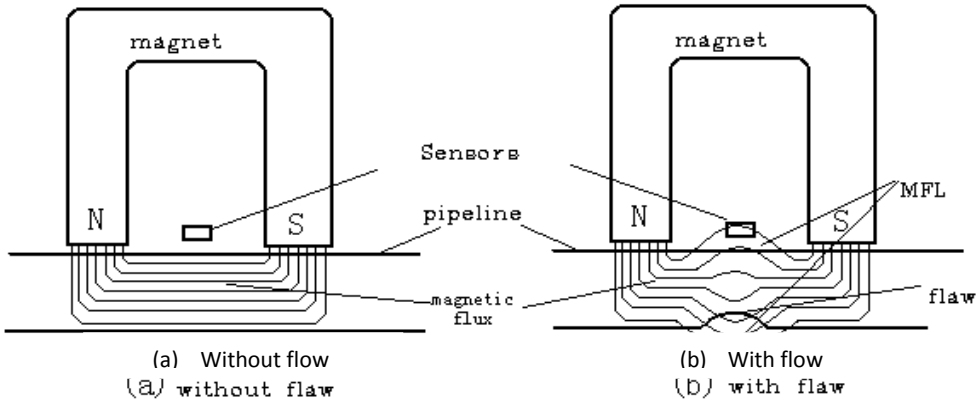

FIGURE 1-5: MAGNETIC FLUX LEAKAGE

The flux leakage is detected by magnetic field sensors, does not require contact, and can be automated for high-speed testing.

The MFL technique is usually regarded as a qualitative technique, although some estimates of the sizes of defects can be made. Thus, the MFL technique is largely a screening tool that can be followed by ultrasonic inspection for the determination of defect size. Figure 1-5 clearly shows the magnetic flux leakages caused by pipe flaws.

1.3.3 RADIOGRAPHIC METHODS

Radiography uses X-rays or gamma rays to produce a two-dimensional image of the pipe as shown in Figure 1-6. Flaws are indicated by changes in transmitted intensity and wall thickness of insulated piping can be measured during service using radiographic techniques. It is also possible to examine scaling in pipes using radiography.

Conventional tangential radiography requires skilled set up and interpretation. Advancements in digitization and image analysis of radiograms have improved this method. Furthermore, developments in technology now enable filmless, real-time imaging and are discussed by Zscherpel et al., [16] and Hecht et al., [17].

By combining imaging advancements and gamma ray detector technology with robotics, it is possible to perform real-time radiography and scan insulated or insulated piping for corrosion and erosion defects or loss of wall thickness (Gupta and Isaacson, [18]; Walker, [19]).

Gupta and Isaacson [18], state, “This is particularly important since such components are subject to flow accelerated corrosion and erosion. These radiographic techniques appear useful for geothermal applications”.

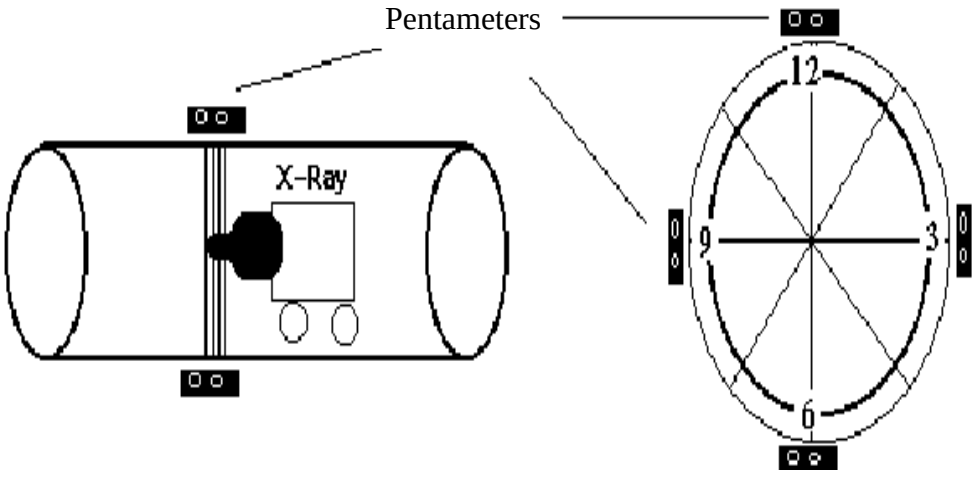

FIGURE 1-6: RADIOGRAPHIC METHOD

1.3.4 THERMOGRAPHIC METHODS

Thermographic testing involves subjecting the object of interest to heating or cooling and measuring the resultant temperatures or thermal gradients with heat sensors. The presence of flaws alters the thermal properties and, consequently, the heat transfer behaviour.

Thermograms are produced, and flaws are indicated by changes in temperature as a result of modifications in heat flow. This is a non-contact method that has broad applications in NDT. Maldague [20] described the use of pulsed active infrared thermography (PAIRT) for the inspection of insulated piping. This technique involves transient thermal perturbation of the object. The resultant sequence of temperature distributions is monitored with an infrared camera, and the data are recorded digitally. It was concluded that thermograph in pipeline applications would be limited to insulated piping systems. Figure 1-7 depicts the capability of thermography technology on indentifying structure related faults within steel pipe.

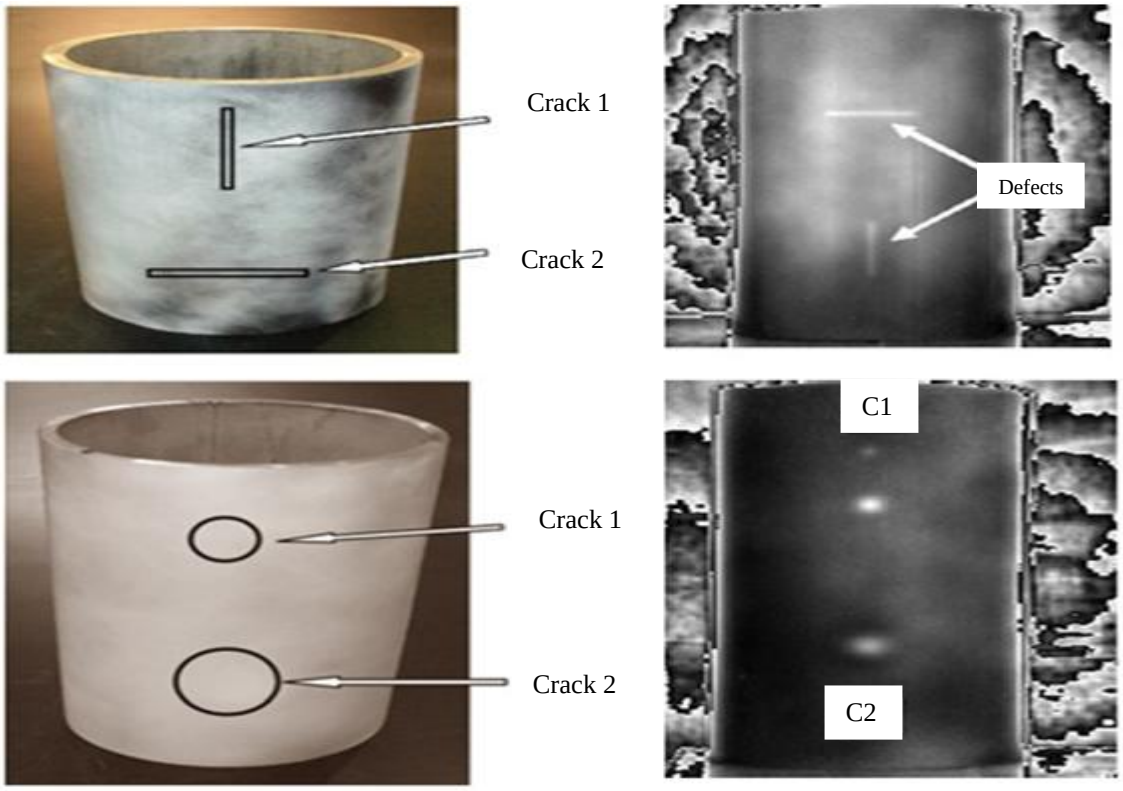

FIGURE 1-7: THERMOGRAMS OF STEEL PIPELINE EMBEDDED WITH VARIOUS FAULTS [145]

1.3.5 DYNAMIC METHODS

Dynamic NDT involves the application of a known vibration to an object or structure and the observation of its vibration response. The dynamic response is sensitive to the presence of flaws. It is also possible to use dynamic methods to determine variations in material properties. Two different methods are used in dynamic testing:

(a) Measurement of natural (resonant) frequencies

Objects or structures can vibrate at different natural frequencies; these frequencies are functions of geometric parameters, physical constants (e.g., elastic modulus, density, and Poisson's ratio), end constraints, modes of vibration include flexural, torsion, longitudinal, radial, diametrical, and annular.

Modal analysis refers to the study of natural frequencies, damping values, and mode shapes of physical systems. The measurement of natural or resonant frequencies involves the application of a vibration force and the determination of the natural frequencies. Measuring ambient vibration and the resultant response is another alternative. The resonant frequency tests require that the object be supported at the nodes for the mode of vibration under consideration [20].

A piezoelectric transducer, electromagnetic vibrator, or other means inducing vibration applies the vibration force. Some form of pickup detects the vibration. Then, a range of physical properties can be calculated based on the measured resonant frequency. Flaws affect elastic properties and resultant resonant frequencies. Use of resonant frequency techniques to detect flaws or damage in structures requires some way to compare the response of the test structure to one that is known to be sound and the use of this information to ascertain the nature and location of the damage. This is where modal analysis becomes applicable in both

theoretical and experimental forms. The deviations in measured global vibration response of the structure must be correlated with localized damage. In order to achieve this, it is necessary to consider local response parameters, such as mode shape data. Although resonant frequency and modal analysis techniques have been applied to assess the integrity of structures such as bridges, the approach is not as well developed as other NDT methods.

(b) Measurement of rate of attenuation, or damping, of the vibration.

In this method, an object is induced to vibrate in one of its natural frequency modes by a vibration pulse. The pulse is then stopped, and the subsequent decay in vibration is measured. Then, the specific damping capacity is determined from the decay curve and because damping capacity is increased by the presence of flaw, this method can be used for NDT of objects.

Kriel and Heyns [21] investigated the applicability of dynamic methods in non-destructive damage detection for insulated piping, in particular, ambient excitation due to flow was considered.

The study examined the important structural modes through finite element analysis and verified these experimentally through frequency-domain and time-domain modal parameter estimation.

The dynamic response to different forms of damage was investigated. It was determined that flow-induced vibration was sufficient to excite modes of interest and that the mode shapes were sensitive to uniform damage rather than localized corrosion [19]. It was also observed that temperature did not affect the results.

The dynamic method of NDT appears to have a potential for use in geothermal piping. Further study is necessary to determine the ability to detect localized corrosion, the minimum size of defect that can be detected, the range of application, and the possibility of using forced

vibration. It is also important to determine the influence of adherent scale on dynamic response and whether scale removal is necessary.

1.4 SIGNIFICANT OF THE THESIS

The research proposed focuses on developing a finite element model to understand the advantages and limitations of ultrasonic methods, in order to develop an oil pipe diagnosing system based on ultrasonic methods.

Hu et al., [23] carried out a case study that demonstrated the application of harmonic wavelet analysis to the problems of detection of small leaks in pipelines using time-frequency domain analysis. A comparison was made between leak detection results of harmonic wavelet and Daubechies wavelet and it was found that harmonic wavelet based small leak detection approach performed better.

The magnetic induction-based sensor detects and localizes leakage throughout the pipeline network and reports to the administration centre in real-time-guided waves and was not affected significantly by the presence of insulation.

Meurer et al., [24] used Lamb wave propagation in the wall of a pipe generated in a standoff manner for defect detection and found that this approach provided accurate measurement of wall thickness for different materials and thicknesses only at the measurement point and not for the circumference of the pipe. Sun et al., [25] used an ultrasonic based sensing network for underground pipeline monitoring by combining measurements of different types of sensors located both inside and around the underground pipelines. However, no recent, rigorous analysis of ultrasonic technology has been carried out combining 3D modelling simulation and CWT analysis so its capabilities have not yet been fully investigated.

1.5 ACADEMIC AIM

To characterise ultrasonic waves propagation into Carbon steel pipelines using 3D finite element modelling and subsequently, propose reliable and sensitive integrity assessment method for oil pipelines based on ultrasonic measurements and wavelet analysis techniques (CWT).

1.6 OBJECTIVES

I. To review state of the art ultrasonic pipeline condition monitoring techniques,

II. To develop 3D finite element model and describe wave behaviours and its propagation into the pipeline structure,

III. To simulate the common fault modes in pipes by introducing into the pipe surface 1 mm diameter holes of different depths,

IV. To build a fully equipped test model for experimental data collection,

V. To develop a sensitive ultrasonic data processing technique based on wavelet analysis for condition feature extraction and classification,

VI. To cry out evaluation of results and review procedure.

1.7 METHODOLOGY

The proposed methodology is in two phases; Phase I: carry out theoretical modelling to investigate the acoustic waves dynamics into the structure of carbon steel pipes; this will be carried out using the ABAQUS finite element software package. Phase II: construct an experimental test rig to carry out real-time measurements on healthy Carbon steel pipes and

with quantified seeded faults using ultrasonic techniques in the Manchester Metropolitan University laboratories.

1.8 THESIS OUTLINE

Chapter 2: reviews the literature of current ultrasonic techniques, wave mode, wave propagation in liquids, ultrasonic fault diagnosis and monitoring and signal processing. It will also review oil transmission pipelines construction, materials, common defects, advantages, and disadvantages of the currently used monitoring techniques.

Chapter 3: presents the mathematical and simulation modelling of ultrasonic wave propagation into steel pipes and some common pipe defects such as small holes (1 mm diameter of depth 25% wall thickness, 50%, 75% and completely through the pipe) using the ABAQUS software.

Chapter 4: The chapter also investigates common signal processing techniques with a focus on fundamental characteristics of ultrasonic transmission in steel pipes combining data analysis with time and frequency domain algorithms. A description is also provided of the experimental setup and then demonstrates and discusses the outcomes results and highlights the research novelty.

Chapter 5: introduces the mathematical tools needed for the research work, including a discussion of analog signals, discrete signals, digital signals and the methods to transition from one of these realms to another. In addition, the chapter introduces the terminology of signal processing and conventional architecture of signal processing systems.

Chapter 6: presents an investigation into the main features of the wavelet transform by comparing wavelet transforms with the Fourier transform, pointing out their common aspects

and main differences and explain the development of a more sensitive signal-processing algorithm based on wavelet analysis techniques; continuous and discrete wavelets.

Chapter 7: presents the achievements of this research study, discusses the extent to which the specified objectives were met, and makes suggestions for future research.

CHAPTER II

LITERATURE REVIEW

This chapter reviews the research literature of ultrasonic pipeline monitoring techniques, wave mode, acoustic wave propagation, ultrasonic fault diagnosis and signal processing. It also reviews construction of oil transmission pipelines including materials used, common defects, and advantages and disadvantages of the currently used monitoring techniques.

2.1 INTRODUCTION

Ultrasound is an oscillating sound pressure wave with a frequency greater than the upper limit of the human hearing range. It has a technique that includes sudden and transient elastic energy waves generated by the rapid release of strain energy caused by deformation, damage or failure mechanisms such as fatigue crack propagation within or on the surface of a material. The signals picked up to ultrasound transducers will generally be high frequency, often above 100 kHz and even above 1 MHz, and will be a complex mix of transients.

Ultrasonic wave are sources radiate energy all directions, and any suitable positioned sensor (e.g. close to the source) will detect the signal. The received signal will be a mix of direct transmission and waves reflected from discontinuities in the material which generally means the received signal will be a mix of direct and reflected waves. If the ultrasonic source is pulsed then the direct and reflected waves will be transients.

Ultrasonic condition monitoring requires the interpretation of this complex signal in a way that provides useful information concerning the condition item of interest (machine component or process). Over the past thirty years ultrasonic techniques have developed for a wide range of applications including: detecting and locating faults in storage tanks, piping systems and pressure vessels [26; 27], monitoring the quality of welds [28], corrosion-erosion processes [29], detecting discharges from high voltage components [30] and failure of protective coatings [31].

This chapter reviews the vast literature concerning ultrasonic monitoring. First the basics of ultrasonic wave propagation and signal transductions are presented, providing a basis for a critique of methods used for source location and the value of attenuation studies. This section ends with an assessment of how an ultrasonic signal is distorted as it travels from source to sensor.

Next, both novel and traditional signal processing techniques used for ultrasonic signal analysis are described with a critical summary.

The final section presents applications, commencing with the most common types of ultrasonic source and a review of ultrasonic applications to pipelines and process vessels.

2.2 ACOUSTIC EMISSION WAVE PROPAGATION AND TRANSDUCTION

Figure 2.8 illustrates AE monitoring, the core problem being to determine as many characteristics of an AE source as possible (e.g. nature, location and magnitude) using signals obtained at one or more surface-mounted transducers. Essentially all AE sources (also referred to as targets) release elastic energy and the AE wave is an elastic wave, but this may be direct from the source or be a reflection as when it is used for assessing particle impacts on the wall of a process vessel.

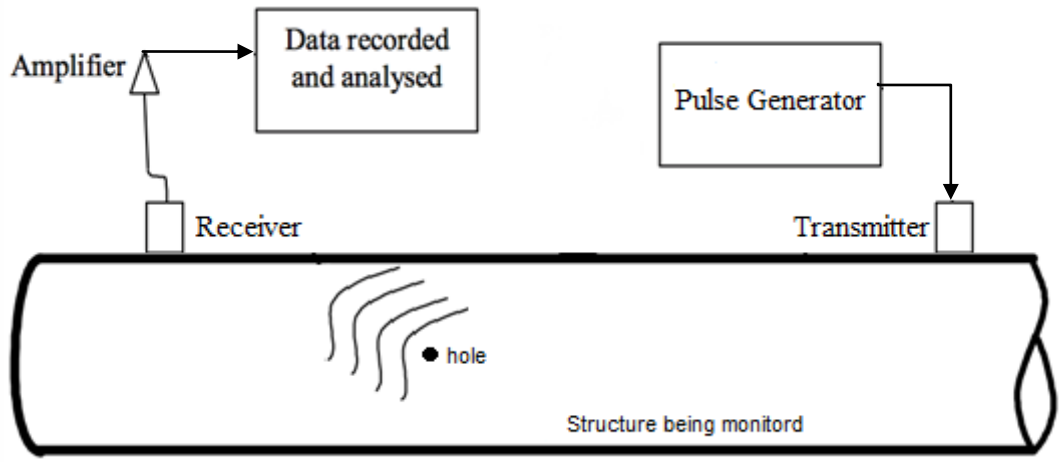

FIGURE 2-8: SCHEMATIC REPRESENTATION OF AE MONITORING

Hamstad et al., [32] have pointed out there are many studies of AE and ultrasonic wave propagation aimed at determining the transfer function (time, frequency, amplitude distortion) introduced by propagation of the wave from source (e.g. the deformation or crack) to the sensor (usually on a peripheral surface).

Once the signal has arrived at the sensor, there is a second transfer function with the transduction of the excitation of the sensor surface into an electrical signal.

The final stage of the process is translating these two transfer functions into a definite physical phenomenon (such as impact or extension of a fatigue crack).

However, AE waves will invariably be complex due to transmission path geometry [33-35]. There have been many attempts to model AE and ultrasonic propagation using classical wave theory but these have had only limited success [36-39].

AE waves are attenuated by attenuation due to viscous effects in the transmitting medium, refraction on passing from one medium to another, reflection from structural features, scattering and mode conversion [35]. Some of these processes result in secondary waves that may themselves be detected by the sensor.

In this section, we concentrate on the propagation and transduction of AE waves and examine the extent to which the extremely complex wave propagation phenomena can be dealt with using simple analytical considerations.

2.3 WAVE MODES

The most common ultrasonic waves are [35; 40];

- Dilatational - longitudinal or compression waves where particle displacement is in the direction of wave propagation, and consists of localized compressions and rarefactions of the medium see Figure 2.9a,
- Distortional - shear waves where the particle oscillations are perpendicular to the direction of wave propagation, see Figure 2.9b,

- Rayleigh or surface waves - the particle motion is a combination of both longitudinal and transverse oscillations so that they move in elliptic "orbits" in planes normal to the surface and parallel to the direction of the wave propagation, see Figure, 2.9c, and

- Lamb or plate waves where separation of modes is generally applicable only for longer source-sensor distances where the wave front is essentially planar.

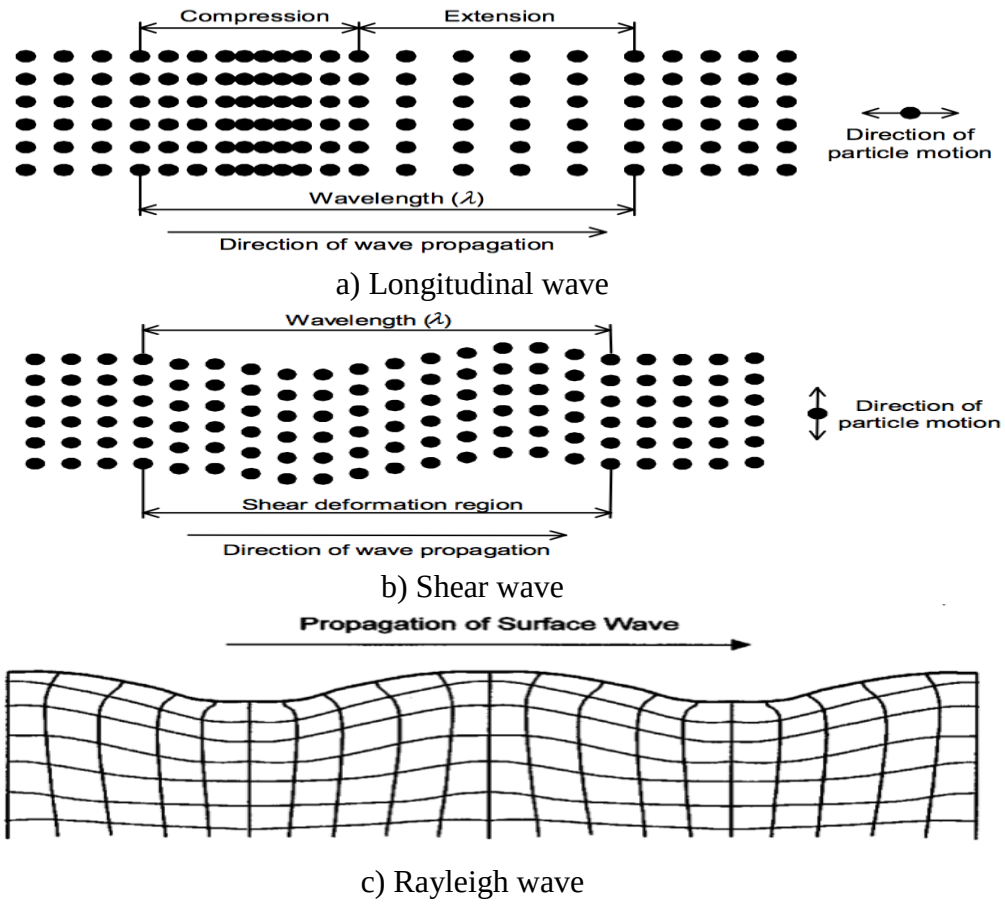

FIGURE 2-9: THE MAIN ULTRASONIC (AE) WAVES IN INFINITE AND SEMI-INFINITE MEDIA

In real structures the type of AE wave cannot be pre-determined, and the different wave types travel at different speeds via different paths, each of which will be a function primarily of the properties of the propagating medium but surrounding media also have an influence. The modes the source will stimulate are not known in advance, and refraction, reflection and mode conversion will take place as the wave travels to the receiver so that distortion of the source

signature will happen. Different modes tend to experience different degrees of attenuation and this contributes to source distortion.

In infinite elastic media waves can propagate only as longitudinal waves or transverse waves. The velocity of longitudinal waves (C_L) is frequency independent:

$$C_L = ((E\ (1-\upsilon))/\ (\rho\ (1+\nu)\ (1-2\upsilon)))^{½} \quad (2.1)$$

Where E is Young's modulus of elasticity for the material, $E_{STEEL} \approx 200 \times 10^9$ N/m^2;

ρ is the density of the material, $\rho_{STEEL} \approx 7800$ kg/m^3; and

ν is Poisson's Ratio for the material, $\nu_{STEEL} \approx 0.28$.

By contrast, shear waves travel as an oscillatory shearing motion between successive atomic planes normal to the direction of travel. The velocity of shear waves (C_S) is also independent of frequency and is given by the following expression:

$$C_S = (E/\ (2\rho\ (1+\upsilon)))\ ½ \quad (2.2)$$

It can be seen that the ratio of speed of the longitudinal wave to that of the shear wave speed is always greater than unity, for steel (and most metals), it is about 2. If the AE wave is incident on an interface, some of the incident energy will be reflected, some will be transmitted into the adjoining medium, and some may propagate along the boundary as a surface-wave [35].

The modes of the reflected and incident waves are usually different so it is often useful to discuss in terms of mode conversion at boundaries even though the transition is not sharp.For semi-infinite media, a third type of wave can also exist, Rayleigh waves, see Figure 2.9c. These waves possess characteristics of both shear and longitudinal waves and propagate at a speed of about 0.9 that the shear wave [34; 35].

In an infinite medium bounded by two surfaces, such as a plate, the waveforms couple at the surfaces to produce more complex propagation modes called Lamb waves. The two basic wave mode classes are shown in Figure 2.10 normally referred to as symmetric (s_o) where both surfaces pinch together, and anti-symmetric (a_o) or flexural wave modes where both surfaces deflect simultaneously in the same direction.

In Lamb waves, the particles move in ellipses, and the relative magnitudes of the motions perpendicular and parallel to the plate depend on frequency and mode of excitation in a complicated manner. Surgeon and Wevers [40] have reported that in plates only extensional and flexural wave modes have been detected in practice.

Gorman and Prosser [41] and Gorman [33] have showed experimentally for aluminium and composite materials that one or two of the Lamb modes can be generated in those cases where the wavelength is much larger than the plate thickness.

They also noted that the classical plate equation governs wave motion where the wavelength is much greater than plate thickness. The wavelength (λ) is related to frequency and velocity by the classic equation $\lambda = V/f$ [34] thus as each generated component depends on the source type and medium through which AE (ultrasonic) wave is propagating each will have a different frequency and velocity [33]. In isotropic materials the in-plane displacement for the extensional mode is governed by the following equations [41]:

$$(\partial^2\mu)/(\partial x^2)+ ((1-\nu)\partial^2\mu)/(2\partial y^2)+(1+\upsilon)(\partial^2\upsilon)/\partial x\partial y = (\rho\partial^2\mu)/(A\partial t^2) \quad (2.3)$$

and

$$(\partial^2 \upsilon)/(\partial x^2)+ ((1-\nu)\partial^2\mu)/(2\partial y^2)+(1+\upsilon)(\partial^2\upsilon)/\partial x\partial y = (\rho\partial^2\mu)/(A\partial t^2) \quad (2.4)$$

Where *x* and y are the coordinate axes in the plane of the plate, *u* and *v* are the displacements along these axes respectively, *v* is Poisson's ratio, ρ is the density, and *A* is given by:

$$A= (Eh)/ ((1-\upsilon^2)) \quad (2.5)$$

Where *h* is the thickness of the sample, A is Amplitude and E is Young's modulus of elasticity for the material. Due to the Poisson effect, the extensional mode may also include of an out-of-plane displacement.

The flexural motion is governed by:

$$D\nabla\wedge(4)\, w+\rho\, (\partial 2\, w)/ (\partial t2) =0 \quad (2.6)$$

Where *w* is the displacement along the z-axis, normal to the plate and D is the bending stiffness per unit breadth given by:

$$D= (Eh)^3/ (12(1-v^2)) \quad (2.7)$$

For Lamb waves the wave velocity is related to the ratio of the plate thickness and wavelength and thus Lamb waves are generally dispersive [33; 35]. At higher frequency-thicknesses, (around 10 mm MHz for steel) AE (ultrasonic) waves are non-dispersive which makes source location easier [35]. For example, Holford and Carter [42] and Surgeon and Wevers [40] showed that AE (ultrasonic) modes in thin plates are dispersive and that the different arrival times of different frequencies could be used to improve accuracy of source location. Jeong and Jang [43] have used the Wavelet Transform of dispersive AE (ultrasonic) modes to accurately locate sources, and have proposed that the AE (ultrasonic) modes should be identified before signal processing to improve accuracy of source location.

For pipelines, wave propagation depend on the transmitting structure (primarily shape and material), the fluid contained in the pipe, the surrounding medium and other environmental aspects, such as temperature and internal gas pressure [27, 35, 44]. The ultrasonic energy is partly reflected and partly transmitted when it encounters a boundary with a surrounding medium or the fluid contained in the pipe [35].

The partitioning between transmitted and reflected waves depends on the angle of incidence and relative material acoustic impedances of the two materials; when the acoustic impedance of the two materials are well matched a large proportion of the energy will be transmitted, e.g. steel and water, but, if they are poorly matched, most of the energy will be reflected, e.g. steel and air.

The reflected and transmitted waves will generally be of a different nature to the incident wave, this change is usually referred to as mode conversion [35]. For two materials of different acoustic impedances, Z_1 and Z_2, the percentage of energy transmitted, E_t is given by:

$$E_t = (4Z_1 - Z_2)/((Z_1 + Z_2)) \times 100 \quad (2.8)$$

And the percentage of energy reflected, E_r is given by

$$E_r = ((Z_1 - Z_2)/(Z_1 + Z_2))^2 \times 100 \quad (2.9)$$

Where $Z = \rho V$; ρ is the material density (kg/m3) and V is the wave speed (m/s).

When the acoustic impedances of two media are well matched ($Z_1 \approx Z_2$), the incident wave is largely transmitted to the other medium, as shown in Figure 2.11a. On the other hand, when the acoustic impedances are very dissimilar ($Z_1 >> Z_2$ or $Z_2 >> Z_1$), the incident wave is mostly reflected, as shown in Figure 2.11b. The acoustic impedances of some common materials can be seen in Table 1.

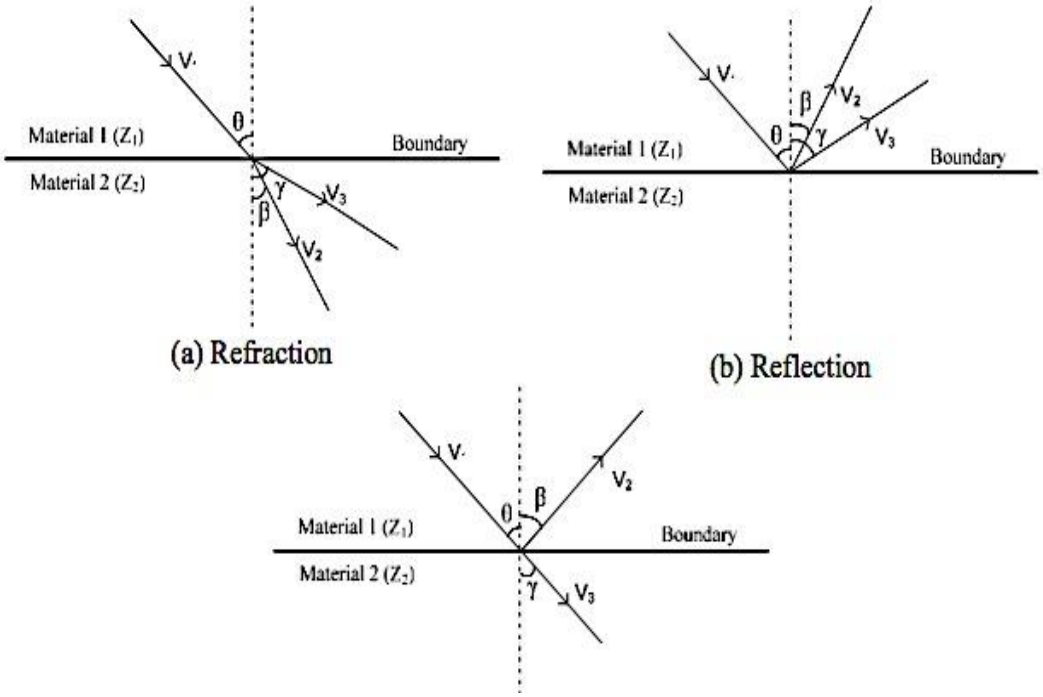

c) Reflection and refraction

FIGURE 2-10: REFLECTION, REFRACTION AND MODE CONVERSION OF WAVE CAST BOUNDARY

Table 1: Acoustic Impedance of some common materials

Material	**Specific acoustic impedance, Kg/m^{2}s**
Air	0.4×10^6
Water	$.05 \times 10^6$
Soil	0.3 to 4×10^6
Concrete	7 to10×10^6
Steel	47×10^6

Both longitudinal waves and shear waves can be reflected or refracted when they impinge on a boundary. The angles of reflection and refraction depend on wave velocities in the material and can be calculated by Snell's Law:

$$Sin\theta/V_1 = sin\beta/V_2 = sin\gamma/V_3 \quad (2.10)$$

Where: $\theta, \beta, and\ \gamma$ are shown in Figure 2-10; and V_1, V_2 and V_3 are the relevant wave velocities. Mode conversion can also occur at a boundary when the acoustic impedances of the two media are different and angle of incidence is not normal to the interface, leading, for example, to longitudinal waves, becoming transformed into shear waves or shear waves transforming to Rayleigh waves [35]. For example, incident wave (V_1) may be reflected as the same type (V_2) while some is transmitted to the other medium as a different type (V_3), as shown in Figure 2.10c. The angle of incidence of each wave can be determined using Equation 2.10 and the relevant wave velocity. In multi-layered structures, the ultrasonic energy may propagate through the different media being partially transmitted and partially reflected at each interface.

Pollock [35] has suggested that Lamb modes can be considered to be multiple reflections and mode conversions of longitudinal and/or shear waves, which may be changed into other Lamb modes on reflection from the plate ends or on transmission into a water-filled pipe. The Lamb wave loses energy as a compression wave in the water. Fuller and Fahy [47] have studied free waves in fluid-filled cylindrical shells and noted that free wave behaviour depends on the thickness of the shell wall and the ratio of the density of the shell material to the density of the contained fluid.

2.4 ATTENUATION

To evaluate and locate ultrasonic signals it is often useful to know how much the signal has been attenuated in the material or structure of interest. If nothing else, knowledge of the attenuation is necessary to ensure that sensors are placed appropriately, especially with large or complex structures [48, 49]. Attenuation of ultrasonic waves can be due to geometric, absorption, "leakage" or dispersion effects [35].

Ultrasonic waves generated by a localised source in an infinite medium spread outwards as spherical waves in all directions from the source. Geometric attenuation arises from the law of conservation of energy, where the energy of the wave front remains constant along the propagation path, but the area of the wave front increases as the square of the distance from the source. Thus the amplitude of the wave (A) will decrease inversely with propagation distance (r), $A=k_1/r$. In plates, wave propagation can be considered to be two-dimensional, expanding as a cylindrical wave front, so the wave amplitude decreases inversely as the square root of the propagation distance (r), $A=k_2/\sqrt{r}$, in order to maintain a constant total energy at the wave front.

In pipelines, the wave front becomes effectively plane after travelling a short distance from the source and so geometric attenuation is very small. Ultrasonic waves are also subject to absorption or damping in the propagation medium; the ultrasonic signal amplitude and energy usually falling exponentially with distance. The attenuation coefficient is depends on material properties but is usually directly proportioned to the frequency which can lead to a kind of structural filtering where some frequencies are attenuated more than others [35, 42].

Leaking of the wave energy into adjacent media can occur at internal or external boundaries. In pipes, this is particularly significant, since both boundaries are present along the entire propagation path, which can lead to the situation where much of the energy is carried in the fluid inside the pipe [35].

Dispersive attenuation occurs in waves where velocity varies with frequency so that an initial sharp transient will become more spread in time as it propagates. The main practical consequence of dispersive attenuation [35] is for dispersive modes (e.g. asymmetric Lamb modes) to become more attenuated with distance than non- dispersive modes.

In some structures, the energy attenuation in one dominant transmission path from source to sensor can be described using a simple absorption law [40]:

$$E(x) = E_o e^{-k x} \quad (2.11)$$

Where E*(x)* is ultrasonic energy at distance *x* from the source (V^2.s); E_o is the energy of the source (V^2.s); *k* is an attenuation factor (m^{-1}); and *x* is the source-sensor distance (m).

Ultrasonic wave attenuation is often measured empirically [50, 51] using a logarithmic scale (decibel) [50], where the relative amplitude (A_r) is given by:

$$A_r = 20.\log_{10}(A_i/A_o) \quad (2.12)$$

Where A_i is the maximum signal at a receiver, a distance, x from the source, and A_o is the maximum signal amplitude at the source position. The amplitudes can be measured in volts provided that the amplifiers are consistently calibrated.

Wave attenuation can then be determined from a plot of the relative amplitude versus distance and can be expressed as decibels per unit distance [50], determined by:

$$\propto = (20 \log_{10}(A_2/A_1))/D = A_r/D \quad (2.13)$$

Where $\propto$ is the attenuation coefficient (dB/m),

A_1 is the amplitude of the signal at Sensor 1, (V)

A_2 is the amplitude of the signal at Sensor 2, (V) and;

D is the distance between Sensor 1 and Sensor 2, (m).

A practical example of differential attenuation effects is given by Holford and Carter [42] who recognised two distinct Lamb wave modes in 12 m long structural steel girders. The signal

was generated by a Hsu-Nielsen source and measured at various source-sensor distances, and it was observed that the non-dispersive mode is essentially an extensional longitudinal wave, which travels faster than the highly dispersive flexural mode. A low pass filter at 100 kHz was used to separate the two modes, since the extensional mode was of higher frequency. Holford and Carter [42] also suggested that, for the near-field zone, the higher attenuation was attributed to geometric spreading and, for the far-field zone; the attenuation was caused by absorption or conversion of ultrasonic wave energy into heat.

2.5 SOURCE LOCATION

Source location is central to ultrasonic based inspection, such as proof testing of metallic and composite vessels, and in monitoring of pipe lines for leakage [96]. Many applications of source location are on relatively uncomplicated structures, such as pipes and plates and with sensors that are assumed to be points in time and space. The time of arrival of the ultrasonic wave propagating from source to sensor is the main feature that is extracted from the detected signal and, by measuring this arrival time with a number of sensors in an array, the position of the source can be determined. The following two sections review the types of geometric algorithms that are used to determine source position given arrival times at the sensors, and this is followed by a discussion of methods used in less clearly- defined cases.

2.5.1 LINEAR SOURCE LOCATION

Two sensors are sufficient to calculate the location of a source where the direction and velocity of wave propagation are known. A common equation used for linear source location (Figure 2-11) is [97]:

$$X_1 = (½)\,(D - \Delta t\, V) \tag{2.14}$$

Where D is the distance between sensors, V is the constant wave velocity, Δt is the time difference between hits, and X_1 is source location measured from the first hit sensor.

For pipes, linear location is most appropriate when the sensor separation is large compared to the diameter of the test object. As this ratio reduces, sources close to the sensors can be mis-located if they are away from the direct axial line through the participating sensors.

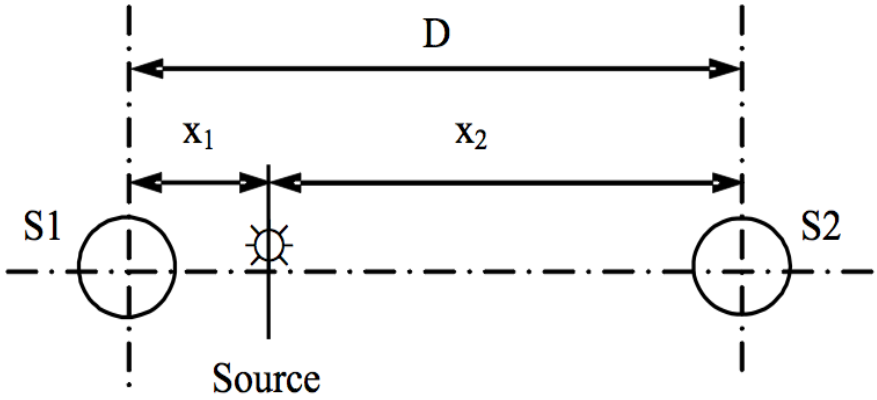

FIGURE 2-11: LINEAR SOURCE LOCATION

Depending on the wall thickness, a source may generate an ultrasonic signal that contains Rayleigh, shear and the two basic Lamb wave modes. Since these modes are produced at the same location, but propagate at different velocities, they will arrive at a sensor at different times. For Lamb waves, using the arrival time difference between the extensional and the flexural mode and knowing the propagation velocity of both modes makes it possible to back-calculate the source location with a reduced number of sensors.

Lamb wave arrival time techniques depend on isolating the different frequency components, which travel at different velocities. For two velocity components with the higher,V_H, the lower, V_L, and the time lag (Δt) between their arrivals at a given sensor, then the source to sensor-distance (x) is given by [97]:

$$x=\Delta t\ ((V_H\ V_L)/\ (V_H - V_L)) \tag{2.15}$$

It is important to emphasise that application of this technique to a given structure requires a thorough understanding of source behaviour, wave propagation and attenuation effects as a

function of structural detail. Prior consideration of the implications of the relationships between structure thicknesses, frequency and source velocity, as described by dispersion curves is vital if the method is to be successfully applied.

2.5.2 2D SOURCE LOCATION

Two-dimensional source location can be applied to plane or curved surfaces. The simplest analysis assumes an infinite plane and the ideal condition is where the stress waves propagate from the source at constant velocity, *V*. If the source is at P_1, and two sensors are placed at S_1 and S_2 (Figure 2-12) the equation of a hyperbola can be written as:

$$R= (½) ((D^2- \Delta t^2 V^2)/ (\Delta t V +D \cos \theta)) \quad (2.16)$$

Where any point satisfies the input data, (the hit sequence and time difference measurement Δt). Equation 2.16 can be used for most cases of 2D source location on a plate, because any point on the hyperbola satisfies the input data, wave arrival sequence and arrival time difference.

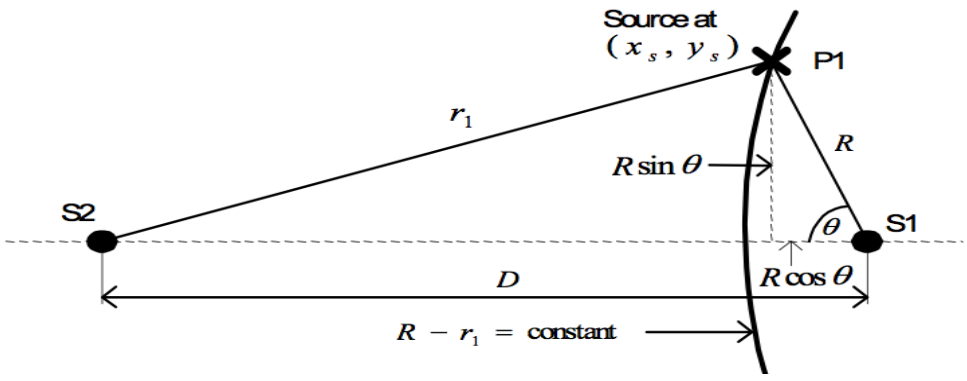

FIGURE 2-12: SOURCE LOCATION IN TWO DIMENSIONS

The energy technique can also be used to locate the source (for continuous emission) in two dimensions by rearranging the Equation 2.10 as [52]:

$$x_i - x_j = \frac{1}{k} \ln\left(\frac{E(x_i)}{E(x_j)}\right) \quad (2.17)$$

Where x_i and x_j are the distances from the ultrasonic source to i^{th} and j^{th} transducers, respectively; *E(x)* is the amplitude of a wave registered by a transducer at a distance *x* from the source; and *k* is the attenuation factor for waves in a given medium. Barat et al., [53] have derived an algorithm to locate an ultrasonic source at coordinates (R, θ, Z) on a cylindrical surface, using three sensors S_o, S_1 and S_2 located at positions $(R, 0, 0)$, (R, θ_1, Z_1) and (R, θ_2, Z_2). They expressed the shortest distance between source and sensor on the cylindrical surface as:

$$\delta_1 = ((R^2)(\theta_1-\theta)^2+(Z_1-Z)^2)^{½} - ((R^2)(\theta^2)+ Z^2)^{½} \quad (2.18)$$

$$\delta_2 = ((R^2)(\theta_1-\theta)^2+(Z_1-Z)^2)^{½} - ((R^2)(\theta^2)+ Z^2)^{½} \quad (2.19)$$

where R is the cylinder radius.

If the arrival times (Δt) between the sensors are determined experimentally, and, assuming the ultrasonic wave speed to be constant (V), the distances between sensors S_o, S_1 and S_2 are respectively:

$$\delta_1 = \Delta t_1 V \quad (2.20)$$

$$\delta_2 = \Delta t_2 V \quad (2.21)$$

Solving Equations 2.18 and 2.19, will aloe R and Z to be determined and hence the source to be located on the cylindrical surface.

2.5.3 LOCATION METHODS IN PRACTICAL SITUATIONS

In practical situations, the source is rarely a true step function, and is often distributed in time. Moreover, it is entirely possible that a number of sources will be operating each with its own temporal and magnitude characteristics. Finally, as pointed out by Pollock [35] it is unlikely that any of the 'pure' modes indicated by plate theory will be present although the propagating

wave can often be split into components that show characteristics of them. Nivesrangsan et al., [48] have approached the multi-source problem on the relatively complex structure of a diesel engine and have demonstrated that characteristic speeds and frequency bands can be used to enhance the quality of information about the relative times and locations of sources. Continuous sources are rather more difficult to locate, since they generally do not contain any reference events that can be used to determine relative arrival times at sensors. Thus, energy-based methods are most commonly used, each sensor being assigned a zone on the structure [97].

The highest output sensor in an array can be used to locate the source, and some improved resolution can be achieved by using the two highest output sensors, Figure 2-13. However, for many real situations it is impractical to deploy sufficient sensors to make zone location accurate. Better source location can be achieved by knowing the attenuation properties of the structure and using these to interpolate for source position between the two sensors with highest outputs using techniques similar to those described in the previous two sections.

If the continuous source has any temporal structure to it, it is possible to use cross- correlation to obtain a time difference, and hence use time and velocity to locate the source, as for burst type emission.

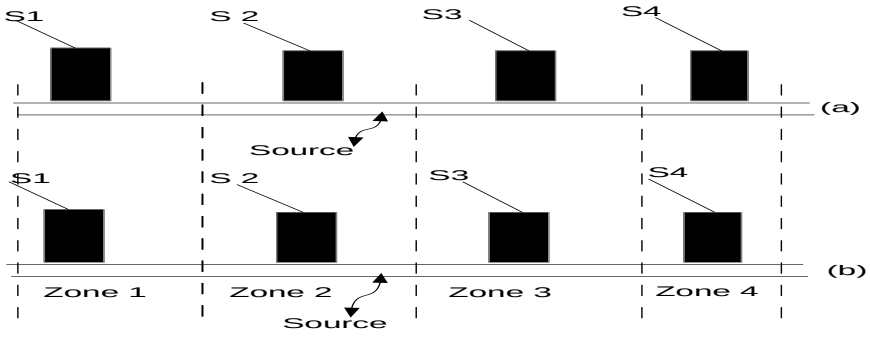

FIGURE 2-13: SCHEMATIC DIAGRAM OF ZONE LOCATION METHOD (ADAPTED FROM [97]) WHERE (A) OUTPUT OF SENSOR 2 IS THE HIGHEST, AND (B) OUTPUT OF SENSOR 2 IS HIGHEST AND SENSOR 3 IS SECOND HIGHEST

2.5.4 TRANSDUCTION

Generally, ultrasonic transducers involve a piezoelectric element, which is most often made from lead zirconate titanate [100]. Commercial transducers are available with different crystal shapes and sizes providing a range of frequency responses. Generally, narrow-band sensors have high sensitivity and broadband sensors lower sensitivity. The frequency response of the sensor/preamplifier combination depends on the electrical impedance of the sensor element, and calibration is important to match the amplitude and phase response of the sensor to the surface displacement over its frequency range [54].

As well as using an appropriate transducer correct mounting of the sensor on the test object is important [55], using suitable acoustic couplant (e.g. grease or water- based gel), is necessary to improve the reliability of ultrasonic detection. Wolfinger et al., [56], for example, working with fibre reinforced plastic structures, improved the efficiency of their monitoring system by using integrated transducers where the high- pass filter was built in. In addition, Grondel et al., [101] investigated Lamb wave modes carried in riveted aluminium plate by stimulating these with a piezoelectric transducer and using calculated dispersion curves to identify an appropriate frequency-thickness product on which to focus ultrasonic analysis. They pointed out that optimizing the dimension and frequency response of the piezoelectric elements was essential to achieve success in fatigue monitoring.

2.6 SIGNAL PROCESSING

Ultrasonic signals can be broadly categorized into burst, continuous and mixed. Burst signals take the form of discrete transients, as shown in the Figure 2.14a, an example being crack growth. The shape of a burst waveform is often approximated by an exponentially decaying sinusoid. Continuous emission has a random oscillatory appearance as shown in the Figure 2.14b, and essentially results from the overlapping of multiple burst type signals that are

indistinguishable separately and give a continuous appearance, and a typical example is process “noise” resulting, say, from fluid flow. In most practical situations, both burst and continuous signals are recorded.

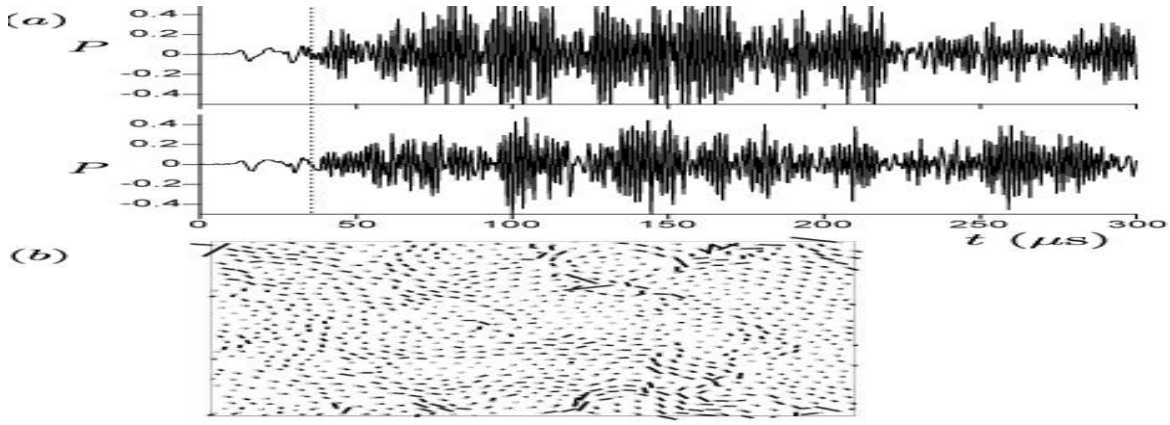

FIGURE 2-14: SCHEMATIC REPRESENTATION OF DIFFERENT ULTRASONIC SIGNAL TYPES [10] (A) IS BURST TYPE AND (B) IS CONTINUOUS TYPE

AE waves are ultrasonic signals that consist of one or more time series with frequencies in the range of 0.1 to 1 MHz and above. As such, the features of the signals can be found in the time and/or frequency domains. Although time domain analysis is widely used in ultrasonic applications and is conceptually simpler [57], frequency analysis can often give a better indication for the source type, and spectral decomposition can be used to distinguish different propagation modes [57, 58]. For example, in support of a patent application, Powell and Dimmick [67] have used a Fast Fourier Transform (FFT) of the detected signal to identify the type of faults in valves each fault having a specific spectral signature. Kwan and Leach [60] have presented a technique for determining the average diameter and average length of cylindrical glass particles using spectral peaks of the ultrasonic signals generated whilst the cylinders were undergoing a tumbling motion. On the other hand, Spall et al., [61] have discussed the difficulties in identifying signals acquired by transducers distant from the source where wave components travel a different speed, and wave-guiding properties in complex structures may distort the signal due to the media being dispersive, reflections, and multiple

paths to the sensors. To avoid distortion of the signal from pencil lead breaks on a cutting tool, Jemielniak [62] modified a Bruel & Kjær preamplifier type 2637 to lower the gain by a factor of 10 (20 dB), and pointed out that the ultrasonic signal should be filtered at the earliest possible stage of processing, just after the initial necessary buffering.

Mathematical transforms are widely applied to raw signals to obtain important information that is not readily available from their time evolutions. The most common tool utilized in signal processing is the Fourier Transform, used to decompose a signal into its frequency components [63]. The Fast Fourier Transform (FFT) is a specific algorithm that converts numerically discrete time domain data into the frequency domain, with very low computation time and avoidance of the round-off errors associated with this computation [64]. Power Spectral Density (PSD) estimation is another tool, using the FFT to indicate how the signal energy is distributed in the frequency domain [63]. The Welch method is an improved PSD estimator [65] and it is implemented in the MATLAB software used in this work. In order to reduce the variance of the PSD estimate, the Welch method calculates PSD by dividing the time series data into segments (possibly overlapping), and, using by the FFT, can calculate each segment of a modified period gram and then average these period grams.

The FFT and PSD require a signal to be stationary, i.e. for the frequency spectrum to be constant in time [66]. For non-stationary signals, a number of time-frequency analysis techniques are readily available such as the Short Time Fourier Transform (STFT) and Wavelet Transform (WT). The STFT is a simple technique that describes the energy distribution of the signal as a time-varying spectrum. The STFT can provide a constant resolution for all frequencies by using same window size for the analysis of the raw signal; accordingly there is a trade-off between time resolution and frequency resolution (Figure 2.15 a).

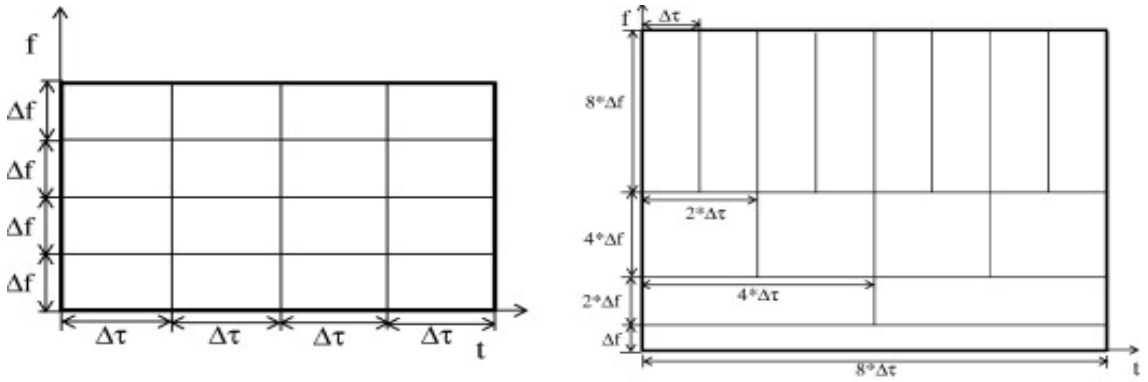

(A) (B)

FIGURE 2-15: RESOLUTION IN (A) THE STFT AND (B) THE WT

The WT also analyses the signal using multi-scaling where the resolution of time and frequency varies in the time-frequency plane (Figure 2.15 b), longer time intervals giving more precise low frequency information and shorter time intervals giving high frequency information, thus improving the overall presentation of the time-frequency characteristics.

The main advantage of the WT over the conventional FFT is that the time domain included in the raw signal is conserved [67, 68]. The WT is implemented in the MATLAB software and it is used in this work to decompose the ultrasonic signal into different levels at different frequencies, each level containing some of information of the original signal, with the ultrasonic sub-signals being in the time domain [79].

The wavelet transform essentially breaks down a signal into components (wavelets), which vary in scale (stretched or compressed) and in location (shifted) [32, 67, 70]. However, some authors have described wavelet decomposition as splitting the signal into an “approximate”, low frequency component and a “detail” (Di), high frequency component [71, 72], as shown in Figure 2.16. The wavelet tree method is a generalization of wavelet decomposition that offers a wide range of possibilities for signal analysis [73].

In general, the wavelet transform (WT) is used to decompose any signal into frequency bands producing a high-resolution time and frequency information about the signal by using a variable sized window. The WT is a function of f (t) at time t [70]:

$$WT_f\ (a,b) = \frac{1}{\sqrt{a}} \int_{-\infty}^{\infty} f(t)\Psi^* \left(\frac{t-b}{a}\right) dt \qquad (2.22)$$

Where a > 0, the superscript * denotes a complex conjugate and *t* is time. The analysis function for the WT can be defined as the" mother wavelet":

$$\Psi_{(a,\,b)}(t) = 1/\sqrt{a}\ \Psi((t-b)/a) \qquad (2.23)$$

Its elements are generated by shifting and scaling a basic wavelet Ψ (t). The parameters *a* and *b* stand for the scale and shift of the basic wavelet. Many authors have suggested that the location of a peak value on the (*a*, *b*) plane indicates the arrival time of a signal [32, 67, 70].

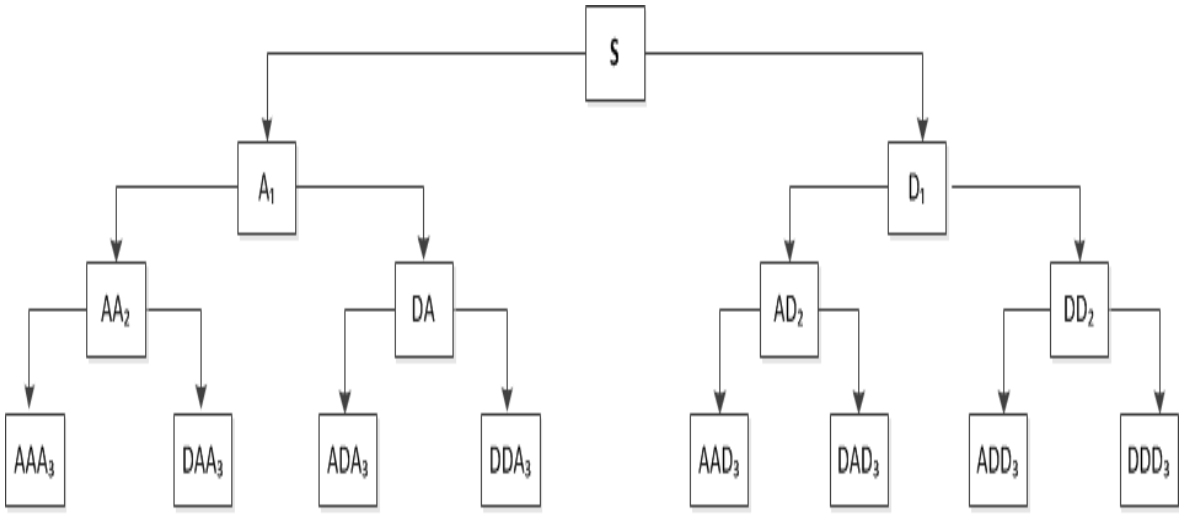

FIGURE 2-16: WAVELET ANALYSIS TREE

Ultrasonic signals normally contain some noise, such as from the environment, which must be removed to aid signal analysis. Time-frequency analysis can be used to describe the ultrasonic signal components and hence remove noise. For example, Ng and Qi [69] have presented a wavelet-based ultrasonic energy technique, in which they use the ratio of reconstructed energy

to sum the original signal energy to identify the insignificant components in the ultrasonic signal without affecting the integrity of the original signal.

Using this approach, they were able to correlate the wavelet-bas*ed* ultrasonic energy with fatigue parameters. Also, Kishimoto et al., [74] and Jeong et al., [43] have suggested that the wavelet transform with the Gabor wavelet is an effective tool for analysing wave propagation phenomena in structures. The dispersion behaviour of the group velocity can be accurately evaluated by the information extracted using the WT.

Generally, the WT is an effective way to analyse ultrasonic signals and both frequency and time information can be obtained. For example, Qi [75] has noted that the failure modes for composite materials can be quantified and that each failure mode frequency band has a different bandwidth.

2.6.1 ULTRASONIC SIGNAL ENERGY

As well as the time and frequency changes as a signal propagates from source to sensor, it is important to note changes in energy, and this can be particularly important for continuous signals where there is no other easy way of locating sources. Generally, the amount of energy emitted from a fault is often used as an indicator of fault severity [102]. The energy associated with an ultrasonic signal over a time, *t*, can be determined as follows:

$$E_{\circ} = \int_0^t v^2\,(t)\;dt \tag{2.24}$$

Where *v (t)* is the amplitude of the ultrasonic waveform in volts, *t* is time in seconds, and the ultrasonic energy is given in V^2. s.

It is also possible to use a wide range of time-based parameters to characterise the ultrasonic signal. For burst signals, the amplitude usually rises rapidly to a maximum value and then

decays nearly exponentially to the background noise level where each parameter is described briefly below:

- Ultrasonic energy is the measurement of the relative energy of an ultrasonic signal, which is calculated from the area under the envelope of the square of the signal.

- Ultrasonic count or ring down count is the number of times the burst signal amplitude exceeds the pre-set threshold.

- Ultrasonic event rate is the time rate at which ultrasonic event counts occur.

- RMS of the ultrasonic signal is the root mean square of voltage, which is generally an indicator of average ultrasonic energy over each averaging time.

- Rise time is the time interval between the first threshold crossing and the maximum amplitude of the burst signal.

- Decay time is the time interval between the maximum amplitude and the last time that the burst signal exceeds the pre-set threshold.

- Signal duration is the time interval between the first and the last threshold crossing of the burst signal.

These parameters were mostly used in early ultrasonic studies of material properties, material deformation and crack propagation, although some variants are used later in this work. Harris and Bell [103], besides indicating that the ultrasonic energy can be related to other conventional parameters (such as counts and RMS voltage), found energy to be a useful indicator of some degradative phenomena in metals, particularly where signal levels were low. In addition, Yoon et al., [76] and Radon and Pollock [77] have correlated ultrasonic

energy with energy-based descriptions of various physical phenomena, such as crack extension and dropped weights.

2.6.2 WAVE ARRIVAL TIME ESTIMATION

In large specimen structure, most ultrasonic waves propagate in more than one mode travelling at different speeds so, for pipe applications, it is important to determine arrival times for the different components of the wave. Ultrasonic event source location is based on the arrival times of transient signals measured at a number of transducers. If the propagation velocity is known, the difference in arrival times for an event at sensors a known distance apart can be used to locate the source.

A number of techniques such as cross-correlation, threshold crossing and wavelet transforms have been used [43, 67, 70, 78, and 79] for automatic source location. The error in source location will include any errors in measured arrival time differences. As stated above in the case of large structures in different environments, attenuation, reflection, refraction, mode conversion and interference can all distort the shape of the propagating wave. Also, for some waves, media dispersion effects can cause time of arrival to be triggered at different phase points of the signal.

The most common method for estimating the arrival time is where the arrival time is taken to be the instant when the raw signal amplitude first crosses a pre-set threshold. Many authors such as Steven et al., [78], Ziola and Gorman [80] and Hamstad et al., [32] have discussed the difficulties of using the first threshold crossing to define the source location, for example, where the threshold needs to be set above the noise level that means the signal will not be distinguishable at very long distances.

To increase the location accuracy of the threshold method some authors, e.g. [81], have recommended that the large amplitude, high frequency, dispersive components should be filtered out of the raw signal and sufficient gain used to amplify the lower frequency non-dispersive components.

This obviously depends upon identification of dispersive and non-dispersive components, which is not always easy to do on a new structure, although Gorman [33] has also suggested using non-dispersive components with a threshold for accurate source location. Gorman [33] has used the threshold method to locate sources on a 0.23 cm thick, 23 cm wide, and 46 cm long aluminium plate. He suggested that the flexural component should be filtered from the signal and only the extensional wave be used for most accurate location. Floating thresholds have been suggested by Coulter et al., [79] who have located continuous emission from a fluid leak by allowing the threshold to float with the ultrasonic signal and were thus able to discriminate between the continuous noise and the ultrasonic signal spikes. The arrival time difference between these spikes could then be used to locate the leak.

Cross-correlation is a conventional time-based technique for measuring differences of arrival time between two or more sensors. The cross-correlation function is given by:

$$R_{y_1,y_2}(t) = \sum_{t=1}^{T} y_1(t) y_2(t+\tau) \tag{2.25}$$

Where the variable τ corresponds to the time difference between the signals, y_1 *(t)* and y_2*(t).* The most likely time delay between two complex time series is determined by the position of the highest peak in the cross-correlation function, and the peakedness of this function will indicate how much distortion there is between the two time series. Cross-correlation techniques can be used to estimate the arrival time difference between two signals automatically, and are most effective when used with non-dispersive waves and when the wave propagates from source to sensor without reflection [82]. Wang and Chu [73] working

with an experimental rotor-bearing rig with a complicated dynamic structure (i.e. friction, impacting and coupling effects) found their cross-correlation results to be considerably enhanced when combined with wavelet decomposition.

Wavelet transform methods are also used to locate sources, for example by Inoue et al., [83], who produced flexural waves in a simply supported beam by dropping a steel ball onto the beam mid-span. They then showed that a three-dimensional plot of the magnitude of the WT in time-frequency space has peaks whose locations indicate the arrival times of each component of the wave.

Jioa et al., [70] have also used a WT method to locate sources in a thin steel plate of dimensions 700 mm × 700 mm, 2.76 mm thick, using a single sensor. They used arrival time difference between the "a" and "b" modes (determined using the peaks in the Gabor wavelet transform) to locate sources with claimed errors of less than 5%. Hamstad et al., [32], uniquely, have worked with numerically simulated waves, and have noted that the wavelet transform (WT) coefficients (usually local maxima at a frequency, group velocity pair) can be combined to form a $a_\circ/a$ magnitude ratio, where the $a_\circ$ (flexural) mode is of higher group velocity and lower frequency than the s_o (extensional) mode.

This ratio was found to distinguish different source types (in their simulated data), when the sources were all located at the same propagation distance. Combinations of the above-mentioned techniques (i.e. a novel technique) can improve the arrival time estimation. For example, Ding et al., [67], working with composite plates, have noted that wavelet packet decomposition associated with threshold crossing is more effective than cross-correlation for the arrival times of the dispersive, and the highly damped signals involved**.** They also found a method using maxima in the Gabor wavelet transform to be effective in determining wave speed.

2.7 ULTRASONIC FAULT DIAGNOSIS AND MONITORING

This section will cover monitoring applications for fracture, fatigue, impacts, plastic deformation and general process monitoring. Specific pipeline applications will be dealt with in the following section.

Many researchers [48, 84-86] have proposed ultrasonic methods as an effective monitoring technique that can be applied in three ways to technological problems; testing and surveillance of structures [87], monitoring and control of machines and processes [88], and material characterisation [89].

It has been estimated that savings in loss of production and human cost brought about by modern condition monitoring techniques can amount to as much as 400 times the cost of the equipment [104] as on top of labour and operators training wages, the arrangement to be carry out to access the location of inspection will suspend the operation or might cause damage.

Under static loading, ultrasonic can be generated by plastic deformation or fracture, or, more commonly, a combination of both. Singh et al., [90] have worked with steel plates in tension with various types of stress concentration (e.g. circular holes) and have found that ultrasonic event rates are higher between yield , Ultimate Tensile Strength (UTS) and those specimens containing stress concentrators started emitting earlier than those without.

Baudouin and Houbeart [91], as part of a study on the effect of plastic deformation on the magnetic properties of electrical steels, carried out some uniaxial tensile tests while monitoring the ultrasonic signals generated. They found ultrasonic emission to be concentrated in three bursts of activity: just before and just after yield; in the advanced stages of work hardening approaching the UTS; and after reaching the UTS, prior to rupture. They attribute all these burst of activity to intense plastic deformation because the steels in question

had a marked yield point, which is normally associated with the initiation of large avalanches of dislocations in solute atmospheres. Hao et al., [92] have used ultrasonic methods to monitor plastic deformation during a deep drawing process, with prior calibration using uniaxial tensile tests.

They developed a model for the ultrasonic energy released, as measured by the RMS value of the ultrasonic signal that predicted it was directly proportional to the product of strain and strain rate, which is similar to an approach used by Carolan et al., [93] who modelled the ultrasonic energy associated with metal cutting. Dunegan et al., [94], have suggested, on the basis of static and dynamic crack extension experiments, that the ultrasonic signals generated are associated with dislocation motion (plastic deformation) in the plastic zone ahead of a crack tip and are credited with the relationship that the total number, N, of ultrasonic counts is proportional to the fourth power of the stress intensity factor.

Later, Palmer and Heald [95], carried out some basic studies on the application of ultrasonic analysis to fracture mechanics of carbon-manganese steels, and agree that crack-tip plasticity is an important generating mechanism, and noted that the total emission count is directly related to plastic zone size which they characterise in terms of the Dugdale strip yielding model, i.e.:

$$N \propto \left[\sec\left(\frac{\pi\sigma}{2\sigma_1}\right) - 1\right] \tag{2.26}$$

Where σ is the applied stress and σ_1 is some characteristic stress, usually the flow stresses. Mukhopadhyay et al., [44], working with notched specimens of stainless steel, have found the power law dependence of the Dunegan crack extension model to vary with specimen thickness (essentially the length of the crack front) thus supporting the Palmer and Heald suggestion to link AE emission with size of the plastic zone and hence plastic yielding

fracture mechanics which was not well developed at the time of the original work of Dunegan et al. On the other hand, some early workers such as Radon and Pollock [77] considered linear elastic fracture mechanics to be adequate to explain the energy associated with ultrasonic during fracture and for brittle fractures related the AE energy to strain energy release rate.

Substantial literature exists on the use of ultrasonic for detection of fatigue crack propagation, beginning with the pioneering work of Dunegan, Harris and co-workers [46] who reported sensitivity to crack growth rates of less than 2.5×10^{-5} mm / cycle. They related ultrasonic counts per cycle to the energy released by crack extension, as measured by the peak value of stress intensity factor and crack growth increment. They noted that the nature of the relationship changed as the crack size increased and went through the plane-stress/plane-strain transition.

Later workers, such as Roberts and Talebzadeh [27, 45], Brkovits and Fang [39] and Jiang et al., [29] have confirmed these findings. Shi et al., [94], have carried out more detailed studies of the nature of the AE associated with fatigue crack extension, and have identified three different classes of waveform (Figure 2.17) associated with small sub-grain sized cracks at initiation, micro-cracking across grain boundaries and the coalescence of micro-cracks into larger, but still localised, cracks.

Larger cracking rates and greater degrees of crack plasticity have been considered by Lindley et al., [98], Bassim and Emam [99] and Hartbower et al., [105], the general consensus about the relative importance of fracture and plastic deformation at the crack tip being similar to that found for static fracture above, where consideration of the degree of crack tip plasticity becomes increasingly important as the plastic zone size increases, for example in low-cycle fatigue or with relatively ductile materials.

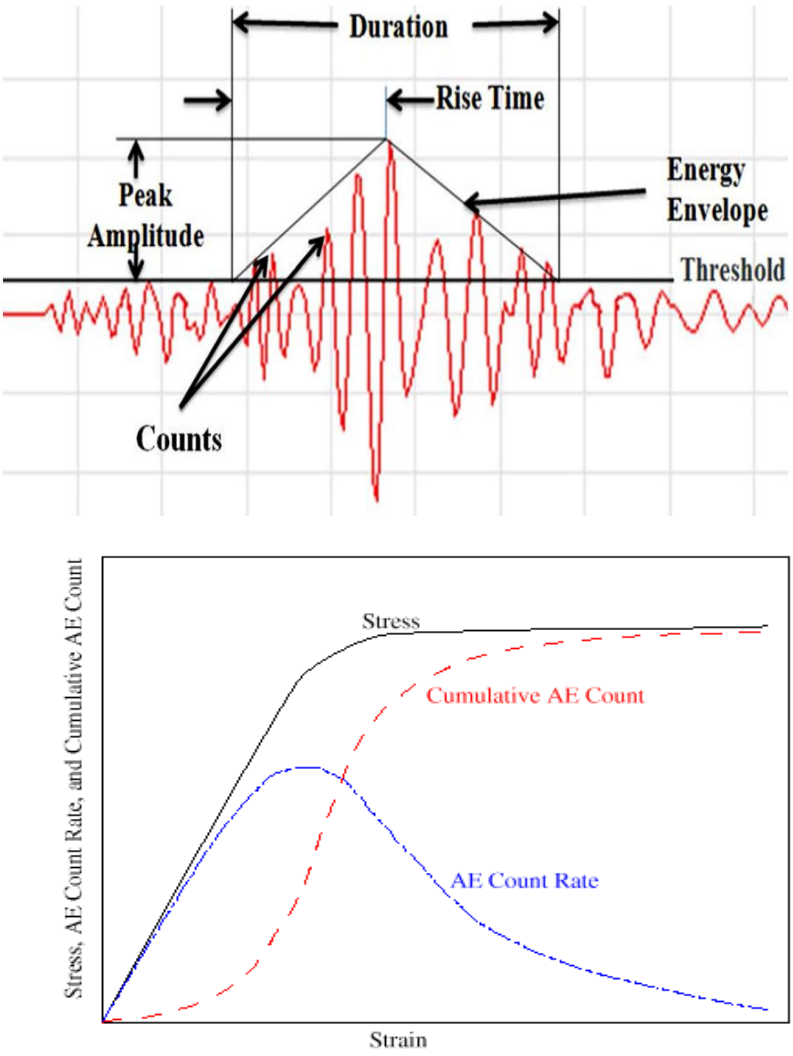

FIGURE 2-17: CUMULATIVE AE COUNTS FATIGUE CYCLES [143].

Impact is a significant potential source of damage in many operating systems, and identifying the type and location of damage is important for reliability and safety of structures and processes [117]. Prosser et al., [107] have studied the AE generated by impact worked on aluminium and graphite/epoxy composites plate using two different types of projectile; a low velocity (0.21 kms^{-1})) impact from a steel projectile fired from an air-gun, and a higher velocity one (1.8 to 7 kms^{-1}) from a nylon projectile fired using a gas gun. They suggested that quantitative information for assessment, including source location and differentiation between penetrating and non-penetrating impact events, could be obtained but that much more work was required on the effect of projectile type (size and material), projectile velocity,

propagation distance and structural shape, before a fully functioning impact monitoring system for aircraft and spacecraft was possible. Working with a suspended steel plate and a pendulum impact, Gaul and Hurlebaus [108] have been able to identify impact location by using the maximum of the wavelet magnitude to calculate arrival times and hence were able to locate the source of the impact. Their method is mostly concerned with source location and no details were given of the nature of the impact events.

Aside from the specific pipeline applications considered in the next section, a large number of different types of industrial process have been subjected to ultrasonic monitoring, metal forming [19] and metal cutting [93] in addition to those mentioned above. For example, Tonshoff et al., [109] have used ultrasonic monitoring to determining work piece quality in hard turning and grinding operations applied to hardened steels. In particular, they have been able to relate sub-surface quality, which influences component life, to RMS ultrasonic energy generated during the process and to residual stress, presumably brought about by a martensitic transformation-taking place in the surface layers. Finally, Boyd and Varley [88] have commented on the very wide potential applications of ultrasonic in chemical engineering, and have included monitoring of gas-liquid, solids and solids-fluid dispersions, monitoring of chemical reactions and the monitoring of equipment as potential areas for development.

2.7.1 PIPE AND PIPELINE SYSTEM CONDITION MONITORING

Pipeline condition monitoring is used both to monitor the condition of the pipeline (structural integrity monitoring) and the condition of the process itself (process monitoring). Hence, a monitoring system must be able to recognise structural defects (such as cracks or leaks) and process defects (such as undesirable fluid characteristics, for example erosion or cavitation). When material characteristics are known, ultrasonic assessment can be used as the basis for continuous plant monitoring, increasing structural safety and reducing shutdown costs for

inspection. For example, Wood and Harris [114], based on 20-year data on large cryogenic storage vessels, have suggested that remnant life can be predicted and structural integrity classified. In addition, Hou et al., [110] have carried out an experimental study of online ultrasonic monitoring of flow and related process parameters for small diameter pipelines conveying dense slurries of fine silica particles, at varying solids concentration, mass flow and volume flow rates. The results showed that ultrasonic signals can be used to characterise slurry flow and that a characteristic frequency in the power density spectrum of the signal was a manifestation of the speed of the positive displacement pump.

Leaks in pipes and vessels can be detected in two general ways, either by detecting the substance that escapes, for example by aircraft or satellite surveillance, or by detecting certain leak-related properties such as pressure drops, acoustic emission, volume balance changes and temperature changes.

Conventional continuous monitoring is based on the physical effects that can be measured directly or by calculation from a mathematical model of the pipeline [86, 111]. For example, a nonlinear model to locate multiple leaks in pipelines has been presented by Verd [115], which discretises a spatial variable, such as pressure, into three non-uniform sections of unknown sizes. Generally, leak detection is perhaps the most successful practical application of ultrasonic to pipelines [19]. For example, Savic [116] has built a leak simulator consisting of an actual 40 mile long pipeline of internal diameter 6 inches and 1 inch wall thickness. The pipeline was built for ethylene gas with an internal pressure of 1500 psi and was buried in wet soil. In the simulation, the line was filled with nitrogen gas to its working pressure and valves opened to allow a controlled leak to be simulated at selected points along the line. The leaks consisted of round holes and both wide and narrow slits and both the size and shape of the leak were found to influence the “acoustic signals”. There are many factors (such as environment) to considered when using an ultrasonic signal to locate a source, see Rajtar and

Muthiah [27], who have studied the capacity of ultrasonics to locate a leak position in low pressure, low flow rate, oil and gas production flow lines using ultrasonic signal attenuation. They noted that the acoustic emission signal is sensitive to the external and internal environment of the pipeline, i.e. supports, soil properties and fluid viscosity, and the results showed that, at a pressure of 0.68 MPa with sensors placed at 61 m and 122 m, the ultrasonic signals resulting from a very small simulated leak (of the order of 0.01% of the pipeline flow rate) could be detected.

Generally, they provided suggestions on determining how many sensing points will be necessary to monitor the operation of a given length of a pipeline, the practical spacing being a compromise between leak sensitivity and the cost of the detection system. However, ultrasonic waves can be used not only to locate a leak in long pipes, but also can characterise the shape of the holes through which the leak is taking place, see Yoshida et al., [112] who have studied the ultrasonic characteristics of pinholes and slits in a 20 mm diameter pipe using a range of backing pressures. They found a variety of interesting characteristics in the frequency domain that could be used to determine the size and shape of the breaches in the pipe wall.

2.8 SUMMARY OF LITERATURE REVIEW

In this chapter, three main aspects of the state of knowledge of ultrasonic technology have been reviewed; ultrasonic propagation, signal processing and ultrasonic applications. This research project will focus on pipelines and pipework, on which there has been limited study outside the principal application of leak detection. This work will investigate what information can be deduced about a source within a pipe using small sensors (Transmitting/ Receiving) situated axially along the pipe.

To do this, it is recognised that some contribution to knowledge will be required in the area of propagation and source recognition and in signal processing, although the latter will be the combining of established processing methods rather than developing a very new technique. In propagation, there is a need for greater clarification of the main "modes" by which ultrasonic energy is carried along pipes and the effects that the internal and external environments have on signal generation and transmission.

Regarding source recognition, it is expected that a contribution to knowledge will be made during the investigation and analysis of how signals are distorted as they travel from source to sensor, and in defining the ultrasonic characteristics of non-leak sources.

CHAPTER III

FINITE ELEMENT MODELLING AND SIMULATION

This chapter presents the mathematical simulation, using the ABAQUS modelling software, of ultrasonic wave propagation in steel pipes with some commonly found pipe defects; small holes in the pipe of 1 mm diameter and varying depths from the outside towards the inside – 25%, 50%, 75% and 100% (wholly through) of the pipe diameter.

3.1 INTRODUCTION

Traditional design and condition monitoring of piping is based primarily on propose events and permissible vibration levels; these approaches only provide indirect information on the loading at critical locations and generally lead to underestimated assessments [118]. A mathematical model is based on collected data; these models can be more or less reliable but in general, their verification can only be carried out when the model quality is tested by reality. Thus, it is important to be able to predict and/or monitor developing pipe failures so that any maintenance work that is required can be anticipated and conducted during normal outages.

More appropriate direct measurement techniques, which can provide information about the actual loading state and condition of the piping, are very limited. Many actual structural situations can be somewhat difficult to model since they may deviate significantly from what the design documents indicate. Therefore, an iterative process is frequently needed to obtain sufficient agreement between computational and experimental results. This may be attained using special purpose tools designed to update finite element analysis models with experimental data.

3.2 DYNAMIC MODELS AND ANALOGIES

Any system may be described as a set of interacting elements or components, each of which has an input and output (e.g. cause and effect). With dynamic system the variables representing the system response are functions of time, with significant rates of change, and here we define vibrating systems as dynamic systems.

A model is a representation of a system, and an analytical (or mathematical) model is a set of equations that approximates the behaviour of the system; often the set of equation may take

the form of stored numerical data in the form of tables or sets of curves. Experimental models are developed by exciting a system in a controlled manner and measuring the resulting response.

Models may, generally, be grouped into the following;

- Physical models (prototype),
- Analytical models,
- Computer (numerical) models, and
- Experimental models (using input/output experimental data).

The main use of analytic models is to predict the response of a system when it is subjected to a given excitation. To obtain, understand and control the practical vibration response of a system requires a good understanding of its dynamic behaviour as can be obtained by developing a suitable model for the system. One use of such a model is the design a mechanical system for control of the vibration performance, in fact dynamic models of vibrating systems are widely used to develop necessary control devices and systems. When a product is "qualified" by analysis, a test specimen is replaced by a suitable analytical model.

3.3 FINITE ELEMENT MODELLING

In continuum mechanics a solid body is described by a continuous mathematical model whose geometrical points are identified with the place of the material elements of the body. When such a continuous body changes its configuration under some physical action, we impose the assumption that the change is continuous. Any introduction of new boundary surfaces, such as caused by tearing of a membrane or fracture of a test specimen, is regarded as an extraordinary circumstance requiring special attention and explanation [23].

3.4 THE STRUCTURAL ELEMENT AND THE STRUCTURAL SYSTEM

To introduce the general concept of discrete systems we shall first consider a structural engineering example with linear elastic behaviour. Figure 3-18 represents a two-dimensional structure assembled from four individual components and interconnected at the nodes numbered 1 to 6. The joints at the nodes, in this case, are pinned so that moments cannot be transmitted. As a starting point it will be assumed that by separate calculation, or for that matter from the results of an experiment, the characteristics of each element are precisely known. Thus, if a typical element labelled (1) and associated with nodes 1, 2, 3 is examined, the forces acting at the nodes are uniquely defined by the displacements of these nodes, the distributed loading (p) acting on the element, and its initial strain. The last may be due to temperature, shrinkage, or simply an initial 'lack of fit'. The forces and the corresponding displacements are defined by appropriate components (U, V and u, v) in a common coordinate system (x, y).

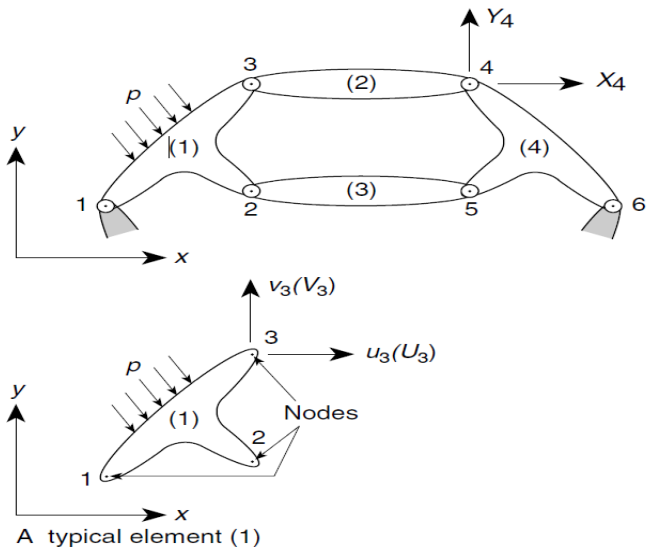

FIGURE 3-18: A TYPICAL STRUCTURE BUILT UP FROM INTERCONNECTED ELEMENTS.

Listing the forces acting on all the nodes (three in the case illustrated) of the element (1) as a matrix† we have

$$q^1 = \begin{Bmatrix} q_1^1 \\ q_2^1 \\ q_3^1 \end{Bmatrix} \qquad q_1^1 = \begin{Bmatrix} U_1 \\ V_1 \end{Bmatrix}, \qquad \text{etc.} \tag{3.1}$$

$$U^1 = \begin{Bmatrix} u_1^1 \\ u_2^1 \\ u_3^1 \end{Bmatrix} \qquad u_1^1 = \begin{Bmatrix} u_1 \\ v_1 \end{Bmatrix}, \qquad \text{etc.} \tag{3.2}$$

Assuming linear elastic behaviour of the element, the characteristic relationship will always be of the form

$$q^1 = k^1 u^1 + f^1 \tag{3.3}$$

Where f^1 represents the nodal forces required balancing any concentrated or distributed loads acting on the element. The first of the terms represents the forces induced by displacement of the nodes.

The matrix K^e is known as the *stiffness matrix* for the element. Equation (3.3) is an example of an element with three nodes with the interconnection points capable of transmitting only two components of force. Clearly, the same arguments and definitions will apply generally. An element (2) of the hypothetical structure will possess only two points of interconnection; others may have quite a large number of such points. Generally, therefore,

$$q^e = \begin{Bmatrix} q_1^e \\ q_2^e \\ . \\ . \\ . \\ q_m^e \end{Bmatrix} \quad \text{and } u^e = \begin{Bmatrix} u_1 \\ u_2 \\ . \\ . \\ . \\ u_m \end{Bmatrix} \tag{3.4}$$

Where each q_a^e and u_a possess the same number of components or *degrees of freedom*. The stiffness matrices of the element will clearly always be square and of the form:

$$\begin{bmatrix} K_{11}^e & K_{12}^e & \cdots & K_{1m}^e \\ \vdots & & \ddots & \vdots \\ K_{m1}^e & \cdots & \cdots & K_{mm}^e \end{bmatrix} \tag{3.5}$$

Where k_{11}^e, etc., are sub-matrices which are again square and of size $l \times l$, where l is the number of forces and displacement components to be considered at each node. The element properties were assumed to follow a simple linear relationship. In principle, similar relationships could be established for non-linear materials, but discussion of such problems will be postponed at this stage. In most cases considered in this thesis the element, matrices k^e will be symmetric.

3.5 ASSEMBLIES AND ANALYSIS OF A STRUCTURE

Consider again the hypothetical structure of Figure 3-19. To obtain a complete solution the two conditions of (i) displacement compatibility and (ii) equilibrium have to be satisfied throughout.

For any system of nodal displacements u:

$$U = \begin{Bmatrix} u_1 \\ \vdots \\ u_n \end{Bmatrix} \tag{3.6}$$

The equation listed in Equation (3.6) for the whole structure containing all the elements automatically satisfies the first condition. As the conditions of overall equilibrium have already been satisfied within an element all that is necessary is to establish equilibrium conditions at the nodes (or assembly points) of the structure. The resulting equations will contain the displacements as unknowns, and once these have been solved the structural problem will be determined. The internal forces in the elements (stresses) can easily found by using the characteristics established a priori for each element. If the equilibrium conditions of

a typical node (a) are to be established, the sum of the component forces contributed by the elements meeting at the node are simply added and we have:

$$\sum_{e=1}^{m} q_a^e = q_a^1 + q_a^2 + \ldots = 0 \tag{3.6}$$

Where q_a^1 is the force contributed to node *a* by element 1, and q_a^2 by element 2, etc, clearly, only the elements which include point *a* will contribute, but for completeness of notation all the elements have been included in the summation. Substituting the forces contributing to node *a* from the definition (1.3) and noting that nodal variables u_a are common (thus omitting the superscript *e*), we have:

$$\left(\sum_{e=1}^{m} k_{a1}^e\right) u_1 + \left(\sum_{e=1}^{m} k_{a2}^e\right) u_2 + \cdots + \sum_{e=1}^{m} f_i^e = 0 \tag{3.7}$$

The summation again only concerns the elements which contribute to node *a*. If all such equations are assembled, we have:

$$Ku + f = 0 \tag{3.8}$$

In which the sub matrices are

$$k_{ab} = \sum_{e=1}^{m} k_{ab}^e \quad \text{and} \quad f_a = \sum_{e=1}^{m} f_a^e \tag{3.9}$$

With the summations including all elements, this simple rule for assembly is very convenient because as soon as a coefficient for a particular element is found it can be put immediately into the appropriate ‘location’ specified in the computer. This general assembly process can be found to be the common and fundamental feature of all finite element calculations. If different types of structural elements are used and are to be coupled, it must be remembered that at any given node the rules of matrix summation permit this to be done only if these are of identical size. The individual sub-matrices to be added have therefore to be built up of the same number of individual components of force or displacement.

3.6 THE BOUNDARY CONDITION

The system of equations resulting from Equation (3.9) can be solved once the prescribed support displacements have been substituted. In the example of Figure 3-19, where both components of displacement of nodes 1 and 6 are zero, this will mean the substitution of:

$$u_1 = u_6 = \begin{Bmatrix} 0 \\ 0 \end{Bmatrix} \tag{3.10}$$

This is equivalent to reducing the number of equilibrium equations (in this instance 12) by deleting the first and last pairs and thus reducing the total number of unknown displacement components to eight. It is, nevertheless, often convenient to assemble the equation according to Equation (3.9) to include all the nodes.

Because the forces in such a situation cannot uniquely determine the displacements, it is necessary to substitute of a minimum number of prescribed displacements to solve this system. This physically obvious fact will be interpreted mathematically as the matrix K being singular, i.e., not possessing an inverse. The prescription of appropriate displacements after the assembly stage will permit a unique solution to be obtained by deleting appropriate rows and columns of the various matrices. If all the equations of a system are assembled, their form is:

$$K_{11}\, u_1 + k_{12} u_2 + \cdots + f_1 = 0$$

$$K_{21}\, u_1 + k_{22} u_2 + \cdots + f_2 = 0 \quad \text{etc.} \tag{3.11}$$

It will be noted that if any displacement, such as $u_1 = \overline{u_1}$, is prescribed then the total 'force' f_1 cannot be simultaneously specified and remains unknown. The first equation could then be deleted and substitution of known values $\overline{u_1}$ made in the remaining equations. When all the

boundary conditions are inserted, the equations of the system can be solved for the unknown nodal displacements and the internal forces in each element obtained.

3.7 SURFACES

Surfaces could be used to model the connection of two or more notable in mechanical, acoustic or coupled acoustic-structural sections. A rigid surface much stiffer than the others in the model might be introduced into a mechanical or coupled thermal-mechanical system with the limit that no heat will be generated in the unbending form, In acoustic-structural investigations, surfaces could be introduced to define impedance limit conditions, incorporating first-request conditions for displaying acoustic radiation.

Surfaces could be utilized to demarcate a surface on which a dispersed load is recommended; this can help client data of circulated surface stacks for complex models. In addition, surfaces can be used to describe multi-focus or coupling imperatives, moreover, surfaces can outline demand areas used as a component recommended for gathering loads as in ABAQUS/Standard.

The following types of surfaces might be delineated in ABAQUS:

1-Element-built surfaces are demarcated with respect to the edges, or finishes of components. The components might be deformable or rigid, applied forces accelerate a surface whether it is deformable or rigid, however if any part of the deformable components lie on or are part of a rigid surface, the surface as a whole will be incompletely deformable and incompletely inflexible. In ABAQUS/Explicit, a default component-based surface that incorporates all forms in the model is used with the general contact ordered system.

2- Node-built surfaces demarcated with respect to junctions and, henceforth, are by definition broken. It is possible to connect a specified region with every junction on the surface.

3- Analytical surfaces are described in geometric terms and are usually rigid.

4- Eulerian material surfaces, where relevant, are described in an Eulerian segment.

These surfaces are already in ABAQUS/Explicit for general use. Coupled structural-acoustic and uncoupled acoustic investigation methods in ABAQUS/Standard ordinarily utilize symmetric lattice spaces and results. Special cases are the subspace-based consistent-state elements or complex recurrence methods utilized for coupled structural-acoustic simulations, where unsymmetrical grids are a result of the coupling system utilized as a part of these cases. Using acoustic endless components or the acoustic rush velocity choice triggers an unsymmetrical grid space and results plot in ABAQUS/Standard, with the exception of characteristic recurrence extraction using the Lanczos-Eigen solver, which utilizes symmetric grid operations.

3.8 SPECIFYING A FREQUENCY RANGE FOR THE ACOUSTIC MODES

Because structural-acoustic coupling is disregarded throughout the automatic multi-level sub structuring (AMS Eigen) examination, the registered resonances will usually be higher than those obtained for the completely coupled framework. This is due to ignoring the mass of the liquid in the structural stage and vice versa. For the normal metal in air case, the structural resonances may be comparatively unaffected; but some acoustic modes that are very important to the coupled reaction may be overlooked because of the air's upward recurrence move throughout Eigen investigation. Thus, ABAQUS permits the user to select a multiplier, to allow for the fact that most extreme acoustic recurrence in the investigation is taken to be higher than the greatest structural.

3.9 DISPLACEMENT NORMALIZATION

Assuming that dislodging standardization is chosen, the eigenvectors are standardized so the greatest dislodging passage in every vector is unity. Depending on if the relocations are insignificant, as in a tensional mode, the eigenvectors are standardized for the purpose that the greatest pivot section in every vector is unity. In a coupled acoustic-structural extraction, if the relocations and revolutions in a specific eigenvector are modest when contrasted with the acoustic forces, the eigenvector is standardized with the goal that the greatest acoustic force in the eigenvector is unity. The standardization is finished soon after the recuperation of needy degrees of license that have been a while ago disposed of with multi-focus requirements or mathematical statement requirements. In this way, it is plausible that such degrees of luxury may have esteems more fantastic than unity.

3.10 ACOUSTIC ANALYSIS

Generally, investigation with acoustic components considered as minor-uprooting straight irritation examination, in which the strain in the acoustic components is strictly (or overwhelmingly) volumetric and modest. In numerous provisions the base state for the direct annoyance is basically disregarded: for robust structures interfacing with air or water, the beginning anxiety (if any) buzzing around or water has insignificant physical impact on the acoustic waves. Most engineering acoustic analyses, transient or steady state, are of this type.

A critical exemption is when the acoustic irritation happens in a gas or fluid with rapid underlying rushes. Provided that the greatness of the stream velocity is critical contrasted with the rate of sound in the liquid (i.e., the Mach number is much more excellent than zero), the engendering of waves is expedited in the heading of rush and deterred in the heading opposite the stream. This wonder is the origin of the well-known “Doppler impact.” In ABAQUS /

Standard underlying stream impacts are recommended for junctions making up acoustic components by tagging an acoustic stream velocity.

Acoustic components could be utilized within a static examination, yet all acoustic impacts can be disregarded. A regular sample is the air cavity in a tire/wheel gathering. In quite a reproduction, the tire is subjected to swelling, edge mounting, and foot shaped impression stacks before the coupled acoustic-structural dissection in which the acoustic reaction of the air hole is resolved.

Acoustic elements additionally might be utilized as a part of a substructure era strategy to create coupled structural-acoustic substructures. Just structural degrees of luxury could be held. Since coupled substructures could commonly just be utilized within dynamic examinations, the held Eigen modes could most frequently be chosen besides. In a static examination including a substructure holding acoustic components, the effects will vary from the effects got in a comparable static dissection without substructures. The explanation for why is that the acoustic-structural coupling is considered in the substructure (accelerating hydrostatic commitments of the acoustic liquid), while the coupling is overlooked in a static examination without substructures.

The direct-solution steady-state dynamic harmonic response procedure is advantageous for acoustic-structural sound propagation problems, because the gradient of $\gamma\ /\rho_f$ need not be small and because acoustic-structural coupling and damping are not restricted in this formulation. If there is no damping or if damping can be neglected, factoring a real-only matrix can reduce computational time significantly.

Some fluid-solid interaction analyses include long-length of time dynamic impacts that more nearly look like structural dynamic examination than wave spread; that is, the essential motion of the structure happen around then scale that is as far back as anyone can remember

contrasted with the compressional wave speed of the strong medium and the acoustic wave speed of the liquid. Equally, in such cases, unsettling influences of investment in the structure engender extremely inefficiently in observation to waves in the liquid and compressional waves in the structure. In such cases, demonstrating of the structure utilizing shafts is normal. When applying the ABAQUS/AMS Eigen solver to a coupled structural-acoustic model, ABAQUS by default projects and stores the acoustic coupling matrix during the natural frequency extraction, for later use in coupled forced response analyses. The structural and acoustic regions are not actually coupled during the Eigen analysis; ABAQUS solves the two regions separately but computes and stores the projected coupling operator for use in subsequent steady-state dynamic steps.

3.11 INTERPRETING THE EXTRACTED MODES IN A COUPLED STRUCTURAL-ACOUSTIC NATURAL FREQUENCY ANALYSIS

While all the modes extracted in a coupled Lanczos structural-acoustic natural frequency analysis include the effects of fluid-solid interaction, some of them may have predominantly structural contributions while others may have predominantly acoustic contributions. Coupled structural-acoustic Eigen modes can be categorized as follows:

Most generally, an individual mode may exhibit participation in both the fluid and the solid media; this is referred to as a “coupled mode.” Second, there are the “structural resonance” modes. These are modes corresponding to the Eigen modes of the structure without the presence of the acoustic fluid. The presence of the acoustic fluid has a relatively small effect on these Eigen frequencies and the mode shapes. Third, there are the “acoustic cavity resonance” modes. These are nonzero Eigen frequency coupled modes that have a significant contribution in the resulting dynamics of the acoustic pressure in mode-based dynamic procedures. Fourth, if insufficient boundary conditions are specified on the structural part of a

model, the frequency extraction procedure will extract rigid body modes. These modes have zero Eigen frequencies (sometimes they appear as either small positive or even negative eigenvalues). However, if sufficient structural degrees of freedom are constrained, these rigid body modes disappear. Finally, there are the singular acoustic modes, which have zero Eigen frequencies and constant acoustic pressure; they are mathematically analogous to structural rigid body modes.

The structural part of the singular acoustic modes corresponds to the quasistatic structural response to constant pressure in unconstrained acoustic regions. These Eigen modes are predominantly acoustic and are important in representing the (low-frequency) acoustic response in mode-based analysis in the presence of acoustic loads, in the same way that rigid body modes are important in the representation of structural motion. As is true for the structural rigid body modes, if a sufficient number of constrained acoustic degrees of freedom is specified (one degree of freedom 8 per acoustic region is enough), the singular acoustic modes will disappear. In models with only one unconstrained acoustic region (the most common case), only one singular acoustic mode will be computed, In general there are as many singular acoustic modes as there are independent unconstrained acoustic regions. If these modes are present, they are always reported first by the Lanczos Eigen solver; and a note at the bottom of the Eigen frequency table in the data file provides information about the number of singular acoustic modes.

The generalized masses and effective masses can help distinguish between the various types of modes and can be used to assess which modes are important for subsequent mode-based analyses. In addition, the acoustic contribution to the generalized masses is reported as a fraction for each Eigen mode. The closer the value of this fraction is to unity, the more pronounced is the acoustic component of this Eigen mode. An acoustic effective mass is also computed for each Eigen mode. This scalar quantity is scaled such that when all Eigen modes

in a model are extracted, the sum of all acoustic effective masses is equal to 1.0 (minus the contributions from nodes with restrained acoustic degrees of freedom). The acoustic effective mass can be compared between different modes: the higher the acoustic effective mass, the more important (typically) the mode is for accurate representation of the acoustic pressure.

3.12 SELECTION OF SOFTWARE AND DEVELOPMENT OF THE MODELING SYSTEM

The software package used in this research to analyse the damage in carbon steel pipe structures was ABAQUS version 6.9. As a powerful finite element commercial code, ABAQUS contains an extensive library of elements and material models, which makes it possible to analyse complex geometric structures and non-linear material responses. The applications of ABAQUS are increasing almost every year as developments occur in engineering features and modelling techniques.

ABAQUS offers a number of procedures to solve a variety of engineering problems. Examples are static stress analysis, dynamic stress analysis, and transient heat transfer analysis.

In the present research, the ABAQUS explicit dynamic analysis was applied to stresses resulting from impact, which is a highly non-linear event with complicated contact conditions. In addition, ABAQUS provides a wide range of flexible options to accommodate advanced applications by providing a user sub-routine interface to increase its functionality.

Based on micromechanics, ABAQUS provides accurate analysis techniques to determine the local element failure and can then adjust the element stiffness to precede damage analysis.

For example, ABAQUS can predict element failure by the most common failure criteria, such as those from the theories of maximum stress, and maximum strain. Advanced failure criteria can be added in ABAQUS by implementing the user sub-routine option.

Following the concepts of damage mechanics and the analysis techniques in FEM, a basic model is presented in this chapter to analyse "healthy" pipe in ABAQUS, and a similar modelling process is implemented for modelling damages, which required additional definition of the geometry and physical properties of the model and of the damage process.

3.13 GEOMETRY, MATERIAL PROPERTIES, AND BOUNDARY CONDITIONS

The structure modelled in this analysis is carbon steel pipe (Figure 3-19) subjected to free suspension, which is hereafter called the basic model (a tube with no defects).

The basic geometry of the model is provided in Table 2, in which the structural parameters are L = 1 m, D = 10 cm, and T = 3.5 mm, which represent the length of the pipe, the diameter of the pipe, and the thickness of the pipe, respectively.

In addition, the model was simplified to 3D, definable, homogeneous, plane-shell-revolution analysis with the assumption that the planned force is on the top surface at 15 cm from the edge of the tube.

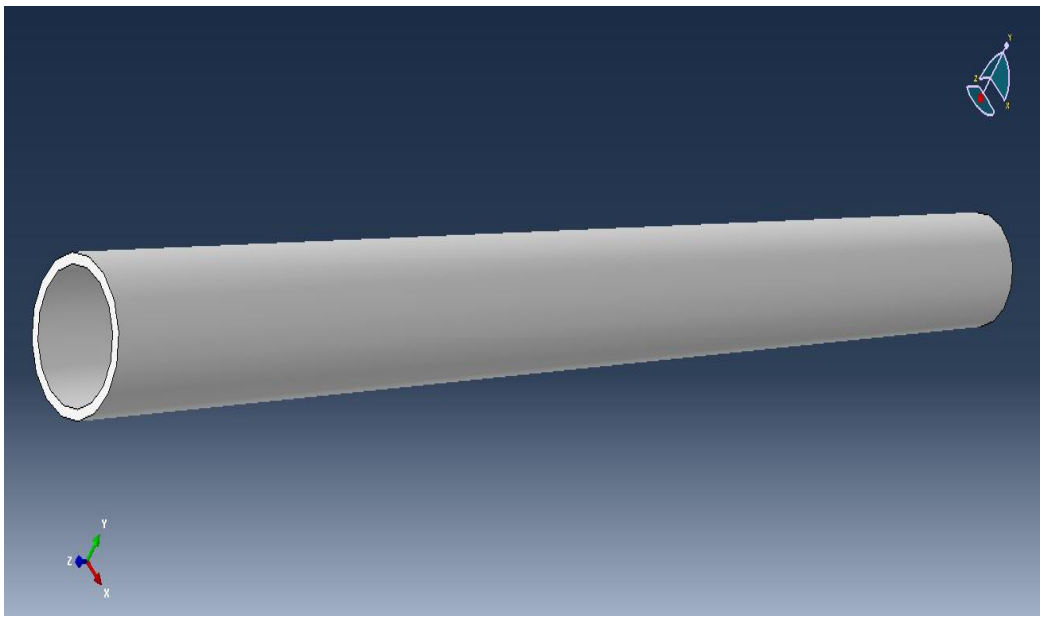

FIGURE 3-19: ABAQUS BASIC PIPE MODEL SIMULATION

Table 2: Specimen properties and parameters of the Model

Model Configurations	
Length of the Tube (*L*)	1 Meter
Outside diameter of the Tube	2.5 Centimetres
Thickness of the Tube (*T*)	3.5 Millimetres
Material Properties	
Stiffness (Young's Modulus)	$E = 200 \times 10^9 \times 10^9$
Poisson's ratio (*v*)	0.3 Pa
Density	7850 kg/m^3
Variables' Parameters	
X	50
θ	25,50,75 and 100% in depth hole
Forced impact at	Acoustic pressure
Impact force	~ 235KHz

In the basic model, uniform tensile stresses were applied in the top surface at each edge of the tube by surface traction frequency of 235 KHz, as shown in Figures (3-20 and 3-21) respectively.

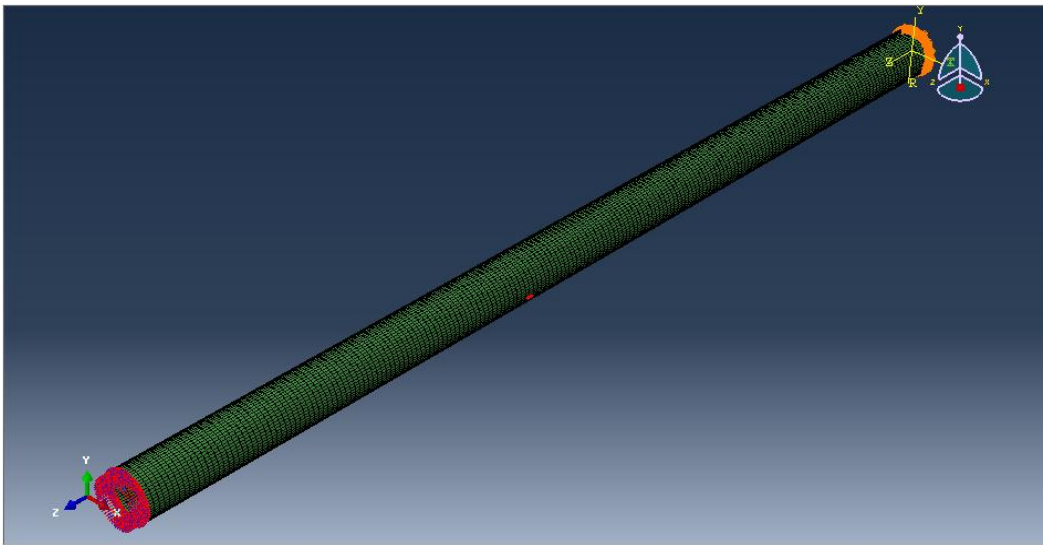

FIGURE 3-20: BASIC MODEL LOAD CONDITIONS

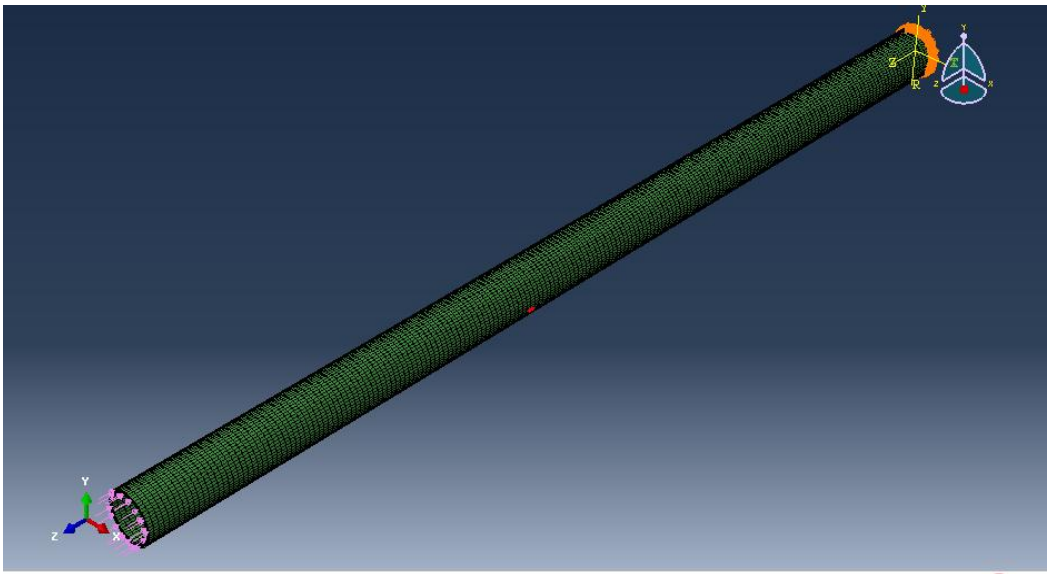

FIGURE 3-21: ABAQUS LOAD DEMONSTRATION

The reliability of the results of FEA depends on how accurately the problem is modelled and analysed. The accuracy of the model depends on including relevant geometrical details, assigning appropriate material properties, and specifying correct boundary conditions. The boundary conditions are included in the model to relate it to reality by constraining the structural response to the applied load and a fixed constraint at a certain location. Therefore, there is a rigorous requirement that the correct boundary conditions be specified before conducting the analysis.

The material properties used in the modelling are elastic and isotropic properties, in terms of stiffness and strength, as listed in (Table 2), and the defects parameter, where (x) represents the distance the hole is from the end of the tube, and ⌀ represents the diameter of the hole. The outputs of the model are acceleration, displacement, and velocity in the time domain.

3.14 MODEL DYNAMIC ANALYSIS USING ABAQUS CAE.

3.14.1 ACOUSTIC EQUATIONS

The equilibrium equation for small motions of a compressible, adiabatic fluid with velocity-dependent momentum losses is taken to be

$$\frac{\vartheta_\rho}{\vartheta_x} + \gamma\,(x,\theta_i)\dot{u}^f + \rho_f(x,\theta_I)\ddot{u}^f = 0 \qquad (3.12)$$

where p is the excess pressure in the fluid (the pressure in excess of any static pressure); x is the spatial position of the fluid particle; $\dot{u}^f$ is the fluid particle velocity; $\ddot{u}^f$ is the fluid particle acceleration; ρ_f is the density of the fluid; $\boldsymbol{\gamma}$ is the "volumetric drag" (force per unit volume per velocity); and θ_i are i independent field variables such as temperature, humidity of air, or salinity of water on which ρ_f and γ may depend.

For an acoustic medium capable of undergoing cavitations', the absolute pressure (sum of the static pressure and the excess dynamic pressure) cannot drop below the specified cavitations' limit. When the absolute pressure drops to this limit value, the fluid is assumed to undergo free expansion without a corresponding drop in the dynamic pressure. The pressure would rebuild in the acoustic medium once the free expansion that took place during the cavitations' is reversed sufficiently to reduce the volumetric strain to the level at the cavitations limit. The constitutive behavior for an acoustic medium capable of undergoing cavitations' can be stated as

$$p = \max\{p_v, p_c - p_0\} \tag{3.13}$$

where a pseudo pressure p_v, , a measure of the volumetric strain, is defined as

$$p_v = -K_f(x, \theta_i)\ \frac{\partial}{\partial_x}\ .u^f, \tag{3.14}$$

where p_c is the fluid cavitation limit and p_v is the initial acoustic static pressure. A total wave formulation is used for a nonlinear acoustic medium undergoing cavitation.

This formulation is very similar to the scattered wave formulation presented below except that the pseudo pressure, defined as the product of the bulk modulus and the compressive volumetric strain, plays the role of the material state variable instead of the acoustic excess pressure. The acoustic excess pressure is readily available from this pseudo pressure subject to the cavitation condition.

3.14.2 FREQUENCY-DOMAIN SOLUTION USING PROJECTIONS ONTO MODEL SPACES

Distinct modal space projection methods for coupled forced structural-acoustic response exist in ABAQUS for the following cases: using coupled modes from Lanczos, using uncoupled modes from Lanczos, and using uncoupled modes from ABAQUS/AMS.

In the Lanczos mode cases, the forced response is computed using the Zienkiewicz-Newton equation, with separate right and left projection operators. In the ABAQUS/AMS uncoupled mode case the Everstine equation is used for the forced response and the right and left projection operators are identical. This case is described in more detail below.

- ***Using uncoupled ABAQUS/AMS modes***

In this case, the Everstine equation is used for the coupled forced response problem and modes are computed from decoupled structural and acoustic ABAQUS/AMS runs. In nodal degrees of freedom the forced response is governed by

$$\begin{bmatrix} K_s & 0 \\ 0 & K_f \end{bmatrix} \begin{Bmatrix} u \\ q \end{Bmatrix} + i \begin{bmatrix} C_s & \Omega S_{fs}^T \\ \Omega S_{fs} & C_f \end{bmatrix} \begin{Bmatrix} u \\ q \end{Bmatrix} - \Omega^2 \begin{bmatrix} M_s & 0 \\ 0 & M_f \end{bmatrix} \begin{Bmatrix} u \\ q \end{Bmatrix} = \begin{Bmatrix} P_s \\ P_f/_{i\Omega} \end{Bmatrix} \tag{3.15}$$

where $C_s$andC_f here are the complete assembled damping matrices for the structure and fluid, including viscous and structural damping, as well as boundary impedance effects. Using transformations constructed from the acoustic and structural modes,

$$\{\phi_i^S\} \mapsto \Phi_S \tag{3.16}$$

$$\{\phi_j^A\} \mapsto \Phi_A \tag{3.17}$$

and representations of the structural and acoustic fields in the spaces spanned by these modes,

$$u \mapsto \Phi_S (\tilde{u} + i\,\tilde{v}) \tag{3.18}$$

$$q \mapsto \Phi_A (\tilde{q} + i\tilde{r}) \tag{3.19}$$

we obtain

$$\begin{bmatrix} \Omega C_s & 0 & -\Omega_{s^T} \\ -K_s + \Omega^2 m_s & -\Omega_{S^T} & 0 \\ -\Omega_{S_{f_s}} & K_f - \Omega^2 m_f & \Omega_{c_f} \end{bmatrix} \begin{Bmatrix} \tilde{u} \\ \tilde{v} \\ \tilde{q} \end{Bmatrix} = \begin{Bmatrix} \Re(\widetilde{f_s}) \\ -\Im(\widetilde{f_s}) \\ \Re(\widetilde{f_s}) \end{Bmatrix} \tag{3.20}$$

The terms in this matrix correspond to the nodal degree-of-freedom operators, projected onto the modal spaces. The damping and coupling matrices in modal coordinates are full and unsymmetrical.

3.15 ACOUSTIC OUTPUT QUANTITIES

Several secondary quantities are useful in acoustic analysis, derived from the fundamental acoustic pressure field variable. In steady-state dynamics the acoustic particle velocity at any field point is

$$\tilde{v} = \frac{i}{\tilde{p}\Omega}\frac{\partial \tilde{p}}{\partial x} \tag{3.20}$$

The acoustic intensity vector, a measure of the rate of flow of energy at a point, is

$$\tilde{I} = -\frac{1}{2}\,\sigma\,.\,\tilde{v}^{\wedge} \tag{3.21}$$

In an acoustic medium the stress tensor is simply the acoustic pressure times the identity tensor, $\sigma = -pI$, so this expression simplifies to

$$\tilde{I} = \frac{-1}{2i\tilde{p}^{\wedge}\Omega}\ \tilde{p}\frac{\partial \tilde{p}^{\wedge}}{\partial x} \tag{3.22}$$

3.16 RESULTS VISUALIZATION

Below are selected graphs form ABAQUS simulation output (Healthy and 50%) that shows efficiency of simulation to predicted faults in pipeline, the output results display the amplitude, velocity, displacement and strain energy as shown on Figures 3-22 to 3-27 respectively.

The modelling outcomes come up with the following:

- The highest displacement of healthy pipe is 1.460 e^{-7} m while highest displacement of 50 % hole depth pipe is 1.594 e^{-7} m (Figure 3-22 and 3-24)

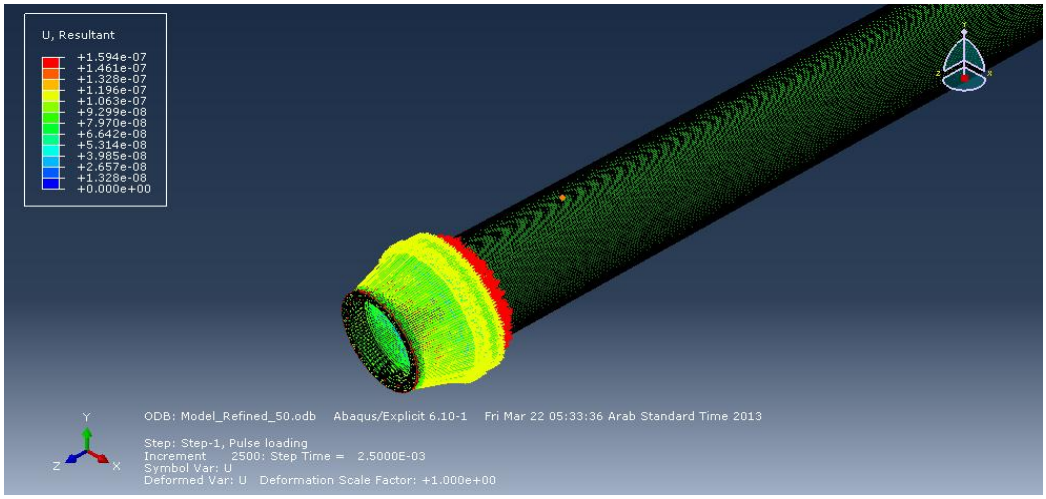

FIGURE 3-22: HEALTHY PIPE DISPLACEMENT RESULTANT

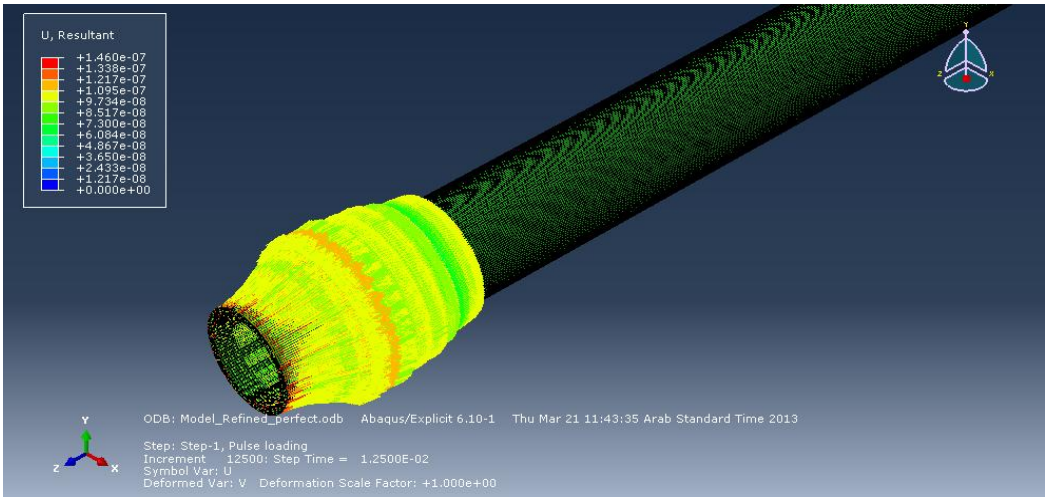

FIGURE 3-23 : 50% HOLE DEPTH PIPE DISPLACEMENT RESULTANT

- Also, the amplitude measurements have shown differences as the highest amplitude of healthy pipe is 6.928 dB while highest amplitude of 50 % hole depth pipe is 7.508 dB as shown in figures 3-24 and 3-24 below,

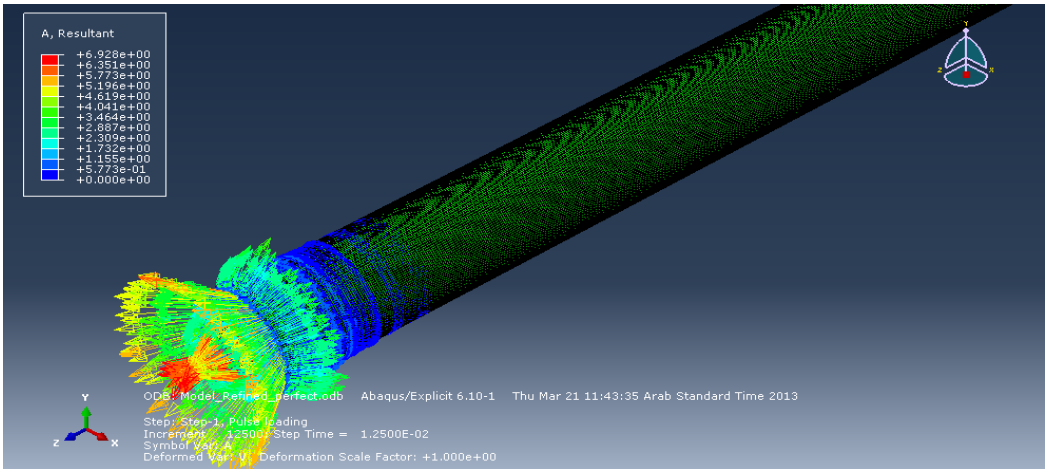

FIGURE 3-24: HEALTHY PIPE AMPLITUDE RESULTANT

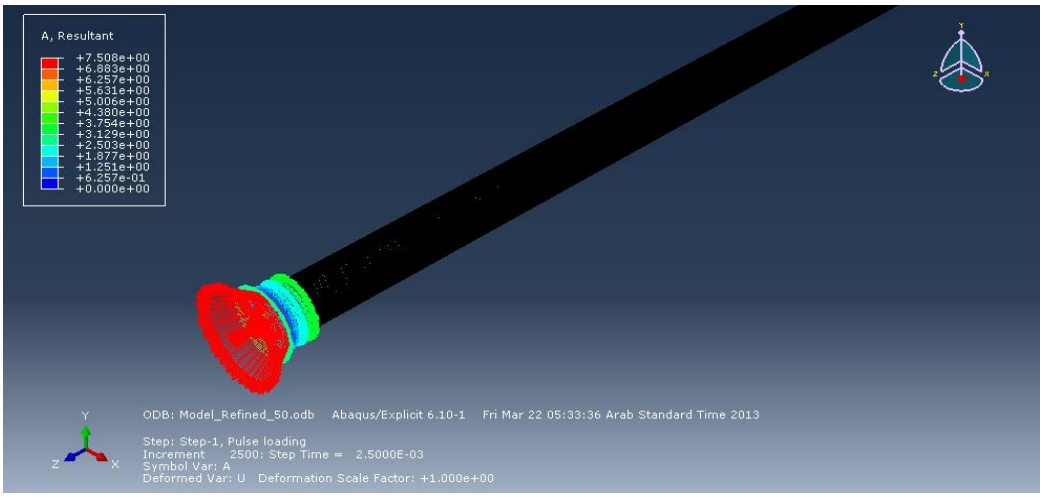

FIGURE 3-25: 50% HOLE DEPTH PIPE AMPLITUDE RESULTANT

For more modeling outcomes results clarification, velocity measurements carried out and come up with highest velocity of healthy pipe is 4.548 e^{-4} m/s while highest displacement of 50 % hole depth pipe is 3.348 e^{-4} m/s as shown in figures 3-26 and 3-27.

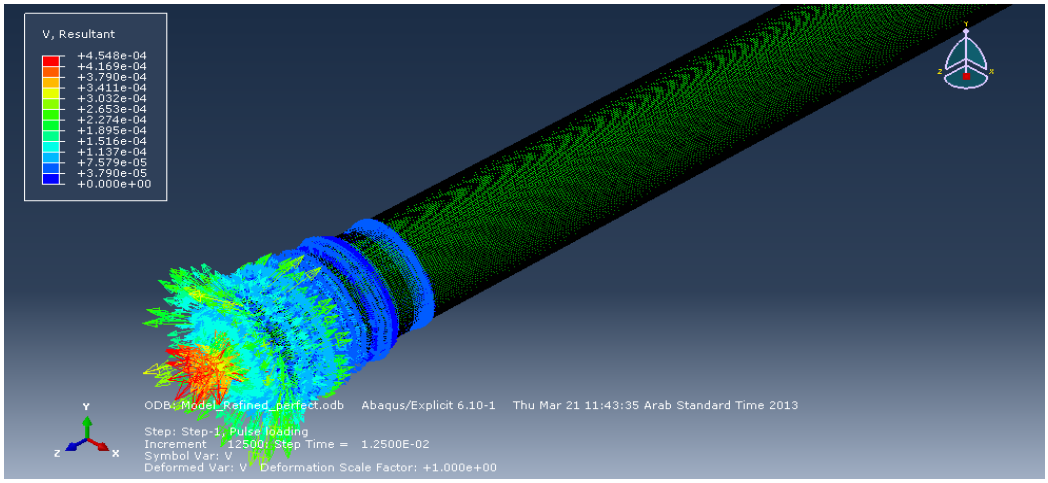

FIGURE 3-26: HEALTHY PIPE VELOCITY RESULTANT

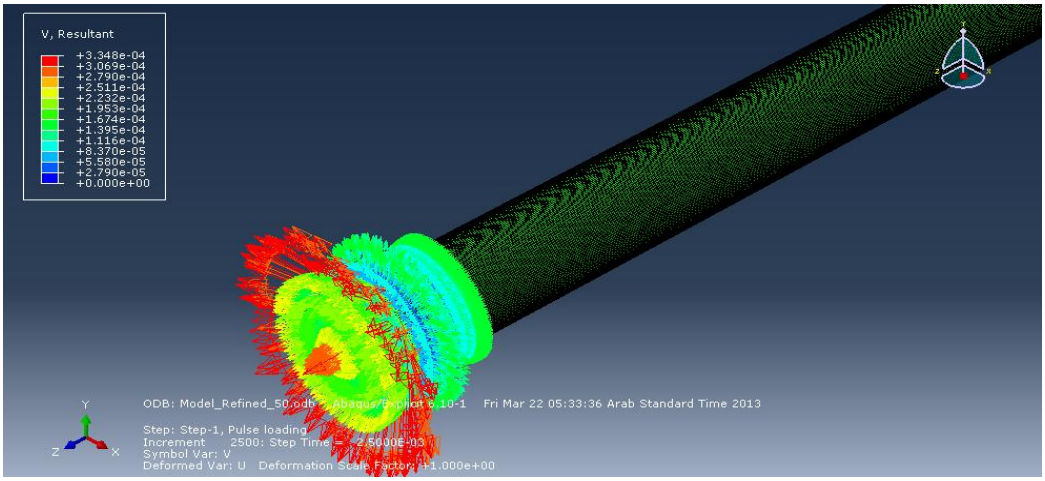

FIGURE 3-27: 50% HOLE DEPTH PIPE VELOCITY RESULTANT

In conclusion, the above findings shows that displacement, amplitude and velocity are in direct proportion with faults size and this underscores the efficiency of the simulation to predicted faults in pipeline smoothly instead of physical inspection that required preparation and arrangement in the vicinity. In addition, the success of the simulation must be verified experimentally as illustrated in the following chapter.

CHAPTER IV

THE EXPERIMENTS SETUP AND PROCUDURE

This chapter provides detailed description of the experimental setup and procedure to investigates the ultrasonic signal processing technique at steel pipes on different conditions and analyzed collected data using conventional and advances techniques to demonstrates the outcomes results graphically and then discuss the results and highlight the research novelty.

4.1 INTRODUCTION

This chapter describes the specifications, experimental apparatus and procedures used for this work. First, the features and specification of apparatus that are common to all the experiments performed are described, and then the details of each experiment are presented. The first experiment was a study of ultrasound wave propagation along a healthy steel pipe. The second series of experiments were the study of ultrasound propagation in defective steel pipes with various defects seeded into them and finally evaluation of the detection and source location capabilities for such sources. All experiments were carried out at room temperature using five different pipes.

4.2 APPARATUS AND PROCEDURE

The system generally consists of pulse generator linked to transducers (source and receiver) attached to the pipe circumference with linked to an oscilloscope that has data acquisition system to capture the signals for analysis and data was analysed offline using MatLab software package. The experimental set-up and block diagram used in this work is shown below in Figure 4-28 (A) (B) respectively. In addition, the experimental procedure and analyses technique flowchart is illustrated in Figure 4-29.

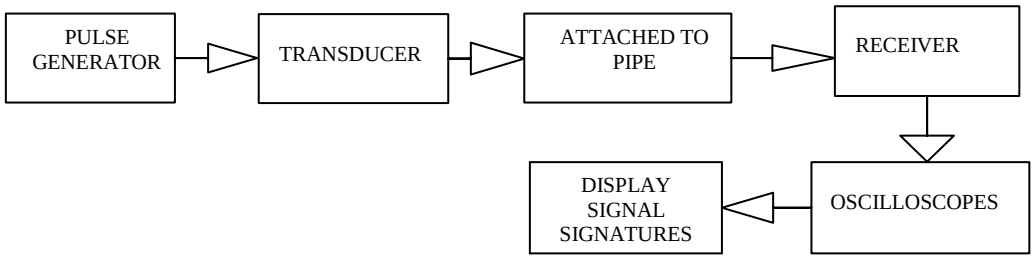

(A)

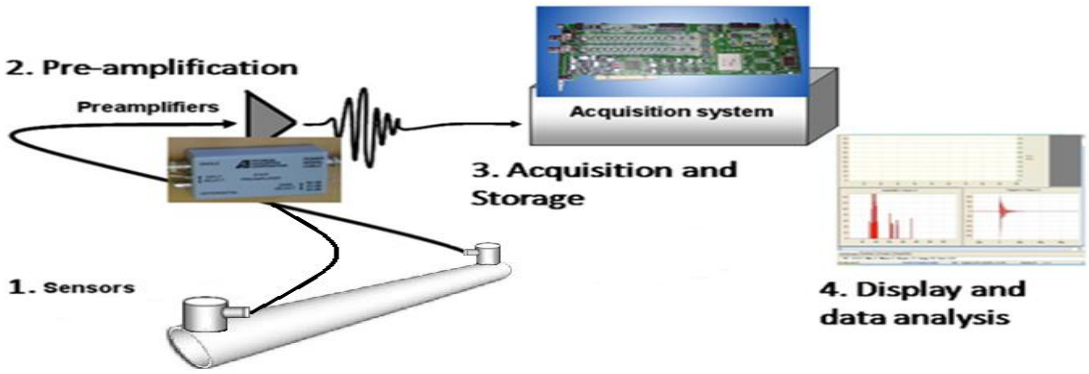

(B)

FIGURE 4-28: THE EXPERIMENTAL PROCEDURE (A) BLOCK DIAGRAM , (B) PROCEDURE

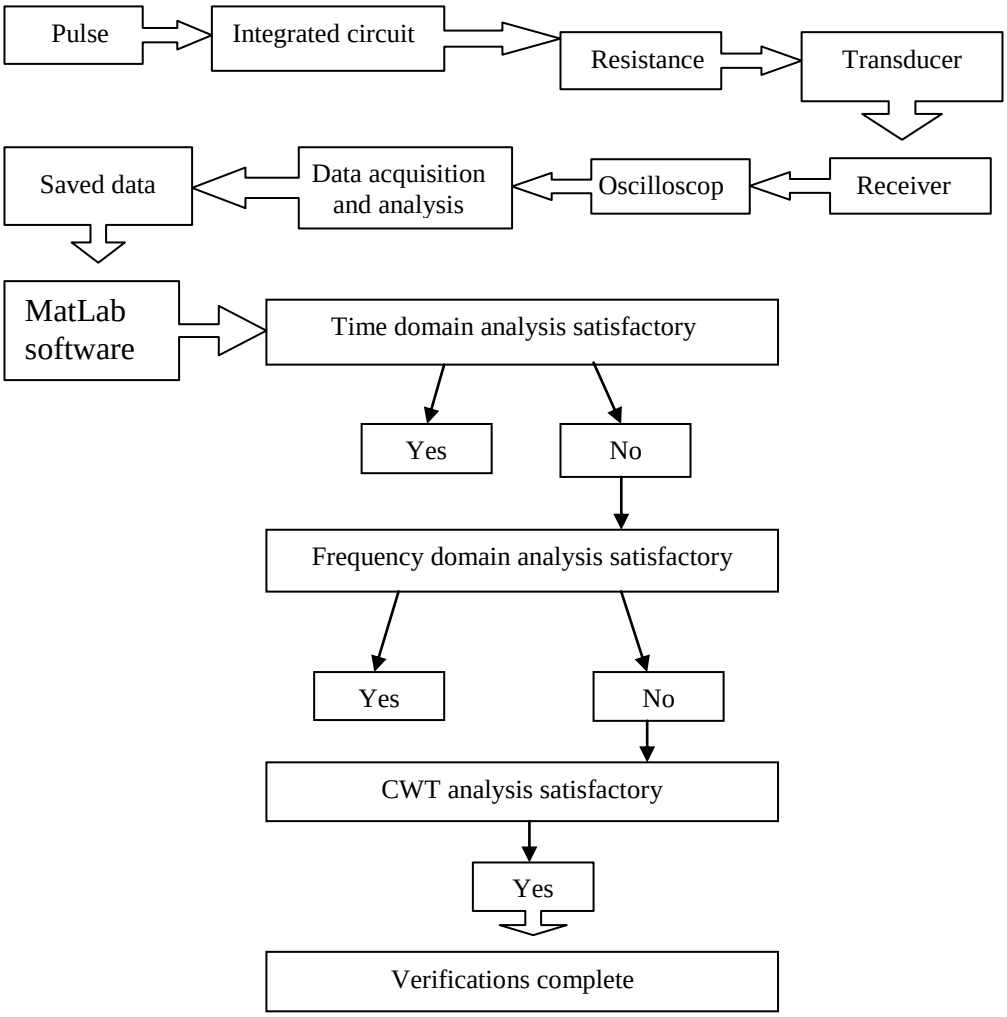

FIGURE 4-29: BLOCK- DIAGRAM AND FLOWCHART OF EXPERIMENTAL PROCEDURE AND SOFTWARE ANALYSIS

4.2.1 ULTRASOUND SENSORS

Air Ultrasonic Ceramic Transducers type 235AC130 was used to generate the signal and detect the response. This transceiver had a centre frequency at 235.0 $\pm$ 10 kHz and two bands of transmitting sensitivity at on 15 dB and -75 dB as receiving sensitivity. The sensor operating temperature range was from -20^{o}C to +60^{o}C, and its diameter was 8.30 mm wide and it was 15 mm high. The transducers were held onto the test object surface as shown on Figure 4-30 and Figure 4-31. To obtain good coupling of transducers to pipe surface the pipe surface was kept smooth and clean and silicone grease was used as coupling to fill any gaps caused by any remaining surface roughness and eliminate air gaps that might otherwise impair any wave transmission. The system was tested using a beam angle of 70^{o} and frequency 235.0 kHz. Calibration certificates for the sensors used in this work are shown in Appendix C.

FIGURE 4- 30: AIR ULTRASONIC CERAMIC TRANSDUCER TYPE 235AC130

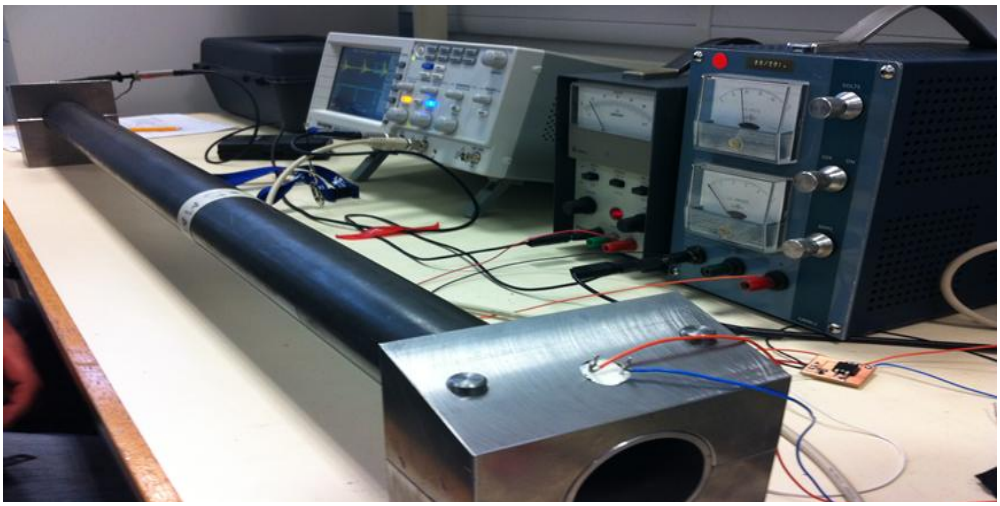

FIGURE 4-31: EXPERMENTAL RIG

4.2.2 PRE-AMPLIFIERS

Pre-amplifiers type LA100.2 was used to amplify the ultrasound signal to a level that could be comfortably transmitted by a short length of coaxial cable to the Analogue to Digital Converter (ADC). Signal conditioning units (Figure 4-32) were built for use with the ultrasonic sensors and pre-amplifiers

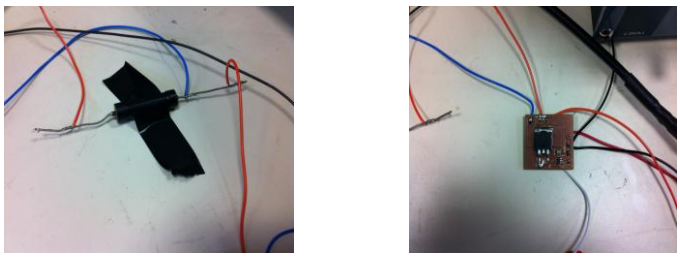

FIGURE 4-32: RESISTANCE AND INTEGRATED CIRCUIT

The ADC could be used to perform analogue RMS processing with the capability of additional amplification or attenuation where necessary as shown in the block circuit diagram in Figure 4-33.

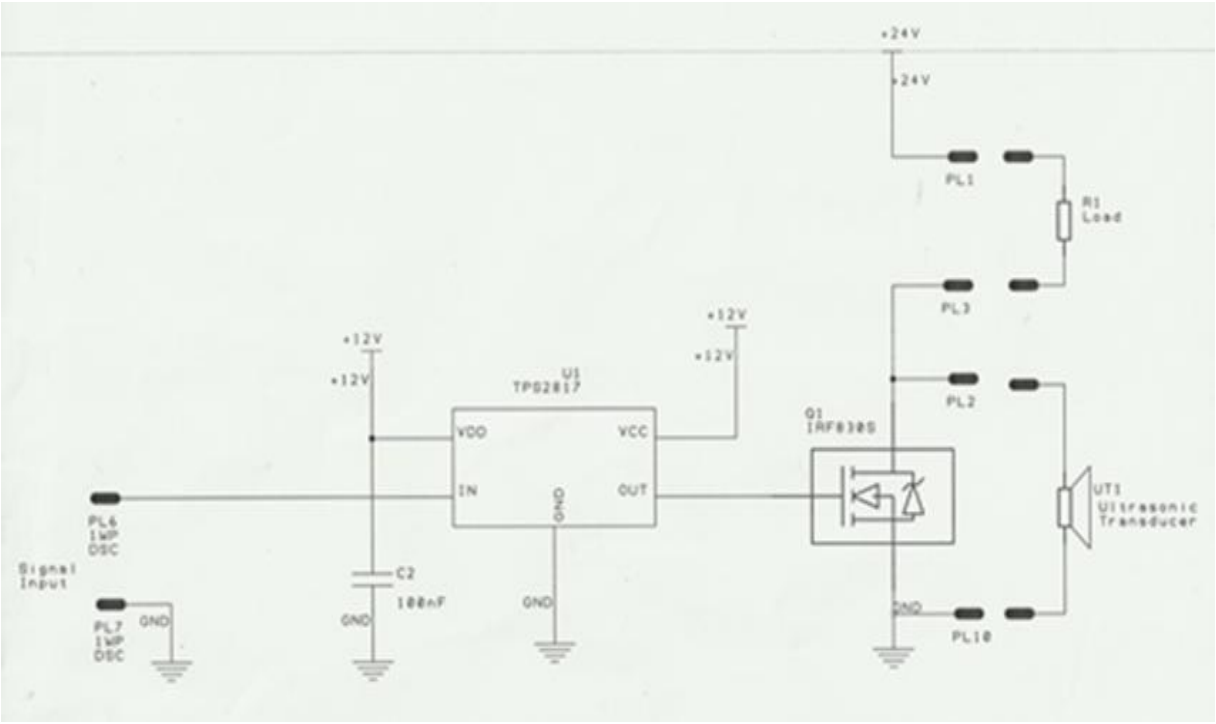

FIGURE 4-33: BLOCK CIRCUIT DIAGRAM

4.3 PULSE GENERATOR

Test systems are often required to generate different types of waveforms and use different families of waveforms, signal and data generators to do this. Traditional types of function and signal generators provide either (i) sine, square, triangular waves or variations and combinations of these, or (ii) high frequency sine waveforms with miscellaneous types of modulation

The first type is used for testing miscellaneous types of analogue, mixed signal or digital circuit blocks, whereas the second type is used for testing communication systems. In general provides a detailed account of these analogue systems and design techniques. With digital instruments, the user is able to produce an arbitrary waveform based on data stored in memory, and many new families of waveforms are now available for use.

A basic pulse generator provides a square wave with a variable period or repetition rate and variable duty cycle. The key evaluation parameter is that the pulse generator must be very much faster than the rise time of the system under test and pulse generators with rise times of 1 and 2 *ns* are now common with rise times of less than 100 *ps* claimed by manufacturers such as Picosecond [www.picosecond.com/product].

A pulse generator provides a wide range and good control of timing parameters but has the disadvantage of not providing the stability of a digital synthesiser. In some pulse generators, built-in calibrators are used to monitor the timing parameters and compensate for the inaccuracies of the analogue circuitry.

In this research an Agilent 33210A 10 MHZ function / Arbitrary, waveform generator was used. The waveforms are generated using Direct Digital Synthesis (DDS) technology that creates stable, accurate low distortion sine waves as well as square waves with fast rise and

fall times up to 10 MHz and linear ramp waves up to 100 kHz. The device setting was as follows:

- Frequency: 235.0 kHz,
- Period: 4.255μ sec.
- Amplitude: 1.88 Volts (Peak to Peak),
- Offset = + 940 mv (DC),
- Duty cycle = 90%, 50%, 10%,
- Pulse width = 3.8 μ sec.
- Edge time 20 *n sec*.,

4.4 DATA ACQUISITION SYSTEM

An oscilloscope display presents for more information than that available from other test and measuring instruments such as frequency counters or digital multi-meters. With the advancement of the solid-state technology, modern oscilloscopes are digital storage oscilloscopes. Signals that can be handled by the modern instruments now reach 50 GHz for repetitive signals and beyond 1 GHz for non-repetitive signals. This gives an idea of the best rise times that can be measured with accuracy. The actual measurement situation may be worsened when probes and cables are used to couple the signal to channel inputs.

The bandwidth of an oscilloscope gives a clear idea of what maximum frequencies of practical waveforms can be measured. For example, an oscilloscope having a 3 dB bandwidth of 75 MHz, means an observed square wave of 75 MHz fundamental frequency will be appear far from square because the third, fifth and higher harmonics which will be heavily attenuated. The resultant wave shape on the oscilloscope screen will be quite close to that of a sine wave. For this reason, an oscilloscope with a bandwidth of at least five times the highest frequency

of the signal to be observed should be used. Failure to do this will lead to the display of seriously distorted wave shapes, particularly for square waveforms.

With the rapid advancement of semiconductor technology, memories, data converters and processors have enabled most reputable manufactures such as Tektronix and Hewlett-Packard (now Agilent Technologies) to produce high quality storage oscilloscopes, which necessitate the digitising, and reconstruction process using analogue-to-digital and (possibly) digital-to-analogue converters in the digitising and reconstruction processes, respectively.

4.5 SAMPLING TECHNIQUES

In all digital storage scopes and waveform digitisers, the input waveforms are sampled before the A/D conversion process. There are two fundamental digitising techniques; (i) real sampling, and (ii) equivalent time sampling. In real time sampling all samples for a signal are acquired in a single acquisition, as in Figure 4-34. In this process a waveform is sampled in a single pass and the sample rate must be high enough to acquire a sufficient number of data points to reconstruct the waveform accurately. Real time sampling can be used to capture both repetitive and single shot events. In equivalent time sampling, the final display of the waveform is built up by acquiring a little information from each signal repetition.

There are two equivalent time sampling techniques: sequential and random sampling. The technique of sequential sampling which samples one point on the waveform every acquisition cycle, this is done sequentially and is repeated until enough points are acquired to fill the memory.

If the memory is 1000 points long it would take 1000 passes to acquire the waveform. The points in time at which these samples are acquired are stored in reference to the trigger point. This type of equivalent time sampling has two advantages.

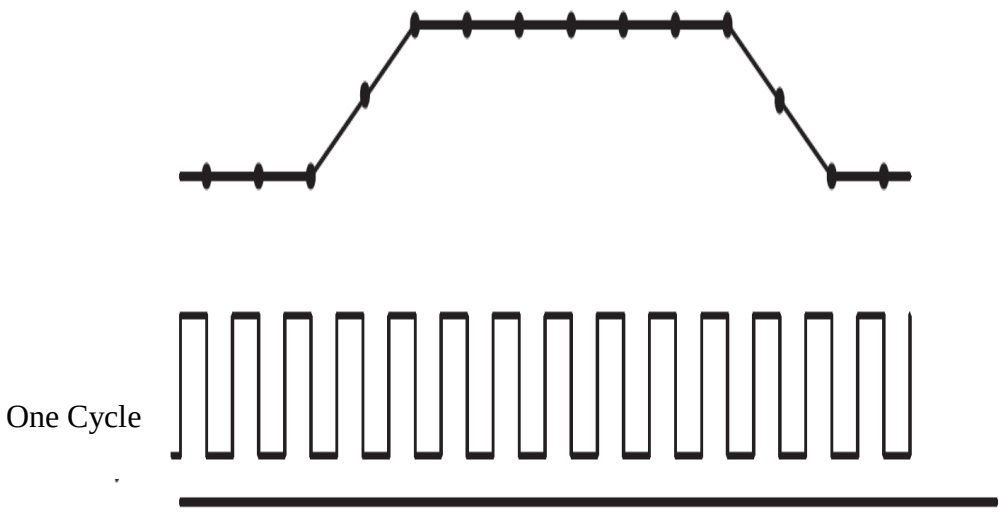

FIGURE 4-34: REAL TIME SAMPLING

First, since the points are reconstructed with reference to the trigger point, it retains the pre- and post-triggering capability, which sequential sampling cannot do. Second, because the sample acquisition is referenced to the trigger signal, the normal digital trigger jitter is not a factor.

Another variation of random sampling is multiple-point random sampling, where several points are obtained in one acquisition cycle. This reduces the acquisition time considerably. It is important to highlight that real time sampling is necessary to capture transient events. Equivalent time sampling is used for repetitive signals and allows capturing of very high frequency components as long as the signal is repetitive.

4.6 DISPLAY TECHNIQUES

There are several methods that may be used to redisplay the waveform after it has been digitised, memorised and processed. Basic techniques include: (i) the use of dots, (ii) linear interpolation (joining the dots), and (iii) sine interpolation or modified sine interpolation. All methods require a digital-to-analogue converter (DAC) to change the data back to a form that the human eye can understand. DACs, when used for reconstructing digital data, do not

require the performance characteristics of ADCs because the conversion rate could be much slower. The main purpose of the DAC is to take the quantised data and convert them to an analogue voltage. In displaying the stored digitised data, aliasing may occur, unless the signal is sampled at more than twice the highest frequency component of the signal.

The diagram in Figure 4-35 shows under sampling of a waveform where sampling is carried out only once per cycle, in this case the alias waveform is of a much lower frequency (approximately 1/19th of the actual frequency), as the information gathered via sampling is inadequate to represent the shape of the actual waveform. More samples per period will eliminate aliasing.

When the sample rate is calculated inside the oscilloscope, the bandwidth of the signal, which can be displayed, is estimated easily. Since we must always digitise twice as fast as the highest frequency in the signal, the simplest way to do so is to make sure that the user picks a time div^{-1} setting that determines a high enough sample rate. When this cannot be done, an antialiasing filter can be used to eliminate frequencies above the Nyquist limit.

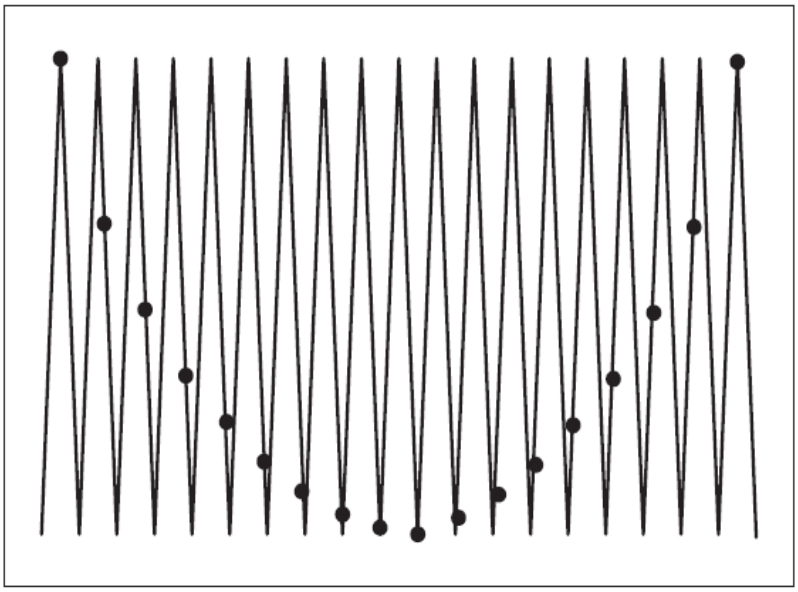

FIGURE 4-35: EFFECT OF UNDER-SAMPLING

4.7 DOT AND VECTOR DISPLAYS

Dot displays are, as their name implies, made up of points on the CRT. These displays are useful providing there are sufficient points to reconstruct the waveform. The number of points required is generally considered to be about 20 to 25 points per cycle. However, with dot displays fewer dots will be available to form the trace when the frequency of the input signal increases with respect to sample rate.

This could result in perceptual aliasing errors, especially with periodic waveforms such as sine waves. This perceptual aliasing is a kind of optical illusion as our mind is tricked to imagine a continuous waveform by connecting each dot with its nearest neighbours when viewing a dot display. The next closest dot in space, however, may not be the closest sample of the waveform. As shown in Figure 4-36 (a), a dot display can be interpreted as showing a signal of lower frequency than the input signal. This effect is not a fault of the scope but of the human eye.

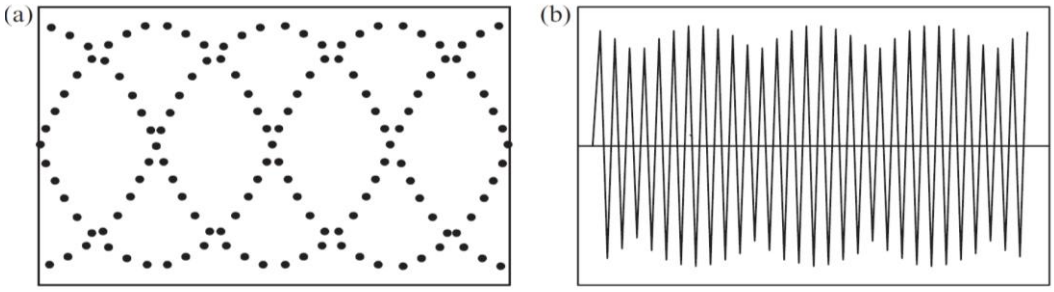

FIGURE 4-36: EFFECT OF ALIASING AND VECTOR DISPLAY: (A) PERCEPTUAL ALIASING; (B) VECTOR DISPLAY

Perceptual aliasing, as in Figure 4-36(a), is easily corrected by adding vectors to the display, as shown in Figure 4-36(b). But this vector display can still show peak amplitude errors when the data points do not fall on the signal peaks because the vectors are only straight lines joining the points. When digital storage oscilloscopes use vector generators, which draw lines

between data points on the screen, perceptual aliasing is eliminated and only about ten vectors are needed to reconstruct a recognisable display.

4.8 SAMPLING RATE

The sampling rate, a primary characteristic of the Digital Storage Oscilloscope (DSO), is commonly expressed as a frequency such as 20 MHz. This may be expressed as the information rate, that is, the number of bits of data stored per second For example, 160 x 10^6 bps for an 8-bit ADC and a sample rate of 20 MHz. In a practical oscilloscope the sample rate varies with the time base setting and the corresponding relationship is

$$\textbf{\textit{Sample rate}} = \frac{\textbf{\textit{record length of waveform time}}}{\textbf{\textit{base setting}} \times \textbf{\textit{sweep length}}}$$

When the sample rate is selected using this criterion it occupies the entire memory and fills the screen. As the time base is reduced (i.e. more time per division), the digitiser must reduce its sample rate to record enough signal samples to fill the display screen.

However, reducing the sample rate also degrades the usable bandwidth (discussed later). Long memory digitisers maintain their usable bandwidth at slower time base settings compared with short memory digitisers.

Because the cost of a DSO depends on the cost of memories and data converters used inside, this criterion is an important one in the selection of a DSO.

The GDS-2102 Instek Digital Storage Oscilloscope which features 100 MHz bandwidth with 2 channels that delivers a sample rate of 1 G samples/s and a maximum record length of 25000 samples was used in this research. The scopes can be programmed to take up to 24 different measurements automatically and results are displayed on the 14 cm wide screen.

4.9 PROBES AND PROBING TECHNIQUES

Probes are used to connect the measurement test point in a device under test to the input of an oscilloscope. Achieving optimised performance in a measurement depends on the selection of the probe. A probe that is not appropriate for an application can mean a significant error in the measurement as well as undesirable circuit loadings.

Many oscilloscopes claim bandwidths that exceed 1 GHz, but one cannot accurately measure signals of such high frequencies unless the probe can accurately pass them to the scope. Standard single-ended, 1 M Ω, passive probes work well in many applications, but their bandwidth cut off is around 500 MHz. Above that frequency; active probes are a better choice. Using the correct probe is critical to making accurate, safe measurements.

Single ended probes, whether passive or active, cannot produce a meaningful measurement when you need to measure the difference between two non-zero voltages. Even worse, using a single-ended probe can be dangerous in some applications.

A wide variety of probes suitable for different oscilloscope measurements are available. The basic types are as follows:

- Voltage sensing,
- Current sensing,
- Temperature sensing,
- Logic sensing, and
- Light sensing

Most common are the voltage or current sensing types. These may be further subdivided into ‘passive’ and ‘active’ for voltage sensing and a/c. and d/c. for current sensing. In addition, there are different types of temperature sensing and logic sensing probes available. For

example, word recogniser probes can be used to generate a trigger pulse in response to a particular logic state.

4.10 EXPERIMENTAL PROCEDURES

The overall purpose was to evaluate the potential of ultrasound monitoring and to validate modelling (theoretically) results and findings in detecting defects in real piping systems and acknowledging the effects that external environments may have on the propagation of the waves. To this end, five sets of experiments were carried out to investigate the propagation of an ultrasound wave signal in a real one meter length of healthy carbon steel pipe and in four exactly similar lengths of Carbon pipe seeded with 1 mm holes of varying depth.

Five carbon steel pipes A grade, type HFS 23 were used in research experiments; all were of length 1 m, of internal diameter 25 mm and wall thickness 3.5 mm

Initially aluminum stands were placed at each end to support the pipe, see Figure 4-34. This arrangement was used to obtain a preliminary indication of the type of propagation behaviour shown by a wave generated from an ultrasonic source. The source was mounted at one end of the pipe at 70 °angles, which is the best angle that shows clear results, the receiver was moved incrementally along the axis of the pipe to the other end at the same angle.

CHAPTER V

ULTRASONIC CONVENTIONAL TECHNIQUES

This chapter serves as a brief introduction to the main features of the Fourier Transform, pointing out the main properties, schemes, basic Fourier Transforms analysis. Conventional Ultrasonic techniques used for research work are also introduced and discussion of the results brought about by the time / frequency domain analysis. Results indicate that these techniques are not effective and are not suitable for the purposes of comparison between the signatures of different models.

5.1 INTRODUCTION

Signals from natural processes tend to be analogue and continuous over an interval of time or space. The mathematical model of an analogue signal is a real function and analogue signal conditioning uses conventional electronic circuitry to acquire, amplify, filter, and transmit these signals. At some point, digital processing may take place; today, this is almost always necessary because powerful modern signal processing techniques, including noise suppression and information extraction are much easier to implement on digital computers.

Whatever the rationale for digital processing, the analogue signal is captured, stored momentarily and then converted to digital form. In contrast an analogous signal is continuous and the mathematical representation of a digital signal has values only at the specific points at which the analogue signal has been sampled. The values of digital signal are of finite precision when they are stored in the registers of a computer, determined by the bit size. Today the number of bits available means that the discrete signal is as precisely known as the digital signal.

The development of electromagnetic theory and the growth of electrical and electronic communications technologies required mathematics suitable for signal processing, communications, signal analysis, and information theory. In particular, at the beginning of the twentieth century, Fourier discovered that very general classes of functions, even those containing discontinuities, could be represented by sums of sinusoidal functions, now called a Fourier series [113].

Research efforts into discrete techniques progressed, slowly at first because – for example – while discrete Fourier series calculations were widely understood they were seldom carried out because they required extensive and intensive calculations with pencil and paper. In the 1920s Nyquist found the first theoretical links between analogy and discrete signals [114].

Shannon developed Nyquist's discovery with his famous sampling theorem [115]. He also proved something to be feasible that was previously thought possible: the possibility of error free digital communication over noisy channels.

With technological advances there was the appearance of digital computers, and at the level of theory Cooley's and Tukey's discovery of the fast Fourier transform (FFT) [116–118]. The combination of these two developments made digital computations of Fourier's series practical for real-time signal data.

Today digital systems are the cores of almost all signal processing and analysis systems and analogue techniques handle only the early signal input. A wide variety of texts are available for signal processing, see for example [119–123]. Many presuppose a background in analogy signal processing [124–127].

Discrete signals of interest here are obtained by taking instantaneous samples from analogue signals. They might assume irrational values at some time instants, and the range of their values might be infinite but a digital computer has memory elements that can hold only limited precision values.

This technology has created a true digital signal processing literature, comprised of the technical manuals for various Digital Signal Processing (DSP) chips, their application notes, and general treatments on fast algorithms for real-time signal processing and analysis applications on digital signal processors [126–131].

5.2 FOURIER SERIES

Mathematicians often treat Fourier series and the Fourier transform separately since they involve two different classes of functions. However, engineers have always been taught that Fourier transform is an extension of Fourier series by allowing the period T of a periodic

function to approach infinity. We will follow this route by discussing Fourier series first. The Fourier series representation of a real-valued periodic function *p (t), [p (t) = p (t + T)]*, is given by:

$$p(t) = \sum_{k=1\infty}^{\infty} \propto_{k} e^{jk\omega ot} \tag{5.1}$$

with

$$\propto_{k} = \frac{1}{T} \int_{t_0}^{t_0+T} p(t) e^{-jk\omega_0 t} \tag{5.2}$$

Where α and k are the Fourier coefficients and the period T= $2\pi/\omega_0$ with ω_0 being the fundamental frequency. The set of functions $\{ e_k \} = \{e^{jk\omega 0t}$, k $\in \mathbb{Z}$ forms a complete orthogonal basis in $L^2[t_0, t_0 + T]$:

$$\int_{t_0}^{t_0+T} e_k \bar{e_\ell}\, dt = T\delta_{k,\ell} \tag{5.3}$$

The coefficient α_k written in the form of an inner product represents the orthogonal component of the function *p(t)* in $k\omega_0$:

$$\alpha_k = \frac{1}{T} \langle e^{jk\omega 0t}, P(t) \rangle \tag{5.4}$$

Hence the Fourier series is an orthogonal expansion of *p(t)* with respect to the basis set $\{e_k\}$.

The representation in (5.1) is exact. However, if we truncate the Fourier series to, say ±*N* terms (*k = −N... N)* Then there will be some error. A Fourier series may be represented in other forms. Representation using sine and cosine functions is given by

$$\mathrm{p(t)} = \frac{\mathrm{a_0}}{2} + \sum_{\mathrm{k=1}}^{\infty} (\mathrm{a_k}\ \cos \mathrm{k\omega 0t} + \mathrm{b_k} \sin \omega_0 \mathrm{t}), \tag{5.5}$$

The quantities a_k and b_k are real. Complex representation using only positive harmonics is written as:

$$p(t) = c_0 + \sum_{k=1}^{\infty} (c_k \cos(\omega 0t + \theta_k) \quad (5.6)$$

with

$$|c_k| = \sqrt{a^2 + b^2}\theta_k = \tan^{-1}\left(-\frac{b_k}{a_k}\right), \quad (5.7)$$

Where $c_k = |c_k|e^{j\theta k}$ are complex quantities, computation formulas for a_k and b_k are

$$a_k = \frac{2}{T}\int_0^T p(t)\cos k\omega_0 t \; dt, \quad (5.8)$$

$$b_k = \frac{2}{T}\int_0^T p(t)\sin k\omega_0 t \; dt, \quad (5.9)$$

5.3 FOURIER TRANSFORM

To extend the Fourier series to the Fourier transform, consider Equations (5.1) and (5.2). The time function *p(t)* in (5.1) can be expressed using (5.2) as

$$p(t) = \sum_{k=-\infty}^{\infty}\left[\frac{1}{T}\int_{-T/2}^{T/2} p(t')e^{-jk\omega_0 t'}dt\right] e^{jk\omega_0}$$

$$= \frac{1}{2\pi}\sum_{k=-\infty}^{\infty}\omega_0\left[\int_{-T/2}^{T/2} p\,(t')e^{-jk\omega_0 t'}dt\right]e^{jk\omega_0} \quad (5.10)$$

We extend the period T to infinity so that ω_0 approaches $d\omega$ and $k\omega_0$ approaches ω. The summation in (5.10) becomes an integral

$$p(t) = \frac{1}{2\pi}\int_{-\infty}^{\infty}\left[\int_{-\infty}^{\infty} p(t')e^{-j\omega t'}dt'\right] e^{j\omega t_0}d\omega \quad (5.11)$$

The integral inside the bracket is represented by a function p^(ω)

$$\hat{p}(\omega) = \int_{-\infty}^{\infty} p(t')e^{-j\omega t'}\,dt' \tag{5.12}$$

and (5.11) becomes

$$p(t) = \frac{1}{2\pi}\int_{-\infty}^{\infty} \hat{p}(\omega)e^{j\omega t}\,d\omega \tag{5.13}$$

Equations (5.12) and (5.13) are known as the Fourier transform pair. From here on, we will use *f (t)* to represent a time-domain function, while *p (t)* is restricted to representing periodic time functions. Rewrite (5.12) in the new notation, the Fourier transform of a finite energy function $f(t) \in L^2(\mathbb{R})$ of a real variable t is defined by the integral:

$$\hat{f}(\omega) = \int_{-\infty}^{\infty} f(t)e^{-j\omega t}dt \tag{5.14}$$

The Fourier transform can also be expressed as:

$$\hat{f}(\omega) = \langle f(t), e^{j\omega t}\rangle \tag{5.15}$$

$\hat{f}(\omega) = \langle f(t), e^{j\omega t}\rangle$ is a complex-valued function, which can be expressed in terms of amplitude and phase by:

$$\hat{f}(\omega) = |\hat{f}(\omega)|e^{j\emptyset(\omega)} \tag{5.16}$$

However, the mapping from the domain of $\hat{f}$ to that of $\hat{f}(\omega)$ is from $\mathbb{R}$ to $\mathbb{R}$ i.e., from the time t-axis to the frequency ω-axis, even though the real-valued function f *(t)* is mapped to a complex-valued function $\hat{f}(\omega)$, the interpretation of (5.15) is very important. This equation states that for an ω_1, $\hat{f}(\omega_1$, $\hat{f}(\omega_2)$ represents the component of *f(t)* at ω_1 If we can determine all the components of *f (t)* on the ω-axis, then a superposition of these components should give back (reconstruct) the original function *f(t)*:

$$f(t) = \frac{1}{2\pi}\int_{-\infty}^{\infty} \hat{f}(\omega)\, e^{j\omega t}\,d\omega \tag{5.17}$$

Hence (5.17) can be viewed as a superposition integral that produces *f (t)* from its components. The integral is referred to as the inverse Fourier transform of $f\hat{}\,(\omega)$. If the variable t represents time, $f\hat{}\,(\omega)$ is called the spectrum of *f (t)*.

5.4 PROPERTIES OF FOURIER TRANSFORMS

Since the focus of this chapter is not a detailed exposition of the Fourier analysis, only the properties that are relevant to wavelet analysis will be discussed.

5.5.1 LINEARITY

If $f(t) = \alpha f_1(t) + \beta f_2(t)$, for some constants α and β, then the Fourier transform is:

$$f\hat{}\,(\omega) = \int_{-\infty}^{\infty} f(t)e^{-j\omega t}\,dt = \alpha \int_{-\infty}^{\infty} f_1(t)e^{-j\omega t}\,dt + \beta \int_{-\infty}^{\infty} f_2(t)e^{-j\omega t}\,dt = \alpha f\hat{}_1(\omega) + \beta f\hat{}_2(\omega), \quad (5.18)$$

The extension of (5.18) to the finite sum of functions is trivial.

5.5.2 TIME SHIFTING AND TIME SCALING

Let the function *f(t)* be shifted by an amount t_0. The spectrum is changed by a phase shift. Indeed, the spectrum of the shifted function $f_0(t) := f(t - t_0)$ is expressed by

$$f\hat{}_0\,(\omega) = \int_{-\infty}^{\infty} f(t - t_0)e^{-j\omega t}\,dt = \int_{-\infty}^{\infty} f(u)e^{-j\omega(u+t_0)}\,du = e^{-j\omega t_0}\,f\hat{}\,(\omega) = |f\hat{}\,(\omega)|\,e^{j\emptyset(\omega)-j\omega t_0}, \quad (5.19)$$

Where φ (ω) is the phase of the original function f(t). The magnitude of the spectrum remains unchanged for a shifted signal. The shifting is incorporated into the phase term of the spectrum.

Let a be a non-zero constant; the spectrum of the shifted function $f_0(t) := f(t - t_0)$ is expressed by:

$$\hat{f}_a(\omega) = \int_{-\infty}^{\infty} f(at) e^{-j\omega t}\, dt \tag{5.20}$$

$$= \int_{-\infty}^{\infty} f(u) e^{-j\omega\left(\frac{u}{a}\right)}\, d\left(\frac{u}{a}\right) \tag{5.21}$$

$$= \frac{1}{|a|} \hat{f}\left(\frac{\omega}{a}\right) \tag{5.22}$$

Depending on whether a is greater or smaller than unity, the spectrum is expanded or contracted, respectively. We shall see that this property is important in the development of wavelet analysis.

5.5.3 FREQUENCY SHIFTING AND FREQUENCY SCALING

The results for frequency shifting and scaling follow in a similar way. If $\hat{f_0}(\omega) := \hat{f}(\omega - \omega_0)$, then

$$f_{0(t)=f(t)e^{j\omega_0 t}} \tag{5.23}$$

and if $\hat{f_a}(\omega) := \hat{f}(a\omega)$ for a nonzero value of a, then

$$f_0(t) = \frac{1}{|a|} f\left(\frac{t}{a}\right) \tag{5.24}$$

5.5.4 MOMENTS

The n order moment of a function is defined as

$$M_n := \int_{-\infty}^{\infty} t^n f(t) dt. \tag{5.25}$$

The first-order moment,

$$M_1 = \int_{-\infty}^{\infty} t\, f\,(t)dt = (-j)^{-1}\frac{d}{d\omega}\int_{-\infty}^{\infty} f(t)e^{-j\omega t}dt\,|\omega = 0$$

$$= (-j)^{-1}\frac{d\hat{f}(\omega)}{d\omega}|\omega = 0 \qquad (5.26)$$

The extension of this formula to the nth-order moment results in

$$M_n = (-j)^{-n}\frac{d^n f\quad(\omega)}{d\omega}|\omega = 0 \qquad (5.27)$$

5.5.5 CONVOLUTION

The convolution of two functions $f_1\,(t)$ *and* $f_2\,(t)$ is defined by:

$$f(t) = \int_{-\infty}^{\infty} f_1(y)f_2(t-y)dy \qquad (5.28)$$

We write (5.28) symbolically as:

$$f(t) = f_1(t) * f_2(t) \qquad (5.29)$$

Notice that if f_2(t) is δ (t), the convolution integral recovers the function f_1 (t). It is well known that a linear system has the input–output relation given by:

$$O\,(t) = h\,(t) * i\,(t) \qquad (5.30)$$

Where *h (t)* is the system response functions. Hence if *i (t)* is a delta function, the output function *O (t)* is the same as *h (t)*. For an arbitrary input function *f (t)* the convolution integral represents a superposition of the output due to a series of input delta functions whose amplitudes are modulated by the input signal.

$$O\,(t) = \int_{-\infty}^{\infty} h(\tau)i(t-\tau)d\tau \qquad (5.31)$$

It is easy to show that the spectral domain representation of the convolution integral of (5.28) is given by:

$$\hat{f}(\omega) = \hat{f_1}(\omega)\,\hat{f_2}(\omega) \tag{5.32}$$

5.6 BASIC FOURIER TRANSFORMS ANALYSIS

The Fourier transform is not easily interpreted because we must consider functions defined from -∞ to +∞. The Fourier transform of a given waveform is to decompose or separate the waveform into a sum of sinusoids of different frequencies. If these sinusoids sum to the original waveform (within an agreed accuracy) then we have determined the Fourier transform of the waveform. A straightforward interpretation of the Fourier transform is illustrated in Figure 5-37. It can be seen that as more terms are added the sum approaches the square wave with increasing accuracy.

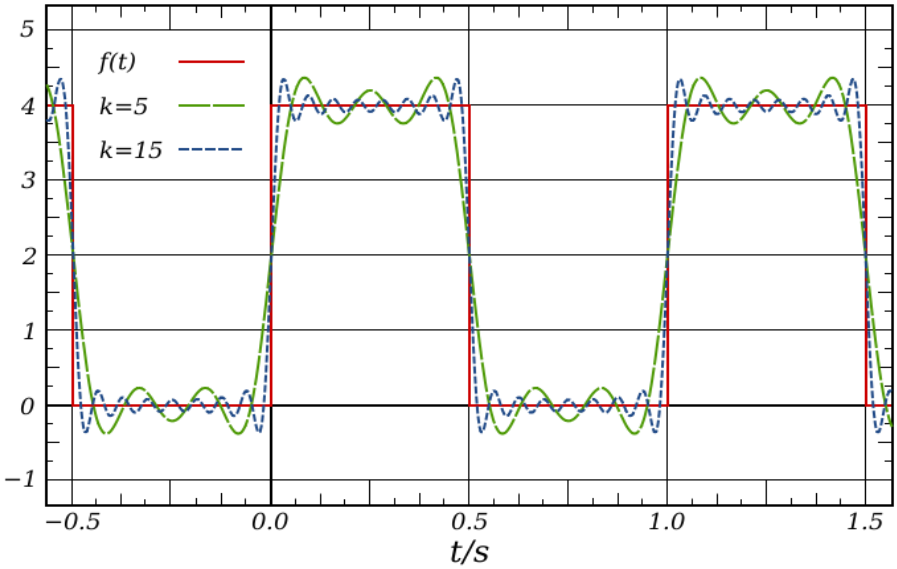

FIGURE 5-37: FOURIER TRANSFORM OF A SQUARE PULSE WAVEFORM

The pictorial representation of the Fourier transform is a diagram, which displays the amplitude and frequency of each of the determined sinusoids. The Fourier transform of the

example waveform is the two sinusoids that add to yield the waveform. As shown, the Fourier transform diagram displays both the amplitude and frequency of each of the sinusoids

The usual convention is to display both positive and negative frequency sinusoids for each frequency; the amplitude has been halved accordingly. The Fourier transform then decomposes the example waveform into its two individual sinusoidal components. The Fourier transform identifies or distinguishes the different frequency sinusoids (and their respective amplitudes), which combine to form an arbitrary waveform. Mathematically, this relationship is stated as

$$S(f) = \int_{-\infty}^{\infty} s(t) e^{-j2xft}\, dt \qquad (5.33)$$

Where *S(t)* is the waveform to be decomposed into a sum of sinusoids, *S(f)* is the Fourier transform of *S(t)*, and $j = \sqrt{-1}$.

If the waveform *s(t)* is not periodic then the Fourier transform will be a continuous function of frequency; that is, *s (t)* is represented by the summation of sinusoids of all frequencies. For example, consider the square pulse waveform and its Fourier transform as shown in Figure 5-1. Here the Fourier transform indicates that one sinusoid frequency becomes indistinguishable from the next and, as a result, all frequencies must be considered and then the Fourier transform is then a frequency domain representation of a function.

Typical applications of the Fourier transform include:

- ***Linear Systems.*** The Fourier transform of the output of a linear system is given by the product of the system transfer function and the Fourier transform of the input signal [134].

- ***Antennas.*** The field pattern of an antenna is given by the Fourier transform of the antenna current illumination [135].

- ***Optics.*** Optical systems have the property that a Fourier transform relation exists between the light amplitude distributions at the front and back focal planes of a converging lens [136].

- ***Random Process.*** The power density spectrum of a random process is given by the Fourier transform of the auto-correlation function of the process [137].

- ***Probability.*** The characteristic function of a random variable is defined as the Fourier transform of the probability density function of the random variable [138].

- ***Quantum Physics.*** The uncertainty principle in quantum theory is fundamentally associated with the Fourier transform since particle momentum and position are essentially related through the Fourier transform [139].

- ***Boundary-Value Problems.*** The solution of partial differential equations can be obtained by means of the Fourier transform [140].

5.7 THE LIFTING SCHEME

The lifting scheme is used to construct wavelets and perfect reconstruction (PR) filter banks. Biorthogonal filter banks having integer coefficients can be easily implemented and can be used as integer-to-integer transform. The two-channel system in Equation (5.33) shows the lifting scheme. The first branch is operated by $A_\circ$ and called dual lifting whereas the second branch is operated by A_1 and is called lifting. We can see that the system is PR for any choices of $A_\circ$ and A_1. It should be noted that $A_\circ$ and A_1 can be nonlinear operations like

rounding or flooring operations, etc. Flooring a value means rounding it to the nearest integer less than or equal to the value.

5.8 FIXED-POINT ARITHMETIC IMPLEMENTATION

One of the factors that primarily affect the cost of the DSP implementation is the resolution of the internal nodes (the size of the registers at each stage). In practice, it is impossible to retain infinite resolution of the signal samples and the transform coefficients. Since the floating-point operation is very expensive, these numbers are often quantized to a fixed number of bits. Two's-complement arithmetic for fixed-point representation of numbers is a system in which negative numbers are represented by the two's complement of the absolute value; this system represents signed integers on hardware, DSP and computers (Table 3).

Each addition can increase the number of bits by one, whereas each multiplication can increase the number of bits by 2^{nd} bits for the multiplication of two n-bit numbers. The nodes in latter stages require more bits than those in earlier stages to store the output after each arithmetic operation without overflows.

As a result, the number of bits required to store the results grows cumulatively as the number of stages increases. In general, the number of bits at each internal node is fixed to a certain number of bits. The Most Significant Bit (MSB) of the result after each operation will be kept up to a certain number of bits for each internal node, and the tail will be truncated. However, this conventional fixed-point arithmetic affects the invariability of the transform because the Discrete Fourier Transform (DFT) coefficients are quantized. Lifting scheme is a way to quantize the DFT coefficients that preserves the invariability property [134,139].

The integer FFT and fixed-point FFT are compared in noise reduction application (Table 4). At low power, i.e., the coefficients are quantized to low resolution, the IntFFT yields

significantly better results than the FxpFFT, and they yield similar results at high power [134,139].

While for two and higher dimensions, the row-column method, the vector-radix FFT and the polynomial transform FFT algorithms are commonly used fast algorithms for computing Multidimensional discrete Fourier Transform (M-D DFT).

Table 3: Computational complexities (the numbers of real multiplies and real adds) of the split-radix FFT and its integer versions (FxpFFT and IntFFT) when the coefficients are quantized/ rounded off to Nc ¼ 10 bits at each stage. [I-6]

N	Split-radix FFT		FxpFFT		IntFFT	
	Adds	Multiplies	Adds	Shifts	Adds	Shifts
16	20	148	262	144	202	84
32	68	388	746	448	559	261
64	196	964	1910	1184	1420	694
128	516	2380	4674	2968	3448	1742
256	1284	5380	10990	7064	8086	4160
512	3076	12292	25346	16472	18594	9720
1024	7172	27652	57398	37600	41997	22199

Table 4: Number of nontrivial complex multiplies. A set of complex multiply is three real multiplies [33]

N	Radix-2	Radix-2^2	Split-radix
16	10	8	8
64	98	76	72
256	642	492	456
1024	3586	2732	2504

5.9 DIGITAL COMPUTER FOURIER ANALYSIS.

Numerical integration of Equation (5.33) implies:

$$S(f) = \sum_{-i=0}^{N-1} s(t_i) e^{-j2xfk^{t_1}} (t_{i+1} - t_i) \qquad k = 0, I, \ldots, N - I \qquad (5.34)$$

For those problems, which do not yield to a closed-form Fourier, transform solution, the discrete Fourier transform (5-34) offers a potential method of attack. However, careful inspection of (5-34) reveals that if there are *N* data points of the function t_i and if we wanted to find the amplitude of *N* separate sinusoids, then computation time was proportional to N^2, thus the Discrete Fourier Transform required excessive machine time for large *N*. In 1965 Cooley and Tukey published their computational algorithm [141], the "Fast Fourier Transform" (FFT), which reduced the computing time of equation to a time proportional to *N* $\log_2 N$, which has completely revolutionized many facets of scientific analysis [137,138].

5.10 THE FOURIER INTEGRAL

The Fourier integral is defined by the expression:

$$H(f) = \int_{-\infty}^{\infty} h(t)e^{-j2\pi}\ dt \quad (5.35)$$

If the integral exists for every value of the parameter *f*, then Eq. (5.35) defines *H(f)*, the Fourier transform of *h(t)*. Typically, *h(t)* is termed a function of time and *H(f)* is termed a function of the frequency. In general, the Fourier transform is a complex quantity:

$$H(f) = R(f) + J(f) = |H(f)|\, e^{j\theta(f)} \quad (5.36)$$

where

- *R(f)* is the real part of the Fourier transform,
- *J(f)* is the imaginary part of the Fourier transform,
- $|H(f)|$ is the *amplitude* or *Fourier spectrum* of *h(t)* and is given by $\sqrt{R^2}(f) + J^2\ (f)$, and
- $\theta(f)$ is the phase angle of the Fourier transform given by $tan^{-1}[\frac{I(f)}{R(f)}]$.

5.11 FFT RESULTS DISCUSSIONS

It is usual to describe sequential signal values as given by time. This is often, but not always, the case; some signals can depend upon a distance measure. It is also possible, and sometimes a very important analytical step, to consider signals as given by order relative to a salient event. However, whether the independent variable is time, some spatial dimension, or a counting of events, when we represent and discuss a signal in terms of its ordered values, we will call this the time-domain description of the signal. Time domain signatures as displayed on an oscilloscope for five sets of experimental results (healthy (A), 1 mm hole at 25% (B) , 50% (C), 75% (D) and 100% depth (E) respectively) as recorded by MatLab software are shown in Figure 5-38. Zoomed results are shown in Figure 5-39, and it can be seen that there are no clear differences between the “healthy” wave and those waves where a hole was present, though differences between the waves with different depth holes is not apparent.

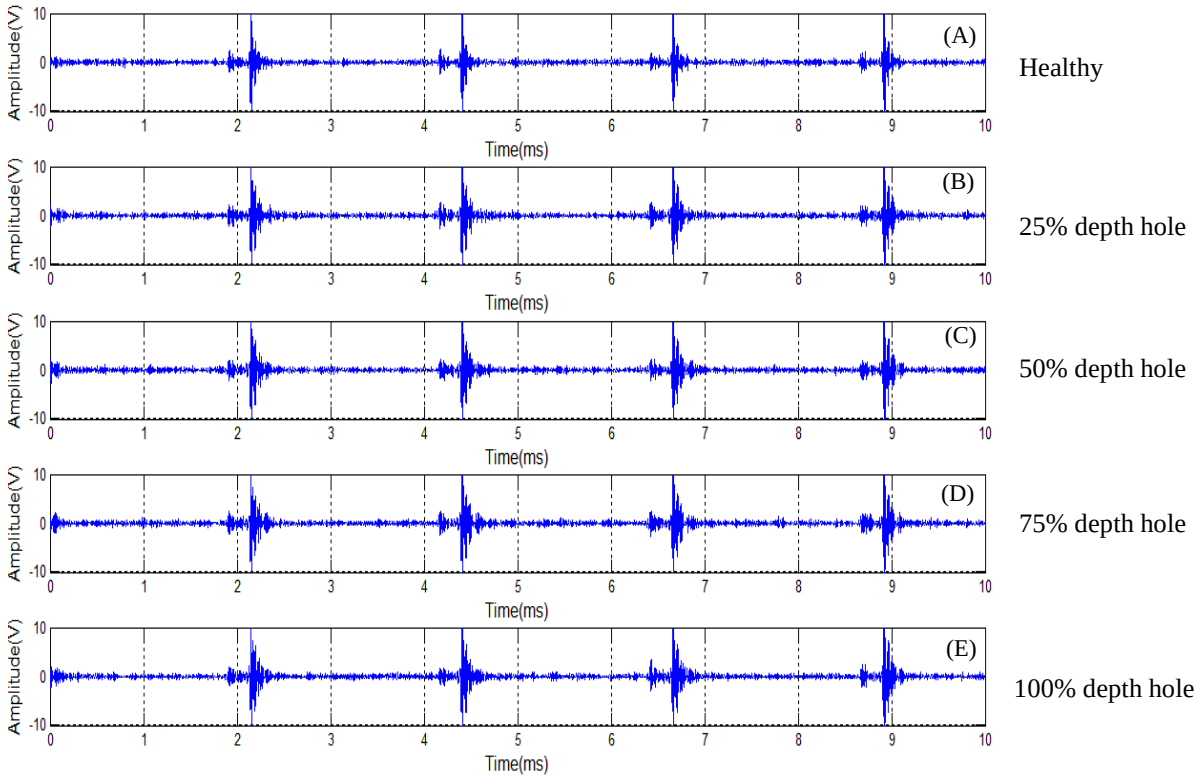

FIGURE 5-38: TIME DOMAIN SIGNATURES FOR FIVE SETS OF EXPERIMENTAL RESULTS (HEALTHY (A), 1 MM HOLE AT 25% (B) , 50% (C), 75% (D) AND 100% DEPTH (E) .

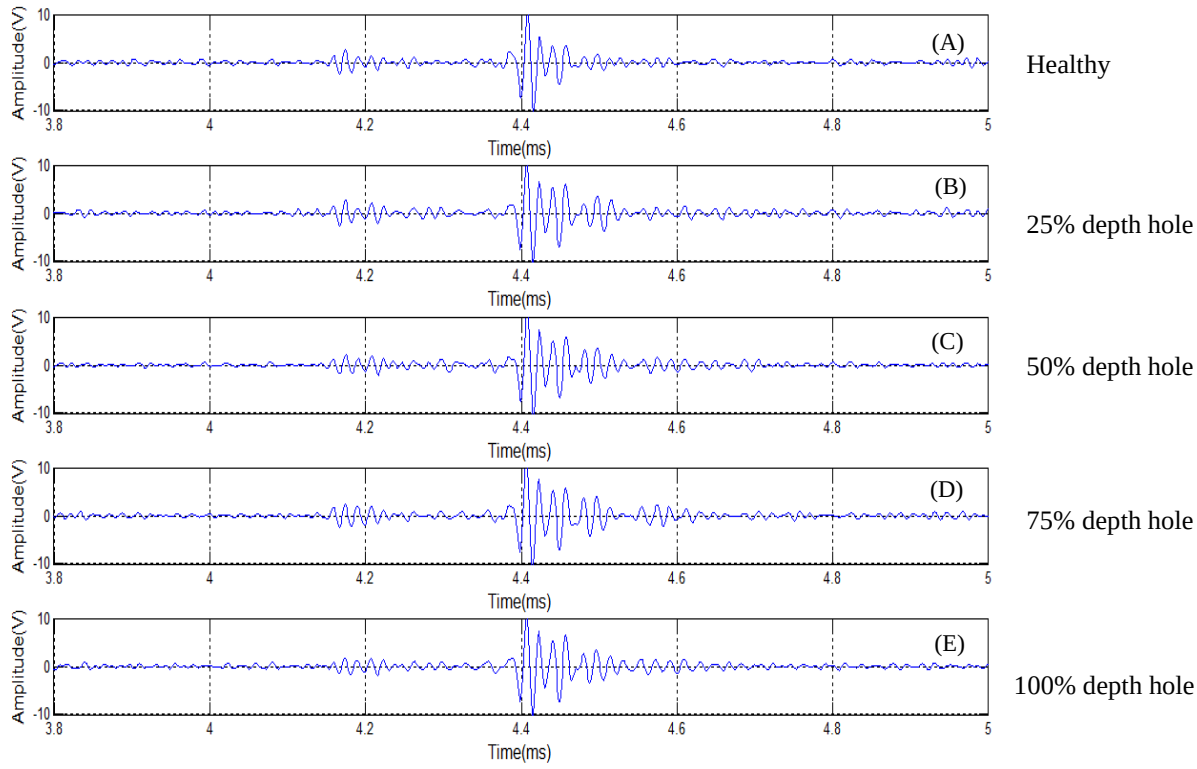

FIGURE 5-39: ZOOMED TIME DOMAIN SIGNATURES FOR FIVE SETS OF EXPERIMENTAL RESULTS (HEALTHY (A), 1 MM HOLE AT 25% (B) , 50% (C), 75% (D) AND 100% DEPTH (E) .

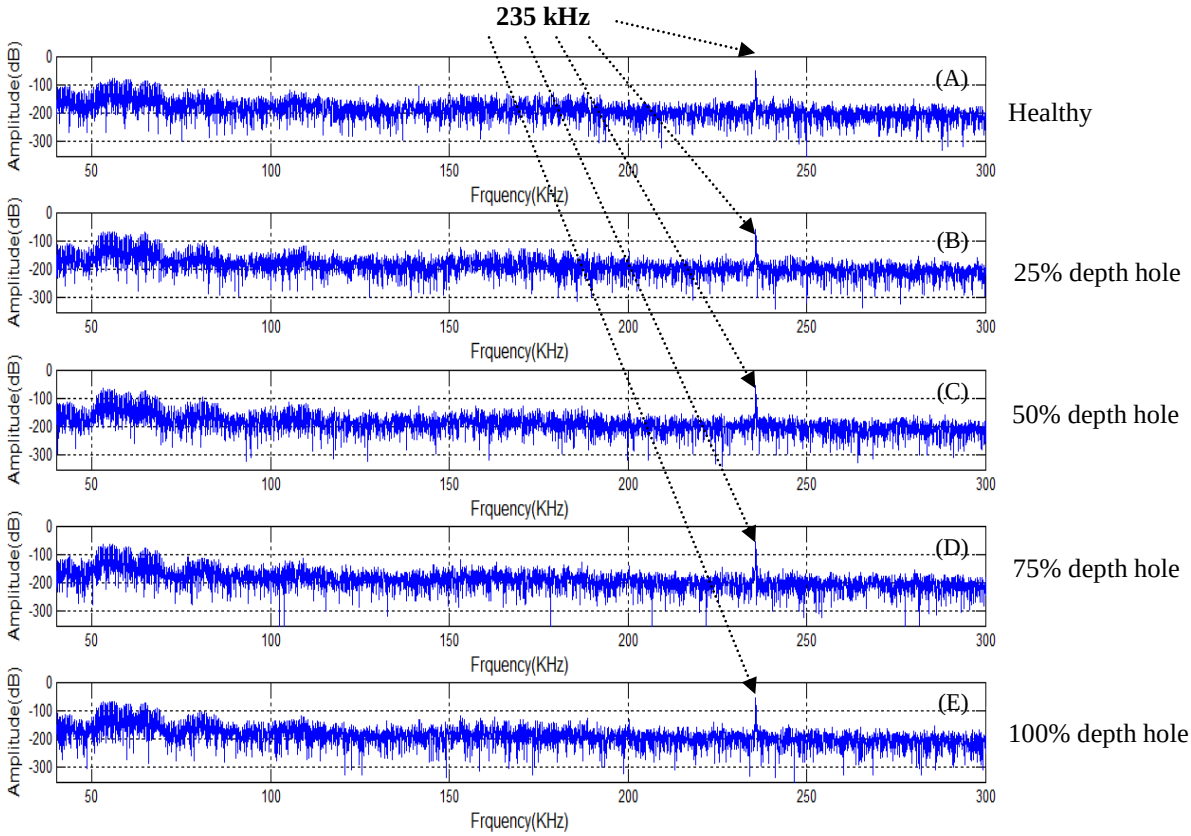

FIGURE 5-40: FREQUENCY DOMAIN SIGNATURES FOR FIVE SETS OF EXPERIMENTAL RESULTS (HEALTHY (A), 1 MM HOLE AT 25% (B) , 50% (C), 75% (D) AND 100% DEPTH (E) .

The frequency domain signature Figure 5-40 above does not show any clear differences at experimentally used frequency (235.0 KHz) and that led to consider those conventional techniques are not sufficient for this type of analysis's which lead to go for advanced techniques as its results are evident in the next chapter.

CHAPTER VI

WAVELET TECHNIQUES

This chapter serves as a brief introduction to the main features of the wavelet transform by comparing wavelet transform with the Fourier transform, pointing out the main differences. This chapter also provides advanced ultrasound techniques used in research and discusses the findings that resulted from the analysis of the continuous wavelet transform; it became clear that these techniques are effective and are suitable for the purposes of comparison between signatures of various models.

6.1 INTRODUCTION

Wavelet analysis had its origins in the mid-eighties. From the very beginning it was driven by application needs and the new technique could be applied successfully to numerous theoretical and practical problems in signal processing. For one of the earliest collections of research and survey papers the reader is referred to [6].

In particular, the detection of discontinuities or irregularities was tackled with wavelets; analysis of electrocardiograms was one of the first reported examples of discontinuity detection [6]. Signal compression is another impressive example of wavelet applications. JPEG 2000, the present version of the international standard on still image compression is based on wavelet techniques [36]

The Fourier transform is probably the most widely used technique to transform the time-domain signal into the frequency-domain but in the process, time information is lost. The Fourier transform of a signal contains no information on when a particular event occurred. This is not a problem for stationary signals which repeat themselves, but can be important when investigating/monitoring the growth of faults where transitory phenomena often constitute the most significant part of the signal.

In an effort to correct this deficiency, the Fourier transform was adapted to analyse only a small section of the signal at a time, a technique called windowing the signal [134]. Essentially Gupta divided the time-domain signal into a series of contiguous sections and the signal contained in each section (or window) is then transformed into the frequency domain. Of course, mathematically the process is not so simple, as the window is a multiplying function, which must be tailored to avoid introducing spurious results. Today a large number of such windows are available and most have the property that the initial and final values are close to zero so that the transform does not “see” the time-domain signal as a series of step

functions. This process is known as the Short-Time Fourier Transform (STFT) and produces a series of spectra, one for each window. As the duration of each window is known the spectra can be layered into a three-dimensional plot (frequency, time and amplitude).

The two drawbacks with this method are: (i) Once a particular window size has been selected it cannot then be changed but many signals can require more precision in determining frequency at some times, than at others, (ii) The uncertainty principle means that good resolutions in both time and frequency-domains cannot be achieved simultaneously. For example, if the signal to be analysed is of short duration, obviously a narrow window should be selected, but the narrower the window the wider the associated frequency band and the poorer the frequency resolution.

The increasing popularity of wavelet transform has meant that today its use rivals that of the Fourier Transform (FT) or Fourier series particularly for time varying signals. Comparing the two, the wavelet transform (WT) uses a so-called mother wavelet instead of the exponential scaling of the FT and translation replaces frequency shift. The essential difference is that a two-dimensional (surface) wavelet coefficient replaces the single dimension Fourier coefficient. The consequent advantage of the WT is that it can provide an analysis that contains information in both the time and frequency domains.

Wavelets used to analyze signals are mathematical functions, which are limited with definite end points along their axis – unlike the sine and cosine functions of the FT they do not repeat to infinity. This makes wavelets different from other transformations because not only can they divide time domain signals into their component frequencies, they can also be expand or compress the (time) scale over which the frequencies are analyzed. This allows the scale to be matched to the required resolution of the signal and gives the WTs the ability to treat non-stationary signals. Thus the WT is used increasingly used for condition monitoring of rotating

machinery, to diagnose the presence of faults such as bearing defects, rotor cracks, rotor misalignment and unbalance, etc. Recently WTs have also been applied to detect stable and propagating cracks.

6.2 TRANSFORMS

All transforms of the signal f (t) described in this section share a common computation principle: The signal is multiplied with a certain "analysis function" and integrated about the time domain. In a symbolic notation the prescription for performing a transform reads

$$f(t)transform \rightarrow \int_{-\infty}^{\infty} f(u)g\bar{u}du \tag{6.1}$$

The "analysis function" g (u) characterizes the chosen transform. In general it may be a complex function; the over line denotes the complex conjugate entity. g (u) in a certain way depends on the parameters, i.e. frequencies or detail sizes to be measured (see below). Thus, by the computation principle given above the transformed entity will be a function that depends on these parameters.

6.3 FOURIER TRANSFORM

The parameter relevant for the Fourier transform is the circular frequency ω, the analysis function reads: $g_{\omega}(u) = e^{ju\omega}$. Thus the transformed signal is a function depending on ω and it is denoted with $f\hat{}$ (ω):

$$f\hat{}(\infty) = \int_{-\infty}^{\infty} f(u)\overline{g_{\omega}(u)}du \tag{6.2}$$

Figure 6-41 illustrates the above computation recipe by plotting both curves required for computing f̂ (π). The signal is shown as a solid curve, the real part of the analysis function $g\pi$ (u) = $e^{ju\pi}$ is dashed. Obviously, it is a harmonic oscillation with circular frequency ω = π.

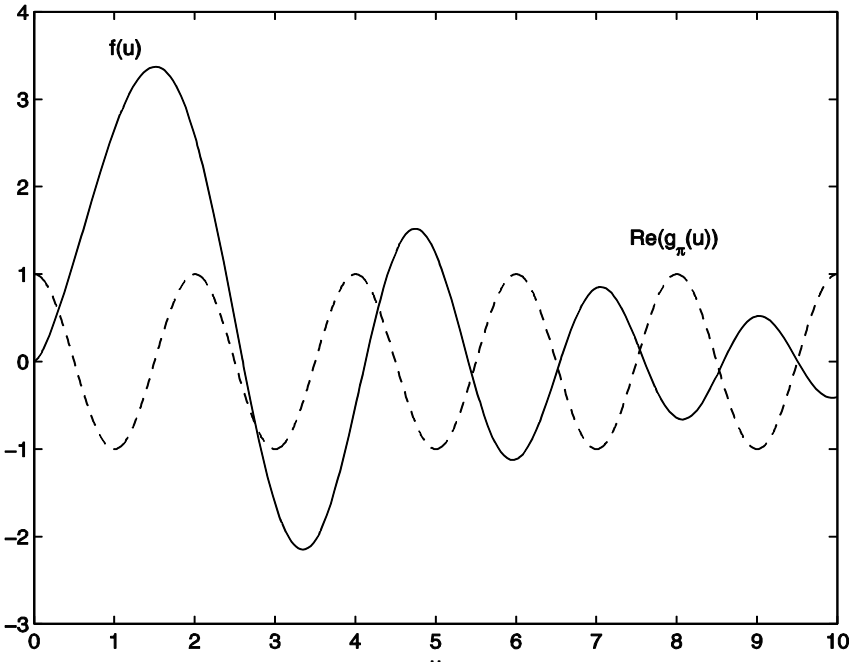

FIGURE 6-41: FOURIER TRANSFORM: SIGNAL AND ANALYSIS FUNCTION (SOLID LINE IS SIGNAL, DOTTED LINE IS REAL PART OF THE ANALYSIS FUNCTION)

The qualitative argument is as follows: If in some time interval the signal oscillates with circular frequency $\omega = \pi$, the signal and the analysis function have a constant mutual phase shift in this interval and therefore provide a nonzero contribution to $\hat{f}(\pi)$.

Yet there is no possibility to localize the appearance of the circular frequency: If (the absolute value of $\hat{f}(\pi)$ is "large", we only know that the signal contains the circular frequency π, but we do not know where it appears, since the analysis function extends over the completely real axis. The only label parameterizing the analysis function is circular frequency.

6.4 SHORT TIME FOURIER TRANSFORM (STFT)

This transform sometimes also is called the "Windowed Fourier Transform". The STFT looks for the appearance of the circular frequency ω at a certain time t. The corresponding analysis function reads:

$g_{(\omega,t)}(u) = e^{ju\omega}$ w (u − t). Here *w (u)* is a "window function", usually centred about the origin (for an example see below). In the expression *w (u − t)* this window is shifted to the desired time, *t*. Now the transformed signal depends on ω and *t*, it also will depend on the shape of the window function, it is denoted with $\hat{f}_w(w,t)$

$$\hat{f}_w(w,t) = \int_{-\infty}^{\infty} f(u)\overline{g_{(\omega,t)}(u)}du \qquad (6.4)$$

For a box window *w* of width 2, centred symmetrically about 0, $\omega = \pi$ and $t = 8$, the computation principle is illustrated in Figure 6-42. Again the dashed curve shows the real part of the analysis function *g (π, 8) (u)*; it is obviously now localized at t = 8, since *w* (*u* − 8) denotes the box window, shifted by 8 units to the right.

In general, the analysis function will be localized at the respective "analysis time" *t*. Therefore, the transform provides not just global information about the appearance of a certain circular frequency, but in addition the time of this appearance.

The procedure described so far has a disadvantage: If in the above example one is interested in small details of the signal around $t = 8$, the corresponding frequency of the analysis function must be increased. As an example Figure 6-42 is redrawn for $\omega = 6\pi$ in Figure 6-43.

The window width is constant and non-adaptive, thus if one is interested in signal details (high frequencies) in only a small neighbourhood of $t = 8$, eventually signal parts, which actually are "not of interest", also will be analysed. Zooming into small details - analogously to a microscope is not supported.

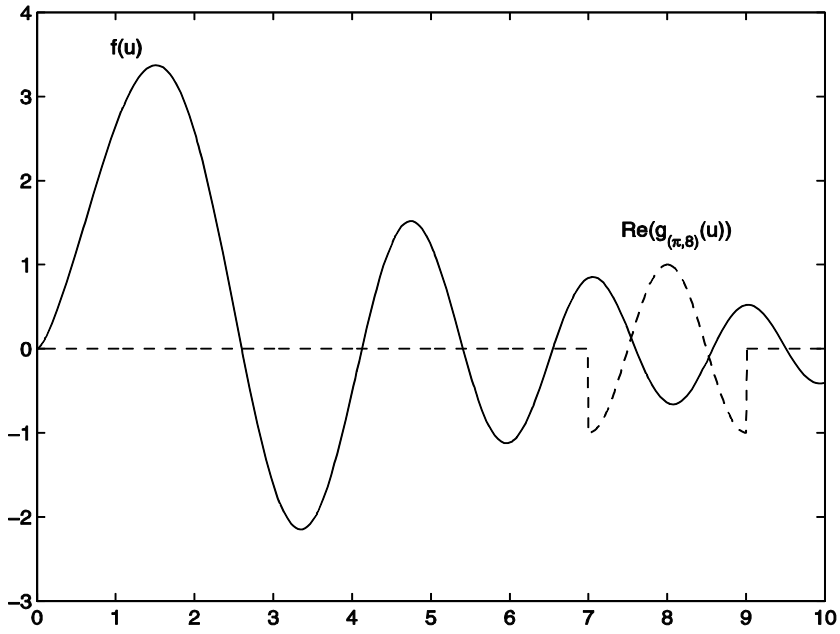

FIGURE 6-42: STFT: SIGNAL AND ANALYSIS FUNCTION FOR Ω = Π

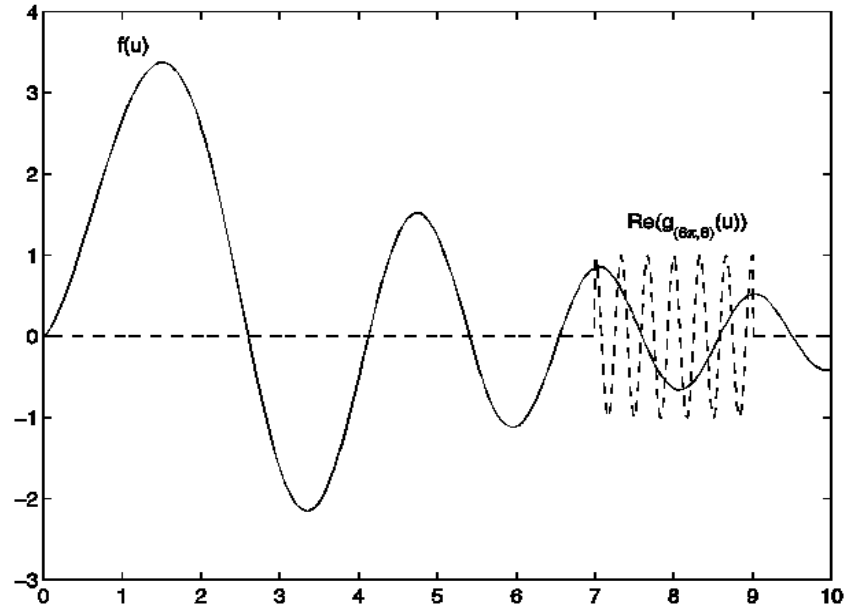

FIGURE 6-43 STFT: SIGNAL AND ANALYSIS FUNCTION FOR Ω = 6Π

6.5 WAVELET TRANSFORM

The wavelet transform (WT) has the property of being able to vary the duration of the "window". In contrast to the Fourier transform, the wavelet transform does not look for

circular frequencies but rather for detail sizes at a certain time *t*. Instead of detail sizes we also will speak of "scale factors", both notions will be used equivalently. As mentioned already, high frequencies correspond to small details and vice versa, thus, when comparing wavelet with Fourier transforms we have to take into account that frequencies and detail sizes are inversely proportional to each other: There exists a constant β such that

$$a = \frac{\beta}{\omega} \tag{6.5}$$

To briefly indicate, how the WT is computed, consider a (real or complex) analysis function *g*, oscillating around the *u*-axis such that $\int_{-\infty}^{\infty} g(u)du = 0$ and decreasing rapidly for $u \to \pm\infty$.

Such a function is called a "wavelet".

In Equation 6.5, relating scale factors with frequencies, the constant β depends on g where: $g_{(a,t)}g(u) = \frac{1}{\sqrt{a}}\, g\left(\frac{u-t}{a}\right)$. The members of this family are generated from g by shifting the function to *t* followed by shrinking (a < 1) or dilating (a > 1) the width of the function. The WT now reads:

$$L_g f(a,t) = \int_{-\infty}^{\infty} \overline{f(u)g_{(a,t)}(u)}du \tag{6.6}$$

For the "Haar-wavelet" the computation of $L_g f\,(a,\, t)$ with a = 1/2 and t = 8 is illustrated in Figure 6-45.

$$g\,(u) = \begin{cases} 1 & 0 \le u < 1/2 \\ -1 & 1/2 \le u < 1 \\ 0 & else \end{cases} \tag{6.7}$$

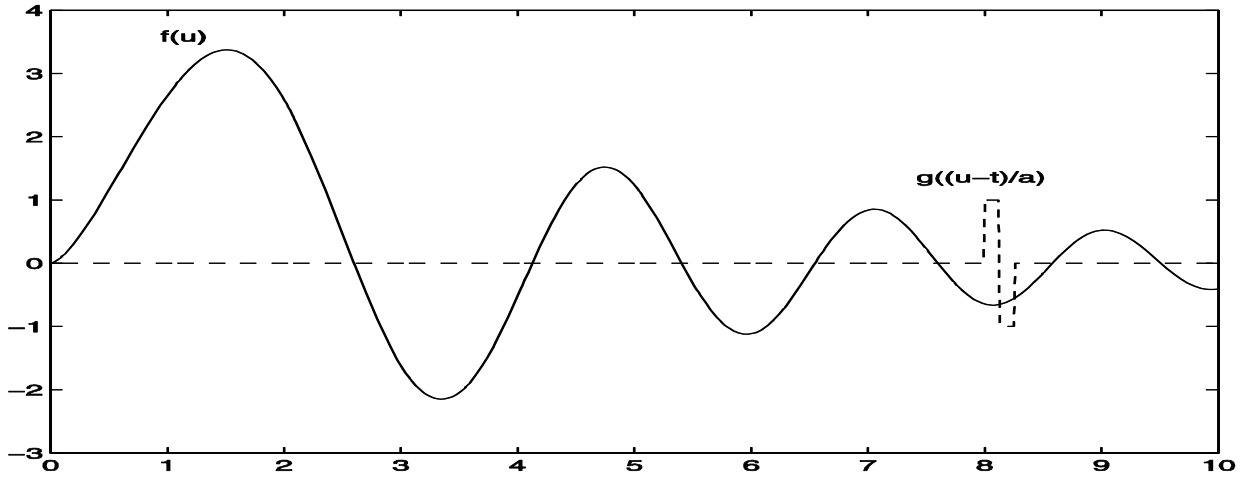

FIGURE 6-45: WAVELET TRANSFORM: SIGNAL AND ANALYSIS FUNCTION $a = -$:

The Haar-wavelet, originally situated in the interval [0, 1] now has been shifted to the right by 8 units and its width has shrunk by the factor 1/2, corresponding to the chosen values of *t* and *a*. For *a* = 1/4 and *t* = 8 we obtain Figure 6-46.

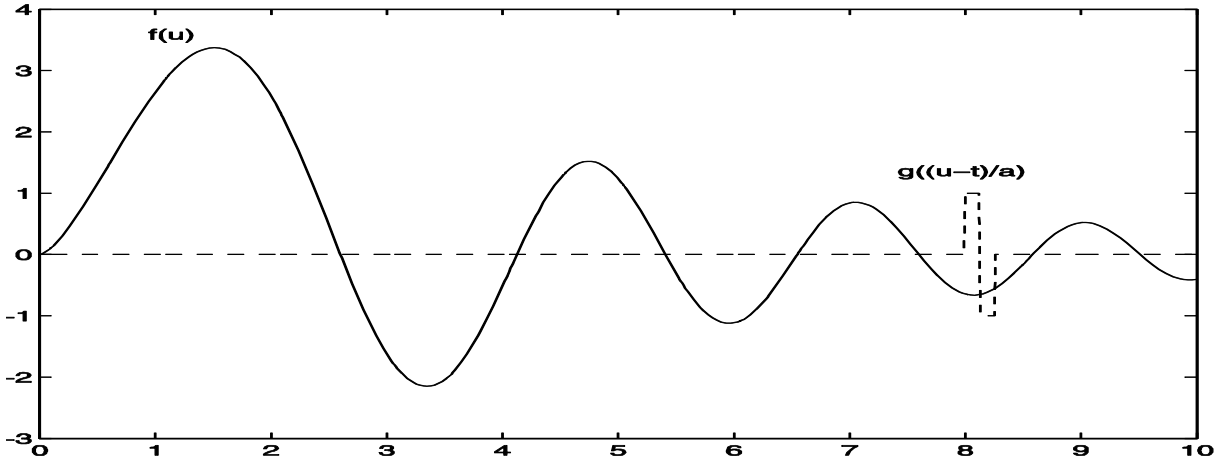

FIGURE 6-46: WAVELET TRANSFORM: SIGNAL AND ANALYSIS FUNCTION $a = -$:

Compare Figures 6-43 and 6-44 with Figures 6-45 and 6-46 and note that the WT shows the desired zooming property in contrast to the STFT. When searching for smaller and smaller details (higher and higher frequencies) with the WT, the corresponding analysis function oscillates faster and is more contracted.

6.6 VISUALIZATION

Both the STFT $f_w(\omega, t)$ and the wavelet transform $L\ f_g\ (a, t)$ are functions that depend on two variables. A suitable visualization of these functions is of essential importance in signal analysis. A widespread graphical representation of two-dimensional functions is the use of contour lines. In signal analysis one usually prefers the visualization of the absolute values of the respective transforms by grey values. High values are coded with bright, low values with dark grey values. Figure 6-46 shows such visualization for the STFT and the WT "chirp" signal $f(t) = \sin(t^2)$.

Since the STFT depends on t and ω, the grey value coding of the STFT has been performed on the t-ω-plane. This plane is also called "phase plane", the corresponding grey value coding "phase space representation" of the STFT. Analogously the t-a-plane is called "scale plane" and the corresponding grey value coding of the wavelet transform "scale space representation" of the wavelet transform.

The increase in frequency with time is clearly visible with the STFT. Equation 6.5 shows a and frequency ω are inversely proportional to each other, for the WT one would expect a behaviour corresponding to a hyperbola and the lower part of Figure 6-47 shows exactly this behaviour.

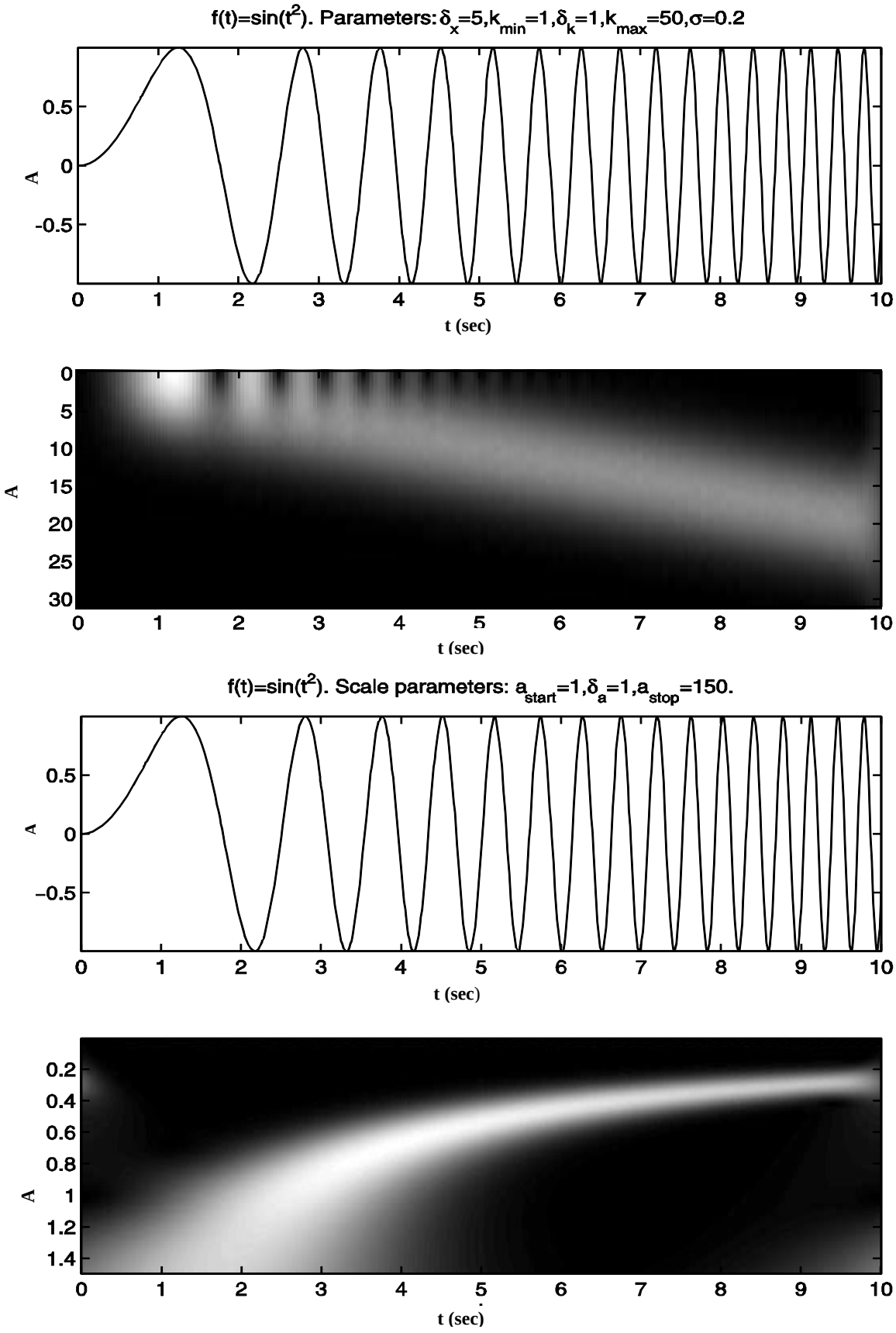

FIGURE 6-47: TOP - STFT OF THE CHIRP-SIGNAL; BELOW - WAVELET TRANSFORM OF THE CHIRP-SIGNAL F (T) = SIN (T^2).

6.7 THE CONTINUOUS WAVELET TRANSFORM (CWT)

Using the symbol ψ for the wavelet in accordance with general use (e.g.), a finite energy function $\psi(t)$ fulfilling the "admissibility condition" is:

$$c_\psi = 2\pi \int_{-\infty}^{\infty} \frac{|\psi\hat{}(\omega)|^2}{|\omega|} d\omega < \infty \tag{6.7}$$

Any finite energy function satisfying Equation (6.7) will be called a "wavelet"; the continuous wavelet transform (CWT) of the signal $f(t)$ is denoted as $L\psi f(a, t)$:

$$L_\psi f(a,t) = \frac{1}{\sqrt{c_\psi}} \frac{1}{\sqrt{|a|}} \int_{-\infty}^{\infty} \bar{\psi}\left(\frac{u-t}{a}\right) f(u) du \; (a \neq 0), (t \in \mathcal{R}) \tag{6.8}$$

Where the over line denotes complex conjugation if $\psi(t)$ is complex valued. It should be noted that:

1. When comparing Equation (6.8) with Equation (6.7), for simplicity in the latter the constant factor $\frac{1}{\sqrt{c_\psi}}$, related to the admissibility condition of Equation 6.7, has been omitted.

2. For practically relevant wavelets the admissibility condition of Equation 6.7 is fulfilled, when

$$\int_{-\infty}^{\infty} \psi(t) dt = 0 \tag{6.9}$$

Thus, ψ will oscillate around the t-axis, since the contributions of positive and negative values to the total area, bounded by the function graph and the t-axis, must cancel each other. Since, moreover, $\psi(t)$ is of finite energy, for $t \rightarrow \pm\infty$ the function $\psi(t)$ will decrease rapidly. Both facts taken together explain the term "wavelet" for the function $\psi(t)$.

3. The CWT shown in Equation (6.8) is a kind of multi resolution analysis, since $L\psi f(a, t)$ provides information about signal details of size $\approx a$, and as explained above a is called the

scale factor and since the proportionality constant in Equation (6.5) depends on the wavelet, the correct relation reads:

$$a = \frac{\beta_\psi}{\omega} \tag{6.10}$$

6.8 FOURIER TRANSFORM VS. WAVELETS - A COMPARISON EXPERIMENT

In a certain sense, the zoom property of the wavelet transform ensures that characteristics of the analysed signal are well represented by the transform values. Moreover, these transform values will be localized at the respective signal parts, where the features are present. These concentration properties both with respect to scale and with respect to time may be formulated mathematically in a more rigorous way; the purpose of this section is, to give a plausible argument for the above statement by performing a comparison experiment with the Fourier transform.

The signal displayed in Figure 6-48 is a section from the beginning of an audio signal. Roughly in the middle, the sudden increase in amplitude can be clearly seen.

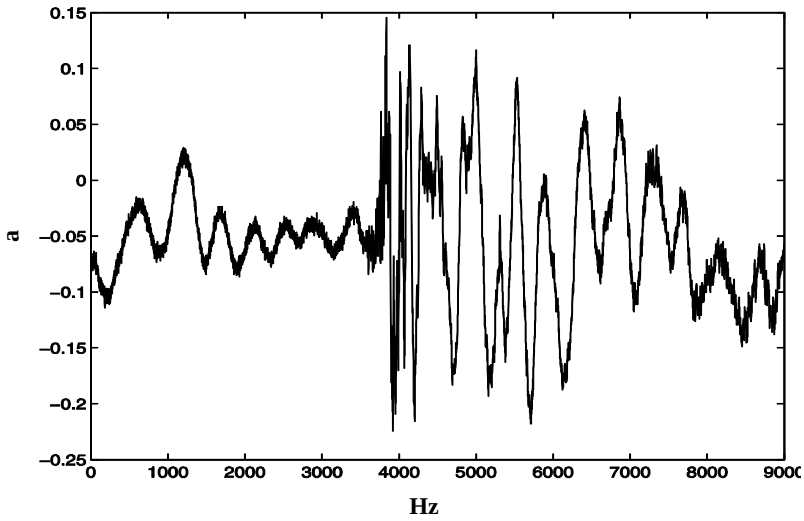

FIGURE 6-48**:** ATTACK-SIGNAL

Such “attack signals” locally, in the neighbourhood of the point at which there is a sudden increase in amplitude contain high frequencies, equivalently it can be said there are drastic changes on a small scale. In such a situation, the zoom property of the wavelet transform should be advantageous when compared with the Fourier transform. To confirm this conjecture, the following experiment was performed:

1- Compute the Fourier transform of the signal, keep those 4% of the values of the transformed signal, having the largest absolute values. Put the remaining transform values equal to zero and reconstruct the signal from this modified transform.

2- Perform the same procedure with the wavelet transform.

The results of the experiment are shown in Figure 6-49. The dashed curve shows the result of the Fourier-reconstruction, the wavelet-reconstruction is displayed by the + symbols; the solid line represents the original signal. The curve represents an enlarged section of the Attack signal in the neighbourhood of the sudden increase in signal amplitude. This is a clear indication for the properties of the WT.

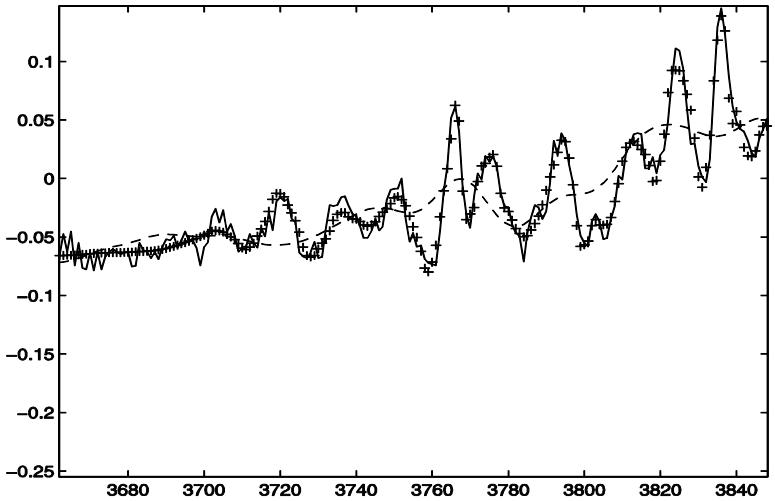

FIGURE 6-49: ATTACK-SIGNAL: RECONSTRUCTIONS (SOLID CURVE IS THE ATTACK SIGNAL. DASHED CURVE REPRESENTS RE-CONSTRUCTION FROM FOURIER TRANSFORM. CURVE WITH + SYMBOLS THE WAVELET RECONSTRUCTION)

Obviously, when using the Fourier transform, the suppression of 96% of the transform signal values - those transform signal values with lower absolute values than the retained ones - leads to a global smoothing (low pass filtering) and therefore the local peaks during the attack phase are not reproduced. In contrast, applying the same suppression procedure to the wavelet transform gives a good reproduction of the peaks in the Attack signal.

The original signal was not presented as a continuous-time signal, but was discretely sampled. For such signals, there exist variants of the continuous formulae given in Equation 6.2 and 6.6, and it was with these that the above experiment was carried out. These discrete transforms" are described in later sections. Moreover, as with any wavelet transform application, the result of the experiment depends on the chosen wavelet *g*. The results displayed in Figure 6-8 were obtained using the db4-wavelet, described in a later section.

6.9 COMPUTATION

Given a sampled signal $\{f\ (kT_s)\}_{k=0}^{N-1}$, we describe an algorithm to compute a sampled version of the CWT. As a result, we will compute the sequence $\{L_\psi f(a, kT_S)\}_{k=0}^{N-1}$ for $a \neq 0$. We describe both the algorithm and the restrictions under which it is valid.

Assume f and ψ to be band-limited and let ω_{max}^{f}, ω_{max}^{ψ} and $\omega_{max}^{\psi a}$ denote the maximum frequencies of f, ψ and ψ_a. Analogously, let ω_{max} denote the maximum frequency of $L_\psi f\ (a, t)$. Then it is not hard to show that:

$$\omega_{max}^{\psi a} = \frac{1}{|a|}\ \omega_{max}^{\psi a} \tag{6.11}$$

Now assume that the sampling is such that the Shannon condition is valid both for $f\ (t)$ and $\psi\ a\ (t)$, i.e.

$$\omega s > 2 \max \left(\omega_{max'}^{f}, \frac{1}{|a|} \omega_{max}^{\psi} \right) \tag{6.12}$$

Then the Shannon condition is automatically satisfied for $L\psi f(a, t)$:

$$\omega s > 2\omega_{max} \tag{6.13}$$

This is true, since by Equation (6.10), the spectrum of $L\psi f(a, t)$ will vanish if the spectrum of $\psi a(t)$ or the spectrum of $f(t)$ vanishes. Thus, Equation (6.11) implies Equation (6.14).

$$\omega_{max} = \min \left(\omega_{max,}^{f} \frac{1}{|a|} \omega_{max}^{\psi} \right) \tag{6.14}$$

Thus, if Equation (6.11) is valid, the spectra of $f(t)$, $\psi a(t)$ and $L\psi f(a, t)$ can be computed with the DFT and this leads to:

- Fast algorithm for the computation of $L\psi f(a, t)$ ($a \neq 0$):

    1. Define the sequence $\{\psi_a(kT_s)\}_{k=0}^{N-1}$, where ψ_a is defined this equation

$$\psi_a(t) := \left(\frac{\overline{-t}}{a}\right) \tag{6.15}$$

    2. Compute the DFT of this sequence resulting in a sequence $\{A_k\}_{k=0}^{N-1}$. then compute the DFT $\{F_k\}_{k=0}^{N-1}$ of $\{f\ (kT_s)\}_{k=0}^{N-1}$.

    3. Apply the IDFT to the product sequence $\frac{1}{\sqrt{c_\psi |a|}} \{F_k A_k\}_{k=0}^{N-1}$ to obtain $\left\{ L_\psi(a, kT_s) \right\}_{k=0}^{N-1}$.

    Schematically: $\frac{1}{\sqrt{c_\psi |a|}} \{F_k\ , A_k\}_{K=0}^{N-1} \xrightarrow{I\ DFT} \left\{L_\psi f\ (a, kT_s)\right\}_{k=0}^{N-1}$ (6.16)

6.10 RECONSTRUCTION

The following calculation shows how the Fourier transform of $\psi a(t)$ may be expressed in terms of the Fourier transform of ψ by intergrade equation 6.8

$$L_\psi f(a,t) = \sqrt{\frac{|a|}{c_\psi}}\,\overline{\omega^{\wedge}}(\omega a) f^{\wedge}(\omega) \tag{6.17}$$

This relation is only a shorthand notation for

$$\int_{-\infty}^{\infty} L_\psi f(a,t) e^{-j\omega t}\,dt = \sqrt{\frac{|a|}{c_\psi}}\,\psi^{\wedge}(\omega a) f^{\wedge}(\omega) \tag{6.18}$$

Multiply both sides of Equation (6.18) with $\frac{\psi^{\wedge}(\omega a)}{|a|^{3/2}\sqrt{c_\psi}}$ and integrate with respect to a. If we recall the definition given in Equation (6.7) of c_ψ it is possible to eliminate all terms depending on $\psi^{\wedge}$ on the right-hand side. After the multiplication and integration procedure, the new right-hand side will read:

$$\frac{1}{2\pi} f^{\wedge}(\omega),$$

Equating this with the corresponding new left-hand side, we obtain a formula which computes $f^{\wedge}(\omega)$ from the CWT, $L\psi f(t, a)$.

1. Now apply the Fourier inversion formula $\left(f(t) = \frac{1}{2\pi}\int_{-\infty}^{\infty} f^{\wedge}(\omega) e^{j\omega t} dt\right)$ to both sides. This gives the desired reconstruction formula:

$$f(t) = \frac{2\pi}{\sqrt{c_\psi}} \int_{-\infty}^{\infty}\int_{-\infty}^{\infty} L_\psi f(a,u) \frac{1}{\sqrt{|a|}}\,\psi\left(\frac{t-u}{a}\right)\frac{du\,da}{a^2} \tag{6.19}$$

With the same reasoning as used for the STFT reconstruction formula;

$$f(t) = \frac{\int_{-\infty}^{\infty}\int_{-\infty}^{\infty} \hat{f}_{\omega}(\omega,\tau)\omega(t-\tau)e^{j\omega t}d\omega d\tau}{2\pi \int_{-\infty}^{\infty}|\omega(u)|^2 du} \quad (6.20)$$

This reconstruction integral is of only limited practical relevance if sampled signals and the corresponding CWT are given and then instead - in analogy to the STFT procedure - one may obtain a reconstruction algorithm by reversing the steps of the computation algorithm.

Assume that the sampling $\{f(kT_s)\}_{k=0}^{N-1}$ of a continuous-time finite energy signal *f*(*t*) is given such that Equation (6.13) is fulfilled. Also assume that the algorithm described above has been performed. After evaluating Equation (6.14), the sequence $\{L_\psi f(a, kT_s)\}_{k=0}^{N-1}$ is given, then the correspondence Equation (6.12) is used again to reconstruct $\{f(a, kT_s)\}_{k=0}^{N-1}$ as follows:

1. Compute the sequence$\{\psi_a(kT_s)\}_{k=0}^{N-1}$, where ψ_a is as defined in Equation (6.11) and compute the corresponding DFT denoted with $\{A_s\}_{k=0}^{N-1}$.

2. Compute the DFT of the sequence$\{L_\psi f(a, kT_s)\}_{k=0}^{N-1}$. Denote this quantity$\{B_k\}_{k=0}^{N-1}$.

3. Compute the sequence $\{F_k\}_{k=0}^{N-1}$ where $F_k = \sqrt{c_{\psi|a|}}\ \frac{B_k}{A_k}$ (6.21)

4. Apply the inverse DFT equation $\left((f_k = \frac{1}{N}\sum_{J=0}^{N-1} Fje^{\frac{-j2\pi jk}{N}}\ (k = 0,1 \ldots N-1)\right)$ to this sequence, resulting in the sequence$\{f(a, kT_s)\}_{k=0}^{N-1}$.

Schematically:

$$\{F_k\}_{k=0}^{N-1} \xrightarrow{IDFT} \{f(kT_s)\}_{k=0}^{N-1} \quad (6.22)$$

6.11 CONTINUOUS WAVELET TRANSFORM RESULTS AND DISCUSSION

A continuous wavelet transform (CWT) is used to divide a continuous function into wavelets; the analysis of acoustic signals recorded during inspection, such a signal may indicate the presence or absence of a defect. In this research the CWT was used for diagnostic purposes. First the local transform is sampled on a grid of discrete values both with respect to time and scale (CWT) or time and frequency (STFT).

In the next step a pattern vector is derived from the sampled transform values and this serves as an input to the subsequent classification procedure. The classifier may be trained with "good" signals, leading to a geometrical description of a "good class" in the space of pattern vectors. A given signal is then classified based on a certain notion of distance to that class. The results indicate that transforms are useful in the context of the research investigation, but the wavelet transform presumably leads to a clearer separation of "good" from "bad" as shown in Figure 6-50 which shows clear differences between the different tests. (Healthy (A), 1 mm hole at 25% (B), 50% (C), 75% (D) and 100% depth (E) respectively)

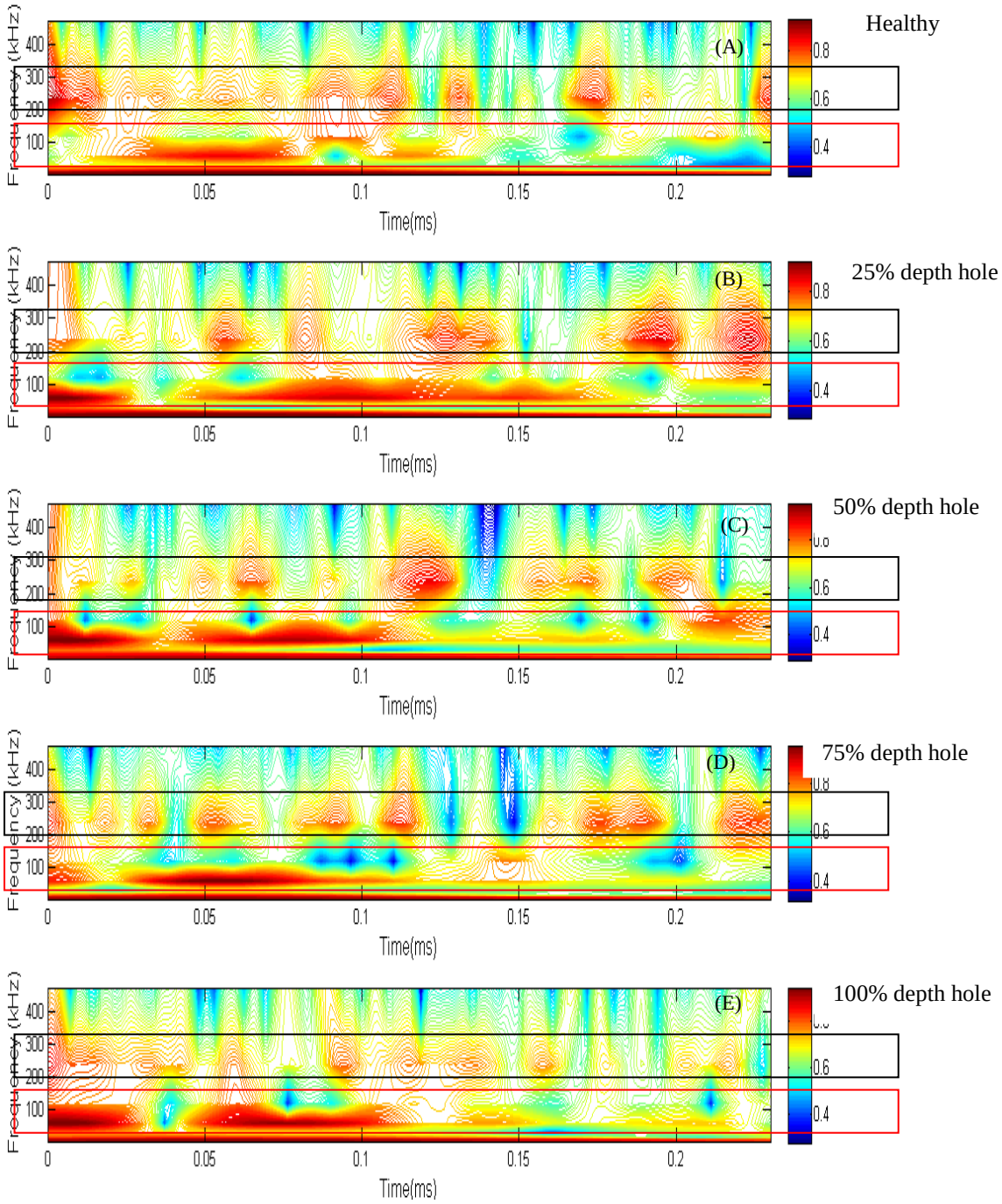

FIGURE 6-50: CWT SIGNATURES FOR FIVE SETS OF EXPERIMENTAL RESULTS (HEALTHY (A), 1 MM HOLE AT 25% (B) , 50% (C), 75% (D) AND 100% DEPTH (E)

6.12 SUMMARY OF EXPERIMENTS

The Conventional techniques used in this research representative in a time domain analysis shown in Figures 5-45 and a frequency domain analysis shown in Figure 5-47 are insufficient

for this type of faults since signatures presented dose not shows any differences between tested pipes.

However, CWT signature (Figure 6-50) shows a clear difference between each pipe case since the density of the red colour that present the energy is change by the change of pipe fault.

Also, this change is found to be in a directly proportional to the increase of the depth of the hole as illustrated in the black rectangular in each diagrams Moreover, the red rectangular indicate that even at low band frequency, red spots density change with change of pipe conditions, based on these finding CWT is consider a sufficient analyses method for this type of fault and material as well as the novelty of this research.

CHAPTER VII

CONTRIBUTION TO KNOWLEDGE, ACHIEVEMENTS, CONCLUSIONS AND SUGGESTED FUTURE WORK

This chapter illustrates the progress made in the research topic as a result of the research work. Research achievements according to the research study plan are also presented and the extent to which targets were achieved and suggestions are presented for future research.

7.1 REVIEW OF THE OBJECTIVES AND ACHIEVEMENTS

Each of the objectives specified in Section 1.6 are presented below, followed by the main achievements related to that each objective.

Objective 1

Understand oil transmission pipelines construction, materials and common failure modes and review state of the art and current ultrasonic pipelines condition monitoring techniques.

Achievement

The achievement of this objective was discussed in Chapter II, based on pipeline integrity management techniques with a review of current monitoring methods advantages / disadvantages and limitation as well as a brief review of ultrasonic (automated and online testing) electromagnetic, radiographic, thermo graphic and dynamic methods. Long-range guided wave and electro-magnetic acoustic transducers were also covered.

A review of the current, non-destructive methods for condition monitoring was presented in Chapter I, along with the advantages and disadvantages of each method. The ideal method for pipeline monitoring would accurately detect the size and location of hole-induced damage on-line without the need for removal of insulation, coatings or scale; it would also be non-intrusive, provide real-time digital information, and be rapid and cost-effective.

The method applied in this research does not require the removal of insulation or coatings, and its grid layout provides a limited point-by-point view of conditions. In addition, it is easy to apply, is less labour intensive, accurate and inexpensive, can be used in confined areas, and does not have to be operated by specialized technicians.

Objective 2

To develop 3D finite element model and describe wave behaviours and its propagation into the pipeline structure.

Achievement

A detailed 3D finite element model was developed and presented in Chapter 3. The developed model successfully described the wave propagation into the structure of the Carbon steel pipe and gave clear understanding of the physics behind such propagation and predicted the effects of pipe's structural deficiencies on the transmitted and received ultrasonic signals.

Objective 3

Build a fully equipped experimental testing model for experimental data collection.

Achievement

This major goal was fully discussed, and the results were demonstrated in Chapter IV. The goal was successfully achieved during a four-month period of diligent work using the University's laboratory apparatus and computer facilities that resulted in an acceptable match between experimental and modeling results.

From these results, it is quite simple to determine the condition of a pipe without having to conduct a physical inspection, which, in some situations might be difficult and require hard work, such as drilling or digging, to access the pipe, which can save a lot of time and money.

Objective 4

Simulate common fault modes; 1 mm size holes at different depth into the pipe surface.

Achievement

The objective of this research was to improve the modelling capabilities of damage in carbon steel pipes and provide better prediction of the response of carbon steel pipe structure; that objective was achieved by developing a better understanding of the application of current damage models and their limitations.

The role of better understanding of the mechanisms of damage modes in improving modelling capabilities was discussed in Chapter III. A major focus of the research was to model the

effects of a hole in the pipe structure, because this is the most common form of damage that occurs. Despite the vast amount of information in the literature concerning the modelling of a hole in the pipe structure, there is still a need for model that can predict the development of such damage and predict its effects on the structural response for pipes subjected to general load conditions.

Objective 5

Develop a sensitive ultrasonic data processing technique based on wavelets for condition features extraction and classification.

Achievement

ABAQUS (2011) software was used to apply the time domain single processing, and Fast Fourier Transformer (FFT) using MATLAB software, version R2012a, was used for frequency domain signal processing, illustrated in Chapters V and VI.

7.2 CONCLUSIONS

This work has advanced oil transmission pipeline condition monitoring methods using ultrasonic systems and wavelet analysis. This was done by re-enacted ultrasonic sources, and legitimate ultrasonic sources with uncontrolled temporal structures. Sensors alignment shows in a significant factor chase for the primary goals, which were to enhance the exactness of source area and to evaluate the level of mutilation connected with ultrasonic wave proliferation along a funnel. Specifically this examination has:

- Developed systems to recognize source area on moderately long pipes; Chapters 1&2,
- Presented an ultrasonic attenuation model for use with wave propagation in pipes under different circumstances using a combination of reflection and transmission laws; Chapter 3,

- Developed techniques for enhancing the resolution of continuous and semi-continuous sources by using appropriate digital filters with attenuation measurements to remove unwanted components; Chapter 4,

- Presented methods of simulating the ultrasonic energy to impact and crack spreading, improving the understanding of how ultrasonic can be used to monitor the mechanical behaviour for pipes under static and dynamic loads; Chapter 3,

- The techniques are believed to be generally applicable, but investigation is required as to the balance of the modes identified in Chapters 1 and 2, and have relied on the effectiveness of the 253 kHz cut-off filter, which had to be found by inspection, and which may only apply to the particular sensors used, or indeed to the particular configurations used. However, it has been shown that a method can be developed to automatically determine an appropriate filter cut-off,

- All of the source location techniques suitable for the air-air environment can be applied to the other environments. The WT technique for source location gives better results with attenuated environments, although still suffers from multiple peaks, which make arrival time estimation unreliable,

- Using a frequency band between 200 kHz and 300 kHz with the energy attenuation technique improved the continuous ultrasonic source location precision to produce an error of less than 14%,

- The CWT can therefore evidently be used to distinguish between healthy and damaged pipes,

- Two novel techniques have been demonstrated (3D ABAQUS software acoustic simulation and CWT analysis) to estimate the resonances of the modes, and hence locate sources in long pipes with an error of less than 3%.

7.3 SUGGESTED FUTURE WORK

The following recommendations are suggested for further research:

7.3.1 FUTURE WORK RELATED TO DIFFERENT MODELING SYSTEMS

The variable window and threshold techniques were found to be the most successful source location techniques when source and sensor were separated by long distances, and both depend on filtering the signal above and below 235 kHz. In view of the possibility of different source frequency contents and variable attenuation, there is room to explore a more dynamic filtering technique, which permits some adaptation according to the source type, the environment and the source-sensor distance.

7.3.2 FUTURE WORK RELATED TO DIFFERENT TYPES OF DEFECTS

The successful application of the simulated ultrasonic technique-using burst, continuous and semi-continuous ultrasonic signals for long distances could be applied to real sources with unknown structures. As a first step, the observed differences in frequency structure of an impact and crack-spreading sources could be used to better understand these sources, perhaps using more controlled dynamic conditions between pipe and indenter and a wider range of pre-crack sizes.

7.3.3 FUTURE WORK WITH DIFFERENT MATERIALS

The modelling of these effects could be studied in more detail by changing the area: length ratio of the pipes and improving the simulation capacity in order to achieve convergence between the results from simulation and those from the more deterministic attenuation model.

REFERENCES

1. 1-BDEW, VEWA-Survey (Summary): Comparison of European Water and Wastewater Prices, Download from /www.bdew.deS, 2010 (accessed January 2013).

2. J. Lighthill; Waves in Fluids ;Cambridge University Press, Cambridge (2001)

3. Papadakis, G.A., "Major Hazard Pipelines: A Comparative Study of Onshore Transmission Accidents", Journal of Loss Prevention, 1999, 12, pp. 91-107.

4. Um, J.S. and Wright, R., "Pipeline construction and Reinstatement Monitoring: Current Practice, Limitations and the Value of Airborn Videography", The Science of the Total Environment, 1996, 186, pp. 221- 230.

5. Gao, Y., Muggleton, J. M., Brennan, M. J., Joseph, P. F., & Hunaidi, O. (2005). On the selection of acoustic/vibration sensors for leak detection in plastic water pipes. Journal of Sound and Vibration, 283, 927–941.

6. A. Crouch, R. Anglisano and M. Jarrah, Quantitative Field Evaluation of Magnetic Flux Leakage and Ultrasonic In-Line Inspection, Pipeline Pigging Conference, Houston, 1996

7. D.N. Alleyne and P. Cawley, Long Range Propagation of Lamb Waves in Chemical PlantPipework, Materials Evaluation, V. 55, No. 4, pp. 504-508, 1997.

8. J. Pei, M.I. Yousuf, F.L. Degertekin, B.V. Honein and B.T. Khuri-Yakub, Lamb Wave Tomography and Its Application in Pipe Erosion/Corrosion Monitoring, Research in Nondestructive Evaluation, V. 8, pp. 189-197, 1996.

9. J.L. Rose, S.P. Pelts and J. Li, Quantitative Guided Wave NDE, 15th World Conference on Nondestructive Testing, Roma, 2000.

10. M.J.S. Lowe, D.N. Alleyne and P. Cawley, Defect Detection in Pipes Using Guided Waves, Ultrasonic, V. 36, pp. 147-154, 1998.

11. A.V. Bray, C.J. Corley, R. Fischer, J.L. Rose and M.J. Quarry, Development of Guided Wave Ultrasonic Techniques for Detection of Corrosion Under Insulation in Metal Pipe, Energy Sources Technology Conference and Exhibition, ASME, 1998.

12. D.N. Alleyne, B. Pavlakovic, M.J.S. Lowe and P. Cawley, Rapid Long Range Inspection of Chemical Plant Pipework Using Guided Waves, 15th World Conference on Nondestructive Testing, Roma, 2000.

13. C.H.P. Wassink, M.A. Robers, J.A. de Raad, and T. Bouma, Condition Monitoring of Inaccessible Piping, 15th World Conference on Nondestructive Testing, Roma, 2000.

14. J.H.J Stalenhoef, J.A. de Raad and P. van Rooijen, MFL and PEC Tools for Plant Inspection, NDT.net, V. 3, No. 12, and 1998.

15. M.J. Cohn and J.A. de Raad, Pulsed Eddy Current Projects for the Detection of Flow- Accelerated Corrosion, PVP-Vol. 380, Fitness-for Service Evaluations in Petroleum and Fossil Power Plants, ASME, pp. 45-57, 1998.

16. U. Zscherpel, Y. One1 and U. Ewert, New Concepts for Corrosion Inspection of Pipelines by Digital Industrial Radiology (DIR), 15th World Conference on Nondestructive Testing, Roma, 2000.

17. A. Hecht, R. Bauer and F. Lindemeier, On-Line Radiographic Wall Thickness Measurement of Insulated Piping in the Chemical and Petrochemical Industry, NDT.net, V. 3, No. 10, 1998.

18. N.IK. Gupta and B.G. Isaacson, Near Real Time In-service Testing of Pipeline Components, Materials Evaluation, V. 59, No. 1,200l.

19. SM. Walker, New NDE Developments Support Rapid, Economical Screening for Flow- Accelerated Corrosion, PVP-Vo1.375, Integrity of Structures and Components: Nondestructive Evaluations, ASME, 1998.

20. X. Maldague, Pipe Inspection by Infrared Thermography, Materials Evaluation, V. 57, No. 9, pp. 899-902, 1999.

21. C.J. Kriel and P.S. Heyns, Damage Identification on Piping Systems Using On-Line Monitoring of Dynamic Properties, Proceedings of 17th International Modal Analysis Conference, Society of Experimental Mechanics, Kissimmee, 1999.

22. M. klann, T. Beuker, Pipeline inspection with the high resolution ultrasonic ili–tool: report on field experience, proceedings of IPC, 2006 6th international pipeline conference, September 25-29, 2006, Calgary, Alberta, Canada

23. J. Hu, L. Zhang, W. Liang, (2011), Detection of small leakage from long transportation pipeline with complex noise Journal of Loss Prevention in the Process Industries, 24, 4, 449-457.

24. T. Meurer, J. Qu, L. Jacobs. (2002), Wave propagation in nonlinear and hysteretic media—a numerical study, International Journal of Solids and Structures 39 (2002) 5585–5614.

25. Z. Sun, P. Wang, C. Mehmet, M. Al-Rodhaan, A. Al-Dhelaan. (2010). Magnetic induction-based wireless sensor networks for underground pipeline monitoring. AD Hoc Networks, 218-227.

26. Lee, H.S., Yoon, J.H., Park, J.S. and Yi, Y.M., "A Study on Failure Characteristic of Spherical Pressure Vessel", Journal of Materials Processing Technology, 2005, 164-165, pp. 882-888.

27. Rajtar, J.M. and Muthiah, R., "Pipeline Leak Detection System for Oil and Gas Flowlines", Journal of Manufacturing Science and Engineering, Trans. ASME, 1997, 119, pp. 105-109.

28. Chen, C.M. and Kovacevic, R., "Joining of A1 6061 Alloy to AISI 1018 Steel by Combined Effects of Fusion and Solid State Welding", Machine Tools & Manufacture, 2004, 44, pp. 1205-1214.

29. Zhang, L., Sazonov, V., Kent, J., Dixon, T. and Novozhilov, V., "Analysis of Boiler-tube Erosion by the Technique of Acoustic Emission: Part I Mechanical Erosion", Wear, 2001, 250, pp. 762-769.

30. Opydo, W., "Study of Elastic Waves of Acoustic Frequencies Generated by Surface Partial Discharges of Solid Insulators in Vacuum", Vacuum, 2004, 74, pp. 85-92.

31. Ma, X.Q., Cho, S. and Takemoto, M., "Acoustic Emission Source Analysis of Plasma Sprayed Thermal Barrier Coatings during Four-point Bend Tests", Surface & Coatings Technology, 2000, 139, pp. 55-62.

32. Hamstad, M.A.,O'Gallagher, A. and Gary, J., "A Wavelet Transform Applied to Acoustic Emission Signals: Part 1: Source Identification", Journal of Acoustic Emission, 2002, 20, pp. 39-59.

33. Gorman, M.R., "Plate Wave Acoustic Emission", Journal of the Acoustical Society of America, 1991, 90(1), pp. 358-364.

34. Carlin, B., "Ultrasonics", McGraw-Hill, New York, 1960.

35. Pollock, A.A., "Classical Wave Theory in Practical AE Testing", Progress in Acoustic Emission III - Japanese Society of Non-Destructive Testing, 1986, pp. 708-721.

36. Giordano, M., Condelli, L. and Nicolais, L., "Acoustic Emission wave Propagation in a Viscoelastic Plate", Composite Science and Technology, 1999, 59, pp. 1735-1743.

37. Pao, Y., Gajewski, R.R. and Ceranolgu, A.N., "Acoustic Emission and Transient Waves in an Elastic Plate", Journal of the Acoustical Society of America, 1979, 65(11), pp. 96-105.

38. Lysak, M.V., "Development of the Theory of Acoustic Emission by Propagating Cracks in Terms of Fracture Mechanics", engineers Fracture Mechanics, 1996, 55(3), pp. 443-452.

39. Andreykiv, O.Y., Lysak, M.V., Serhiyenko, O.M. and Skalsky, V.R., "Analysis of Acoustic Emission Caused by Internal Cracks", engineer Fracture Mechanics, 2001, 68, pp. 1317-1333.

40. Surgeon, M. and Wevers, M., "One Sensor Linear Location of Acoustic Emission Events using Plate Wave Theories", materials science & Engineering A, 1999, 265(1-2), pp. 254-261.

41. Gorman, M.R. and Prosser, W.H., "AE Source Orientation by Plate Wave Analysis", Journal of Acoustic Emission, 1991, 9(4), pp. 283-288.

42. Holford, K.M. and Carter, D.C., "Acoustic Emission Source Location", Key Engineering Materials, 1999, 167-168, pp. 162-171. 176

43. Jeong, H. and Jang, Y., "Fracture Source Location in Thin Plates using the Wavelet Transform of Dispersive Waves", IEEE Transactions on Ultrasonic, Ferroelectrics and Frequency Control, 2000, 47(3), pp. 612- 619.

44. Hunaidi, O. and Chu, W.T., "Acoustical Characteristics of Leak Signals in Plastic Water Distribution Pipes", Applied Acoustics, 1999, 58, pp. 235- 254.

45. NDT Systems, I., Worldwide Excellence in Ultrasonic, http://www.ndtsystems.com/Reference/Velocity_Table/velocity_table.htm.

46. Nivesrangsan, P., "Multi-Source, Multi-Sensor Approaches to Diesel Engine Monitoring using Acoustic Emission", PhD Thesis, Heriot Watt University, Edinburgh, 2005.

47. Fuller, C.R. and F.J. Fahy, "Characteristics of Wave Propagation and Energy Distribution in Cylindrical Elastic Shells Filled with Fluid", Journal of Sound and Vibration, 1982, 81(4), pp. 501-518.

48. Nivesrangsan, P., Steel, J.A. and Reuben, R.L., "AE Mapping of Engines for Spatially Located Time Series, Part I: Preliminary studies", Mechanical Systems and Signal Processing, 2005, 19(5), pp. 1034-1054.

49. Schoorlemmer, I.H., "Advanced Real Time Source Location Applications", 26th European Conference on AE Testing, Berlin, 2004, pp. 623-627.

50. Maji, A.K., Satpathi, D. and Kratochvil, T., "Acoustic Emission Source Location using Lamb Wave Modes", Journal of Engineering Mechanics, 1997, 123(2), pp. 154-161.

51. Langhorne, P.J. and Haskell, T.G., "Acoustic Emission during Fatigue Experiments on First Year Sea Ice", Cold Regions Science and Technology, 1996, 24, pp. 237-250.

52. Braginskii, A.B., Medvedev, B.M. and Platkov, A.I., "Amplitude-Frequency Location Procedure for Acoustic Emission", Soviet Journal of Nondestructive Testing, 1989, 24(9), pp. 620-626.

53. Barat, P., P. Kalyanasundaram and Raj, B., "Acoustic Emission Source Location on a Cylindrical Surface", NDT & E International, 1993, 26(6), pp. 295-297.

54. Theobald, P.D., Esward, T.J., Dowson, S.P. and Preston, R.C., "Acoustic Emission Transducers-Development of a Facility for Traceable Out-of- plane Displacement Calibration", Ultrasonic, 2004, 43, pp. 343-350.

55. Colombo, S., Giannopoulos, A, Forde, M.C., Hasson, R. and Mulholland, J., "Frequency Response of Different Couplant Materials for Mounting Transducers", NDT & E International, 2005, 38, pp. 187-193.

56. Wolfinger, C., Arendts, F.J., Friedrich, K. and Drechsler, K., "Health-Monitoring-System based on Piezoelectric Transducers", Aerospace Science Technology, 1998, 6, pp. 391-400.

57. Hsu, N. N. and Hardy, S.C., "Operation in Acoustic Emission Waveform Analysis for Characterisation of AE Source, Sensors and Structures", Elastic Waves and Non-destructive Testing of Materials, Trans. ASME, 1978, 29, pp. 85-106.

58. Stephens, R.W.B. and Pollock, A.A., "Waveforms and Frequency Spectra of Acoustic Emission", Journal of the Acoustical Society of America, 1971, 50(3), pp. 904-910.

59. Powell, L.E. and Dimmick, J.G., "Apparatus and Method for Testing for Valve Leakes by Differential Signature Method", Patent no. (5650943), USA, 1995.

60. Kwan, H.W. and Leach, M.F., "Characterisation of Cylindrical Particles from their Acoustic Emission", Ultrasonics, 1985, 23(5), pp. 233-238.

61. Spall, J.C., Maryak, J.L. and Asher, M.S., "Neural Network Approach to Locating Acoustic Emission Sources in Non-destructive Evaluation", Journal of Sound and Vibration, 1998, 211(1), pp. 133-143.

62. Jemielniak, K., "Some Aspects of Acoustic Emission Signal Pre- processing", Journal of Materials Processing Technology, 2001, 109, pp. 242-247.

63. Cohen, L., "Time-Frequency Analysis", Prentic-Hall PTR, New Jersey, 1995.

64. Cochran, W.T., et al., "What is Fast Fourier Transform", IEEE Transactions on Audio and Electro acoustics, 1967, 15(2), pp. 45-55.

65. Welch, P.D., "The use of Fast Fourier Transform for the Estimation of Power Spectra: A Method Based on Time Averaging over Short, Modified, pp. 178 Period grams", IEEE Transactions on Audio and Electro acoustics, 1967, 15(2), pp. 70-73.

66. Cohen, L., ""Time-frequency Distributions - a Review", Proceedings of The IEEE, 1989, 77(7), pp. 941-981.

67. Ding, Y., Reuben, R.L. and Steel, J.A., "A New Method for Waveform Analysis for Estimating AE Wave Arrival Times using Wavelet Decomposition", NDT & E International, 2004, 37(4), pp. 279-290.

68. Grosse, C.U. and Reinhardt, H.W., "Signal Conditioning in Acoustic Emission Analysis using Wavelets", NDT.net, 2002, 7(9), pp. 1-9.

69. Ng, E. and Qi, G., "Material Fatigue Behaviour Characterisation using the Wavelet-based AE Technique- a Case Study of Acrylic Bone Cement", Engineering Fracture Mechanics, 2001, 68, pp. 1477-1492.

70. Jiao, J., He, C., Wu, B., Fei, R. and Wang, X., "Application of Wavelet Transform on Model Acoustic Emission Source Location in Thin Plates with one Sensor", Pressure Vessels and Piping, 2004, 81, pp. 427-431.

71. Venugopal, V. and Foufoula, G. E., "Energy Decomposition of Rainfall in the Time-frequency-scale Domain using Wavelet Packets", Journal of Hydrology, 1996, 187, pp. 3-27.

72. Wu, Y. and Du, R., "Feature Extraction and Assessment using Wavelet Packets for Monitoring of Machining Processes", Mechanical Systems and Signal Processing, 1996, 10(1), pp. 29-53.

73. Wang, Q. and Chu, F., "Experimental Determination of the Rubbing Location by means of Acoustic Emission and Wavelet Transform", Journal of Sound and Vibration, 2001, 248(1), pp. 91-103.

74. Kishimoto, K., Inoue, H., Hamada, M. and Shibuya, T., "Time Frequency Analysis of Dispersive Waves by Means of Wavelet Transform", Trans. ASME, Journal of Applied Mechanics, 1995, 62, pp. 841-846.

75. Qi, G., "Wavelet-based AE Characterisation of Composite Materials", NDT & E International, 2000, 33, pp. 133-144.

76. Yoon, D., Jung, J., Kim, K., Park, P. and Lee, S., "AE Parameter Analysis for Fatigue Crack Monitoring", the 15th World Conference on Non-destructive Testing, Roma, 2000. 179

77. Radon, J.C. and Pollock, A.A., "Acoustic Emission and Energy Transfer during Crack Propagation", Engineering Fracture Mechanics, 1972, 4, pp. 295-310.

78. Steven, M., Ziola , S.M. and Gorman, M.R., "Source Location in Thin Plates using Cross-Correlation", Journal of the Acoustical Society of America, 1991, 90(5), pp. 2551-2556.

79. Coulter, J.E., Evans, R.S. and Robertson, M.O., "Acoustic Emission Leak Source Location", Patent no. (4858462), USA, 1989.

80. Ziola, S.M. and Gorman, M.R., "Source Location in Thin Plates using Cross-Correlation", Journal of the Acoustical Society of America, 1991, 90(5), pp. 2551-2556.

81. Gorman, M.R., "Acoustic Emission for the 1990s", Ultrasonic Symposium,IEEE, Orlando, 1991, pp. 1039-1046.

82. White, P.H., "Cross Correlation in Structural Systems: Dispersion and Non-dispersion Waves", Journal of the Acoustical Society of America, 1969, 45(5), pp. 1118-1127.

83. Inoue, H., Kishimoto, K. and Shibuya, T., "Experimental Wavelet Analysis of Flexural Waves in Beams", Experimental Mechanics, 1996, 36(3), pp. 212-217.

84. Buckely, K., Venkatesan, G., West, D. and Kaveh, M., "Detection and Characterisation of Crack for Failure Monitoring and Diagnostics", Acoustic, Speech, and Signal Processing, IEEE, Atlanta, 1996, pp. 2738- 2741.

85. Robertson, A.I.F., Douglas, R.M., Nivesrangsan, P., Brown, E.R., Steel, J.A. and Reuben, R. L, "Source Identification using Acoustic Emission on Large Bore Cylinder Liners", 26th European Conference on AE Testing, Berlin, 2004, pp. 637-643.

86. Lozev, M.G., Clemena, G.G., Duke, J.C., Sison, M.F. and Horn, M.R., "Acoustic Emission Monitoring of Steel Bridge Members", Final Report, Transportation Research Council, Virginia, 1997.

87. Stebut, J., "Multi-mode Scratch Testing-A European Standards, Measurements and Testing Study", Surface & Coatings Technology, 2005, 200, pp. 346-350.

88. Boyd, J.W.R. and Varley, J., "The Uses of Passive Measurement of Acoustic Emissions from Chemical Engineering Processes", Chemical Engineering Science, 2001, 56, pp. 1749-1767.

89. Richter, H., Bohmert, J. and Viehrig, W., "The use of Acoustic Emission to Determine Characteristic Dynamic Strength and Toughness Properties of Steel", Nuclear Engineering and Design, 1999, 188, pp. 241-254.

90. Singh, K.S.,Srinivasan, K. and Chakraborty, D., "Acoustic Emission Studies on Metallic Specimen under Tensile Loading", Materials & Design, 2003, 24, pp. 471-481.

91. Baudouin, P. and Houbaert, Y., "The Study of a Uniaxial Deformation Effect on the Magnetic Properties of a Non-oriented Electrical Steel using Acoustic Emission Characterisation", Journal of Magnetism and Magnetic Materials, 2002, 246, pp. 247-253.

92. Hao, S.,Ramalingam, S. and Klamecki, B.E., "Acoustic Emission Monitoring of Sheet Metal Forming: Characterisation of the Transducer, the Work Material and the Process", Journal of Materials Processing Technology, 2000, 101, pp. 124-136.

93. Carolan, T.A., Kidd, S.R., Hand, D.P. , Wilcox, S.J., P. Wilkinson, Barton, J.S. , Jones, J.C. D. and Reuben, R. L., "Acoustic Emission Monitoring of Tool Wear During the Face Milling of Steels and Aluminium Alloys using a Fibre Optic Sensor - Energy Analysis", Proc. I Mech E, Part B Journal of Engineering Manufacture, 1997, 211(B4), pp. 299-309.

94. Dunegan, H.L., Harris, D.O. and Tetelman, A.S., "Detection of Fatigue Crack Growth by Acoustic Emission Techniques", Materials Evaluation, 1970, 28(10), pp. 221-227.

95. Palmer, I.G. and Heald, P.T., "The Application of Acoustic Emission Measurements to Fracture Mechanics", Materials Science & Engineering, 1973, 11, pp. 181-184.

96. Wevers, M., "Listening to the Sound of Materials: Acoustic Emission for the Analysis of Materials Behaviour", NDT&E International, 1997, 30(2), pp. 99-106.

97. Miller, R. K. and Mclntire, P., "Nondestructive Testing Handbook. Vol. 5: Acoustic Emission Testing", American Society for Non-Destructive Testing, New York, 1987.

98. Lindley, T.C.,Palmer, I.G. and Richards, C.E., "Acoustic Emission Monitoring of Fatigue Crack Growth", Materials Science & Engineering, 1978, 32, pp. 1-15.

99. Bassim, M.N. and Emam, M.H., "Acoustic Emission during the Low Cycle Fatigue of AISI 4340 Steel", materials science & Engineering, 1984, 68, pp. 79-83. 181

100. Reuben, R. L, "The Role of Acoustic Emission in Industrial Condition Monitoring", COMADEM International, 1998, 1(4), pp. 35-46.

101. Grondel, S., Delebarra, C., Assaad, J., Dupuis, J. and Reithler, L., "Fatigue Crack Monitoring of Riveted Aluminium Strap Joints by Lamb Wave Analysis and Acoustic Emission Measurement Techniques", NDT & E

102. Stone, D.E.W. and Dinwall, P.F., "Acoustic Emission Parameters and Their Interpretation", NDT International, 1977, April, pp. 51-61.

103. Harris, D.O. and Bell, R.L., "The Measurement and Significance of Energy in Acoustic Emission Testing", Experimental Mechanics, 1977, 17(9), pp. 347-353.

104. Botten, S.F., "Prevention of Catastrophic Failure using Acoustic Emission Monitoring", Journal of Acoustic Emission, 1989, 8(1-2), pp. 330-333.

105. Hartbower, C.E., Morais, C.F., Reuter, W.G. and Crimmins, P.P., "Acoustic Emission from Low-cycle High-stress-intensity Fatigue", Engineering Fracture Mechanics, 1973, 5, pp. 765-789.

106. Shi, Z., Jarzynski, J., Bair, S., Hurlebaus, S. and Jacobs, L.J., "Characterisation of Acoustic Emission Signals from Fatigue Fracture", Proceedings IMechE, 2000, 214(C), pp. 1141-1149.

107. Prosser, W.H.,Gorman, M.R. and Humes, D.H., "Acoustic Emission Signals in Thin Plates Produced by Impact Damage", Journal of Acoustic Emission, 1999, 17(1-2), pp. 29-36.

108. Gaul, L. and Hurlebaus, S., "Identification of the Impact Location on A Plate using Wavelets", Mechanical Systems and Signal Processing, 1997, 12(6), pp. 783-795.

109. Tonshof, H.K., Jung, M., Mannel, S. and Rietz, W., "Using Acoustic Emission Signals for Monitoring of Production Processes", Ultrasonic, 2000, 37, pp. 681-686.

110. Hou, R., Hunt, A. and Williams, R.A., "Acoustic Emission of Pipeline Flows: Particulate slurries", Powder Technology, 1999, 106, pp. 30-36.

111. Jacob, L.J., "Characterisation of Acoustic Emission Signals from Mode I Crack", Journal of Engineering Mechanics, 1991, 117, pp. 1878-1889.

112. Yoshida, K., Kawano, H., Akematsu, Y. and Nishino, H., "Frequency Characteristics of Acoustic Emission Wavefoms During Gas Leak", 26th European Conference on AE Testing, Berlin, 2004, pp. 321-327.

113. G. B. Arfken and H. J. Weber. Mathematical Methods for Physicists. San Diego: Academic Press, 1995.

114. G. M. Wing. A Primer on Integral Equations of the First Kind. Philadelphia: SIAM, 1991.

115. B. K. Alpert, G. Beylkin, R. Coifman, and V. Rokhlin. "Wavelet-Like Bases for the Fast Solution of Second-Kind Integral Equations." SIAM J. Sci. Comp. 14 (1993), 159–184.

116. J. Mandel. "On Multi-Level Iterative Methods for Integral Equations of the Second Kind and Related Problems." Numer. Math. 46 (1985), 147–157.

117. J. C. Goswami. "An Application of Wavelet Bases in the Spectral Domain Analysis of Transmission Line Discontinuities." Int. J. Num. Modelling 11 (1998), 41–54.

118. J. H. Richmond. "Digital Solutions of the Rigorous Equations for Scattering Problems." Proc. IEEE 53 (August 1965), 796–804.

119. R. F. Harrington. Field Computation by Moment Methods. New York: IEEE Press, 1992.

120. G. Beylkin, R. Coifman, and V. Rokhlin. "Fast Wavelet Transform and Numerical Algorithms I." Comm. Pure Appl. Math. 44 (1991), 141–183.

121. R. L. Wagner, P. Otto, and W. C. Chew. "Fast Waveguide Mode Computation Using Wavelet-Like Basis Functions," IEEE Microwave Guided Wave Lett. 3 (1993), 208–210.

122. H. Kim and H. Ling. "On the Application of Fast Wavelet Transform to the Integral- Equation of Electromagnetic Scattering Problems." Microwave Opt. Technol. Lett. 6 (March 1993), 168–173.

123. B. Z. Steinberg and Y. Leviatan. "On the Use of Wavelet Expansions in Method of Moments." IEEE Trans. Antennas Propagate. 41 (1993), 610–619.

124. K. Sabetfakhri and L. P. B. Katehi. "Analysis of Integrated Millimeter-Wave and Sub- millimeter-Wave Waveguides Using Orthonormal Wavelet Expansions." IEEE Trans. Microwave Theory Tech. 42 (1994), 2412–2422.

125. B. Z. Steinberg. "A Multiresolution Theory of Scattering and Diffraction." Wave Motion 19 (1994), 213–232.

126. R. D. Nevels, J. C. Goswami, and H. Tehrani. “Semi-Orthogonal Versus Orthogonal Wavelet Basis Sets for Solving Integral Equations.” IEEE Trans. Antennas Propagat. 45 (1997), 1332–1339.

127. Z.XiangandY.Lu.“AnEffectiveWaveletMatrixTransformApproachforEfficient Solutions of Electromagnetic Integral Equations.” IEEE Trans. Antennas Propagat. 45 (1997), 1332–1339.

128. Z. Baharav and Y. Leviatan. “Impedance Matrix Compression (IMC) Using Iteratively Selected Wavelet Basis.” IEEE Trans. Antennas Propagat. 46 (1997), 226–233.

129. J. C. Goswami, R. E. Miller, and R. D. Nevels. “Wavelet Methods for Solving Integral and Differential Equations.” In Encyclopedia of Electrical and Electronics Engineering, ed. J. H. Webster. New York: Wiley 1999.

130. B. Z. Steinberg and Y. Leviatan. “Periodic Wavelet Expansions for Analysis of Scattering from Metallic Cylinders.” IEEE Antennas Propagate. Soc. Sym. (June 1994), 20–23.

131. G. W. Pan and X. Zhu. “The Application of Fast Adaptive Wavelet Expansion Method in the Computation of Parameter Matrices of Multiple Lossy Transmission Lines.” IEEE Antennas Propagat. Soc. Sym. (June 1994), 29–32.

132. G. Wang, G.W. Pan, and B. K. Gilbert.“ A Hybrid Wavelet Expansion and Boundary Element Analysis for Multiconductor Transmission Lines in Multilayered Dielectric Media.” IEEE Trans. Microwave Theory Tech. 43 (March 1995), 664–675.

133. W. L. Golik. “Wavelet Packets for Fast Solution of Electromagnetic Integral Equations.” IEEE Trans. Antennas Propagate. 46 (1998), 618–624.

134. GUPTA, S. c., Transform and State Variable Methods in Linear Systems. New York: Wiley, 1966.

135. KRAUS, J. 0. , Antennas. New Y ork: McGraw-Hili, 1950.

136. BoRN, M., and E. WOLF, Prillciples of Optics. New York: Pergamon Press,

137. LEE, Y. W., Statistical 17reory of Communication. New York: Wiley, 1960.

138. PAPOULlS, A., Probability, Random Variables, and Stochastic Processes. New York: McGraw-Hill, 1965.

139. FRENCH, A. P., Principles ofModern Physics. New York: Wiley, 1961.

140. BRACEWELL, RON, The Fourier Transform and Its Applications. New York: McGraw-Hill, 1965.

141. COOLEY, J. W., and J. W. TUKF.Y, "An algorithm for the machine calculation of complex Fourier series," Mathematics o f Computation (1965), Vol. 19, No. 90, pp. 297-301.

142. M.M. Tehranchi, M. Ranjbaran, H. Eftekhari, Double core giant magneto-impedance sensors for the inspection of magnetic flux leakage from metal surface cracks, Sensors and Actuators A: Physical, Volume 170, Issues 1–2, November 2011, Pages 55-61

143. Serife Agcaoglu and Ozan Akkus; Acoustic Emission Based Monitoring of the Microdamage Evolution during Fatigue of Human Cortical Bone; J Biomech Eng 135(8), April 04, 2013.

144. Electromagnetic acoustic transducer. (2013, November 11). In Wikipedia, the Free Encyclopedia. Retrieved 23:51, December 10, 2013, fromhttp://en.wikipedia.org/w/index.php?title=Electromagnetic_acoustic_transducer&oldid=581229576

145. Ir. Dr. Peter W. Tse; Thermography (Active & Passive) in NDT Technique; Croucher Optical Nondestructive testing (CNDT) Laboratory; Department of Systems Engineering & Engineering Management
City University of Hong Kong,2012.

146. Singh, R.; Pipeline Integrity Handbook: Risk Management and Evaluation; Elsevier Science; 2013.

APPENDIX A: ULTRASONIC WAVE PROPAGATION SIMULATION WITHIN ABAQUS CAE

A. Mission

1. The dimension of the SPECIMEN is shown in table 5 below:

Table 5: Specimen characterizations

Length	Diameter	Thickness	Material	Density	Poisson's ration	Young's modulus
1m	2.5 cm	3.5mm	Carbon Steel	7850 Kg/m	0.3	2e9

2. Faults= 1mm hole at different depth (25%, 50%, 75% and 100%)

3. Transceiver = Air Ultrasonic Ceramic Transducer 235AC130

4. Transceiver location = each pipe edge

5. The objective of this simulation is getting the U displacement and total energy at sensing point.

B. Preliminaries

1. File > Set Work Directory: All files, which are generated, will be saved in this directory as shown:

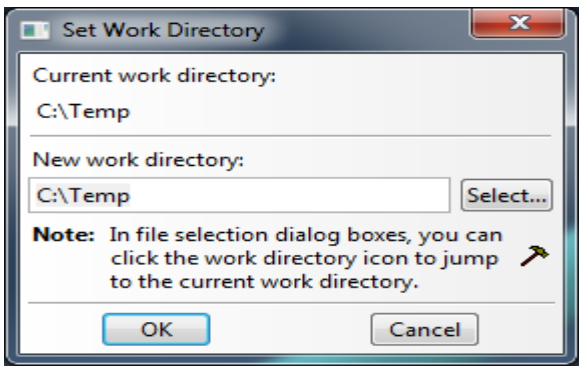

C. Module: Part

- 3D modelling space
- De formable type
- Solid extrusion feature

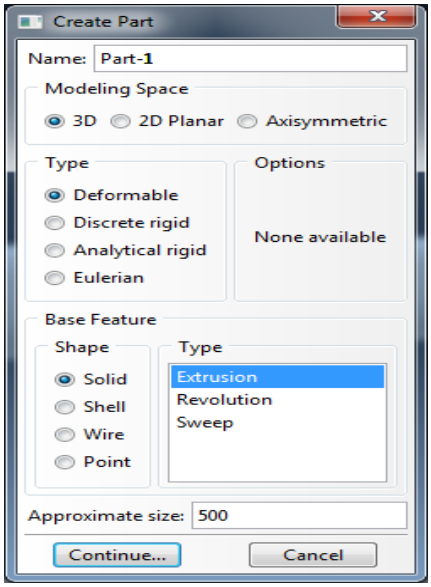

- Create circle >X, Y> 0,0>0,0.025>0,0>0,0.0215

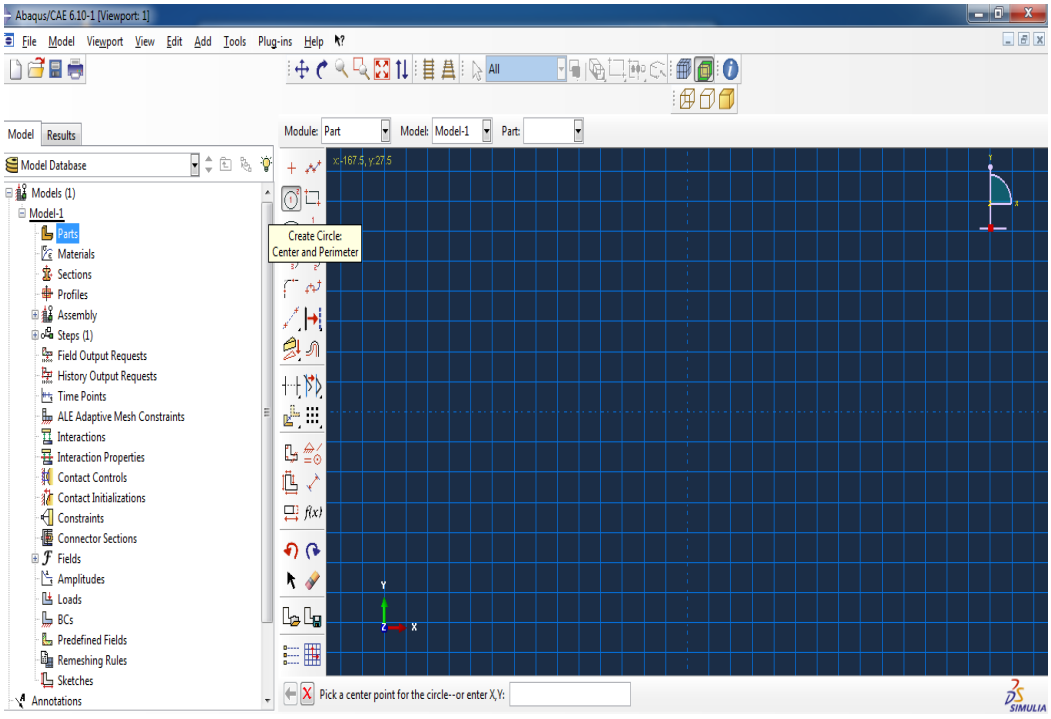

- Blind extrusion at depth of 1 meter

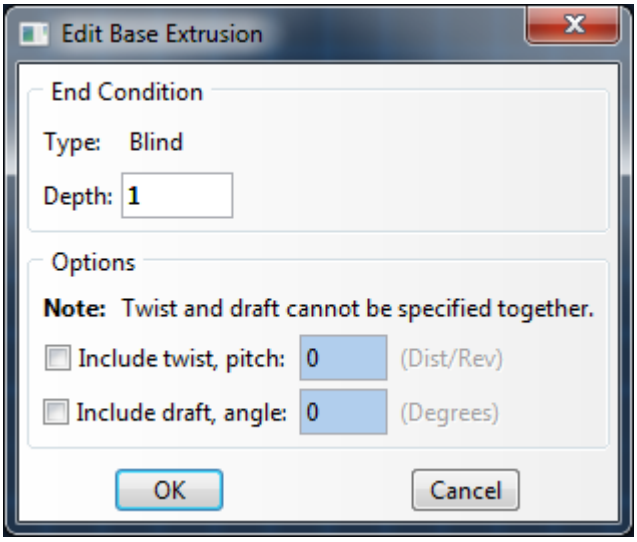

- The finial module shape as shown below

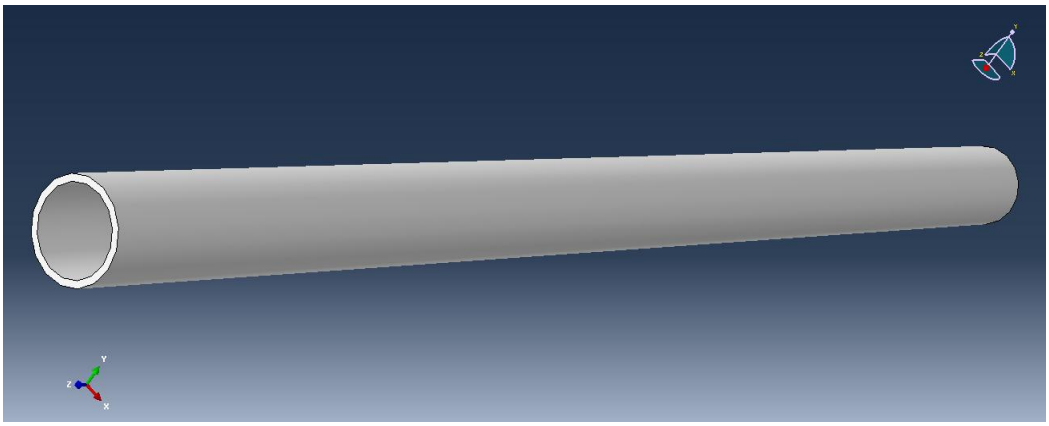

D. Module: Property

- Density = 7850 kg / m^3
- Elastic elasticity
- Paisson ratio = 0.3 Pa
- Stiffness (Young Module) = 2e

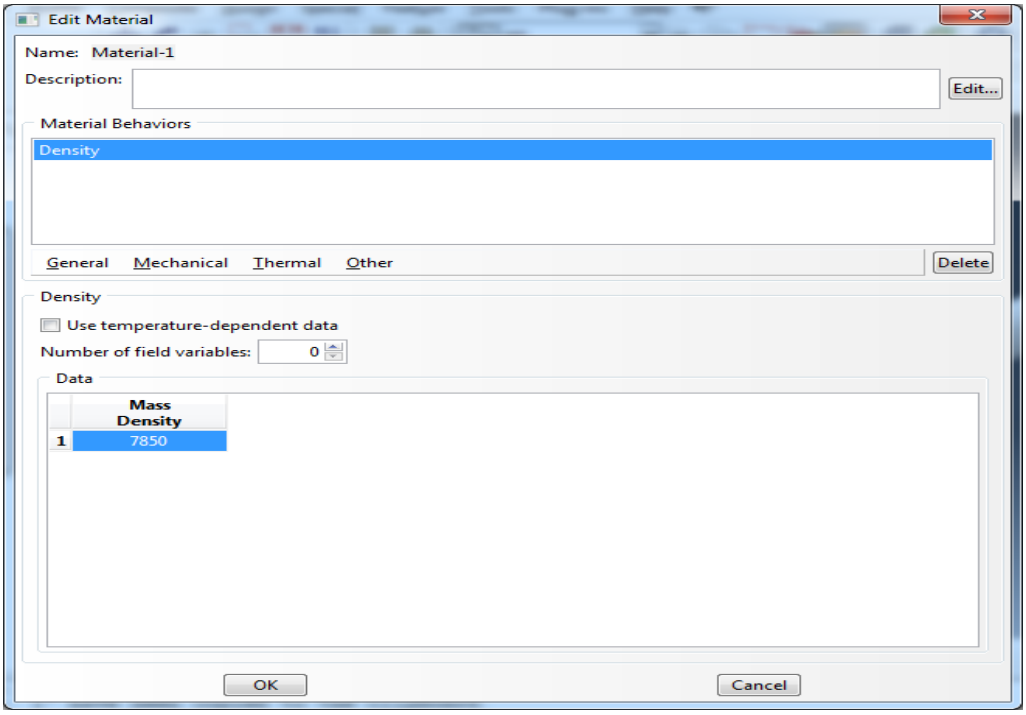
Edit Material
Name: Material-1
Description:
Edit...
Material Behaviors
Density
General
Mechanical
Thermal
Other
Delete
Density
Use temperature-dependent data
Number of field variables: 0
Data
Mass Density
1
7850
OK
Cancel

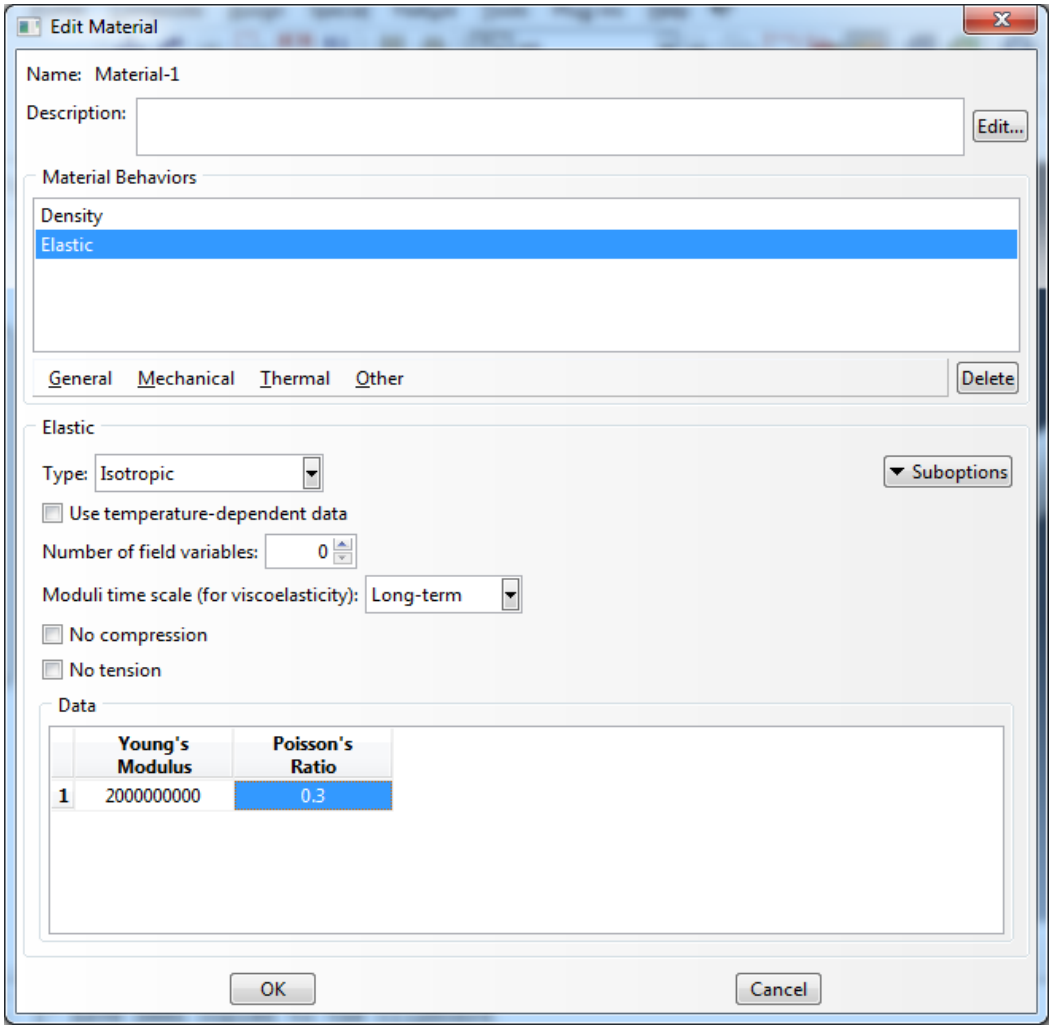
Edit Material
Name: Material-1
Description:
Edit...
Material Behaviors
Density
Elastic
General
Mechanical
Thermal
Other
Delete
Elastic
Type: Isotropic
Suboptions
Use temperature-dependent data
Number of field variables: 0
Moduli time scale (for viscoelasticity): Long-term
No compression
No tension
Data
Young's Modulus
Poisson's Ratio
1
2000000000
0.3
OK
Cancel

- The section properties defined as solid homogeneous.

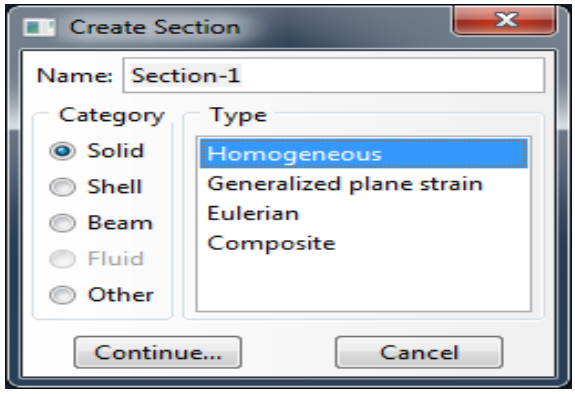

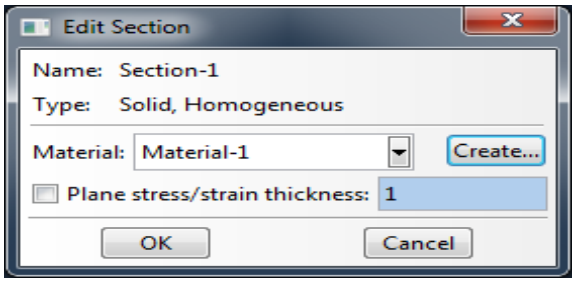

- The section is assigned for the whole model and the result will looks as shown below

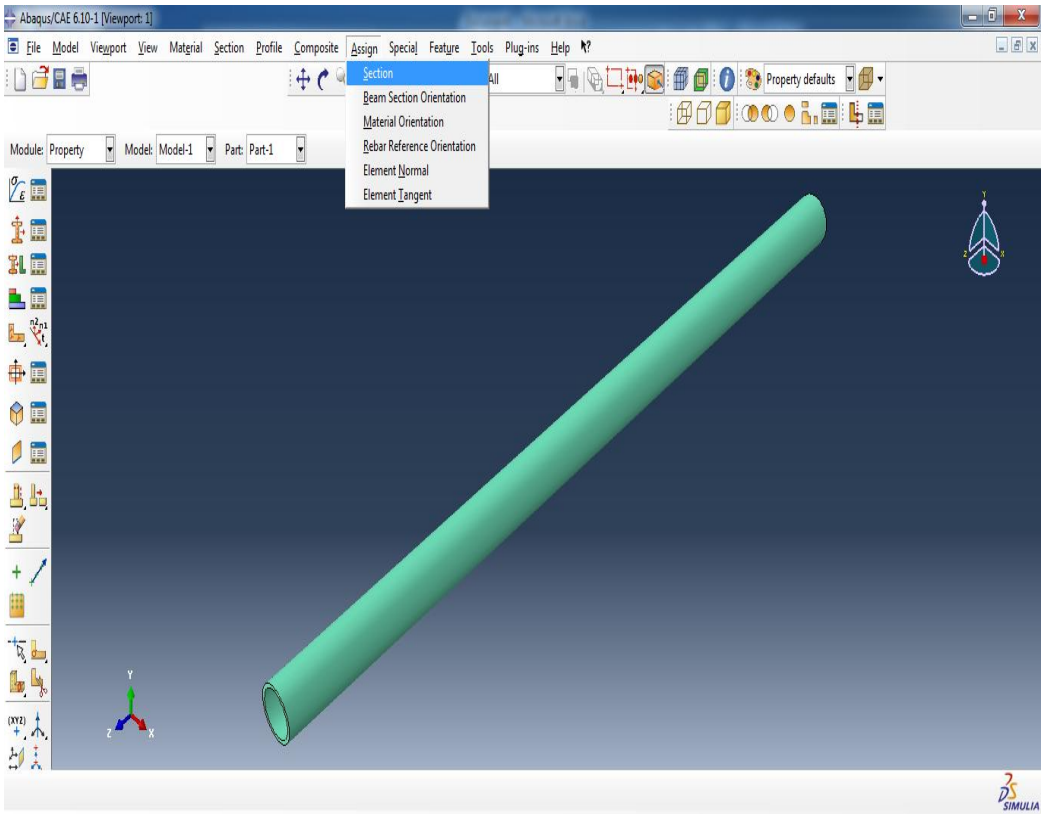

E. Module: Assembly

- Independent instance type

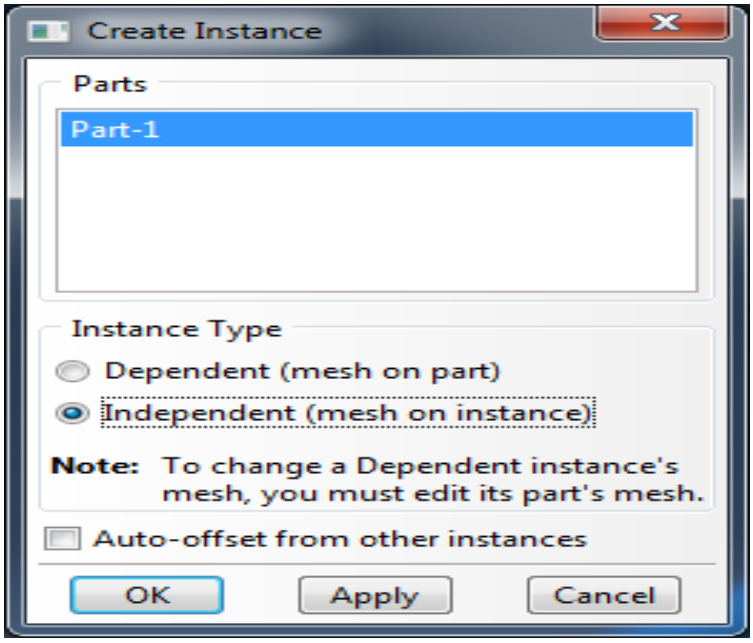

F. Module: Meshing

- Approximate meshing global size is 0.001

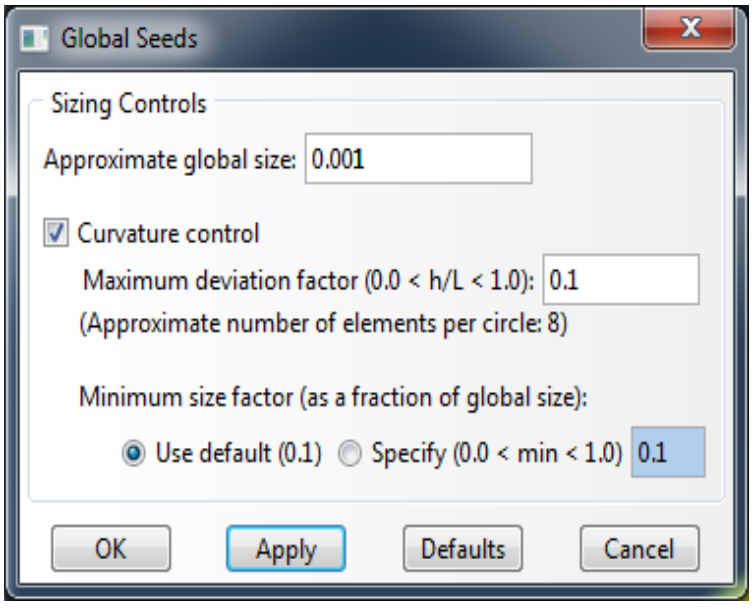

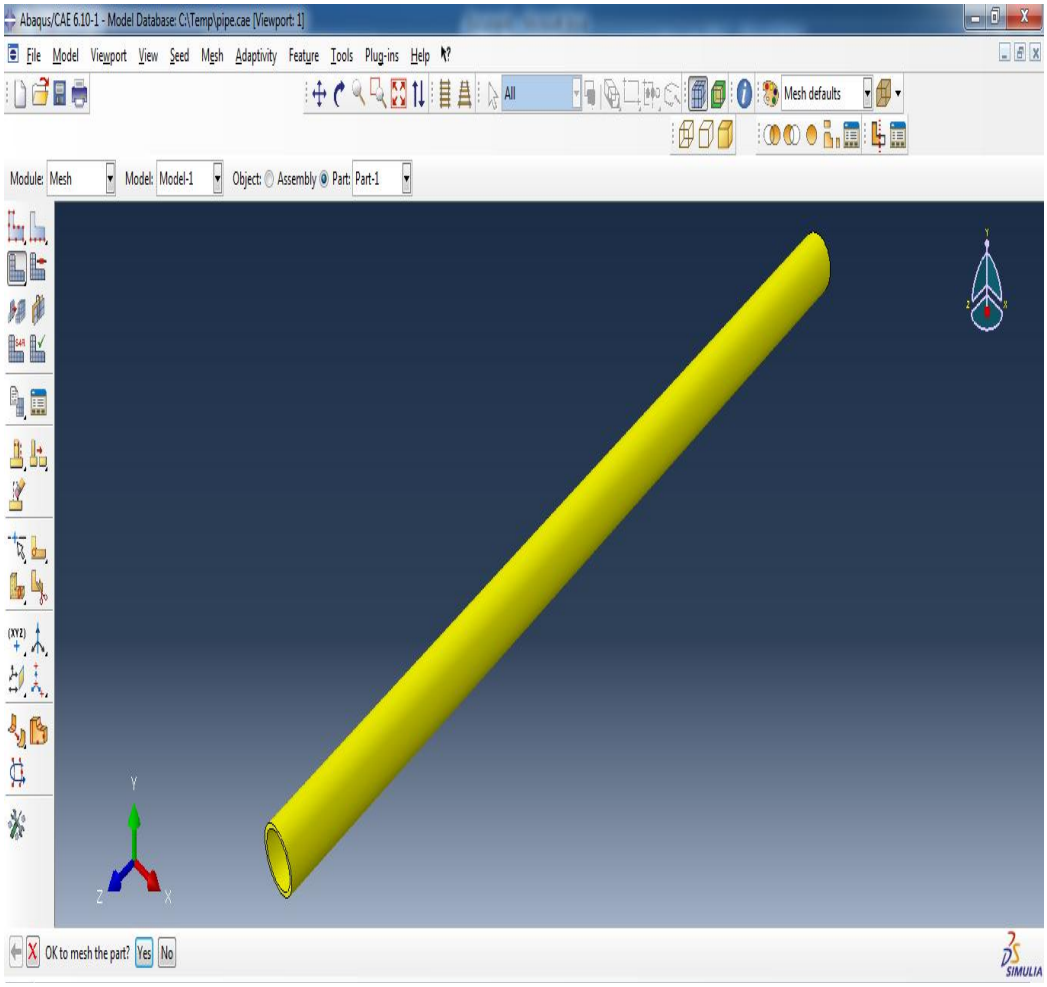

- The resultant shape as follows

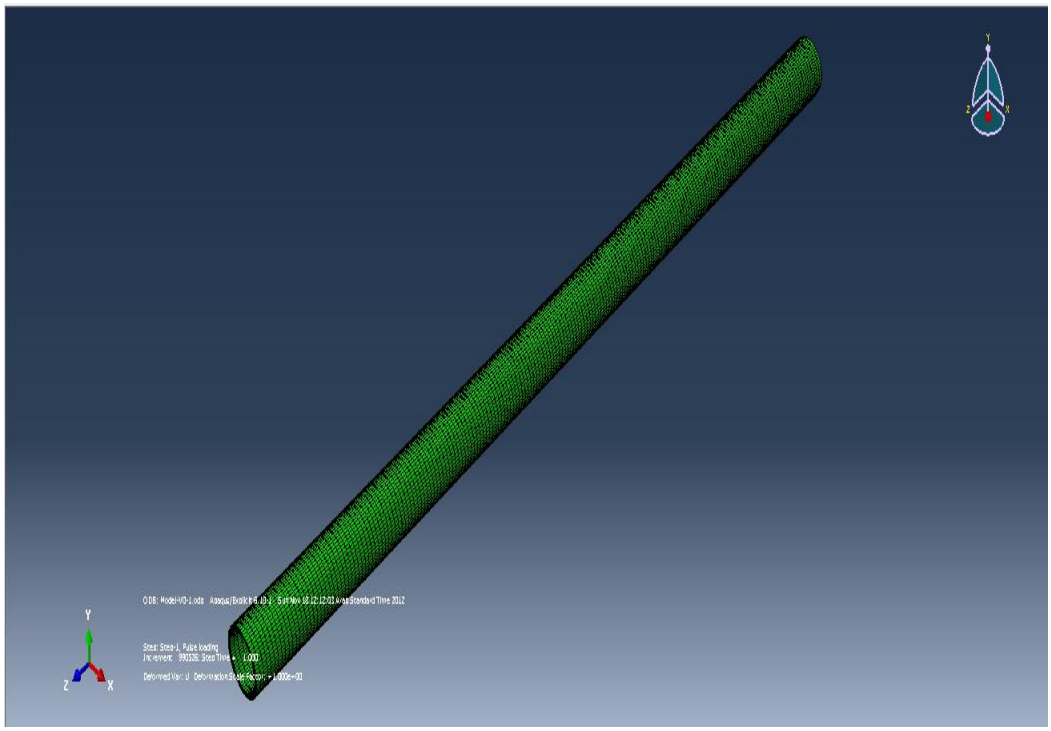

G. Step: Dynamic /Explicit

- Explicit initial step

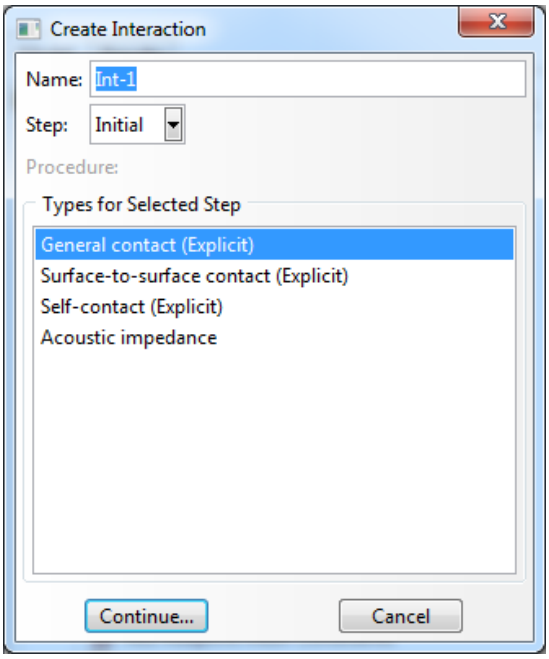

- Initial step boundary condition for U1, U2, and U3

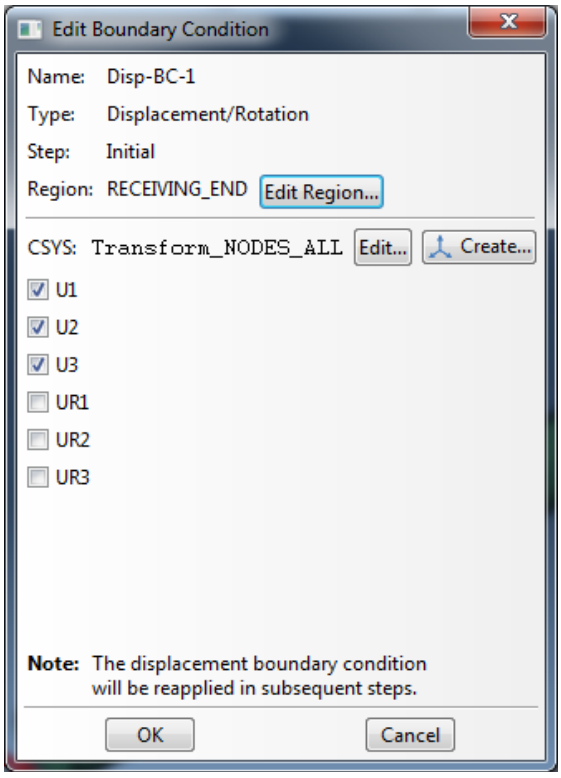

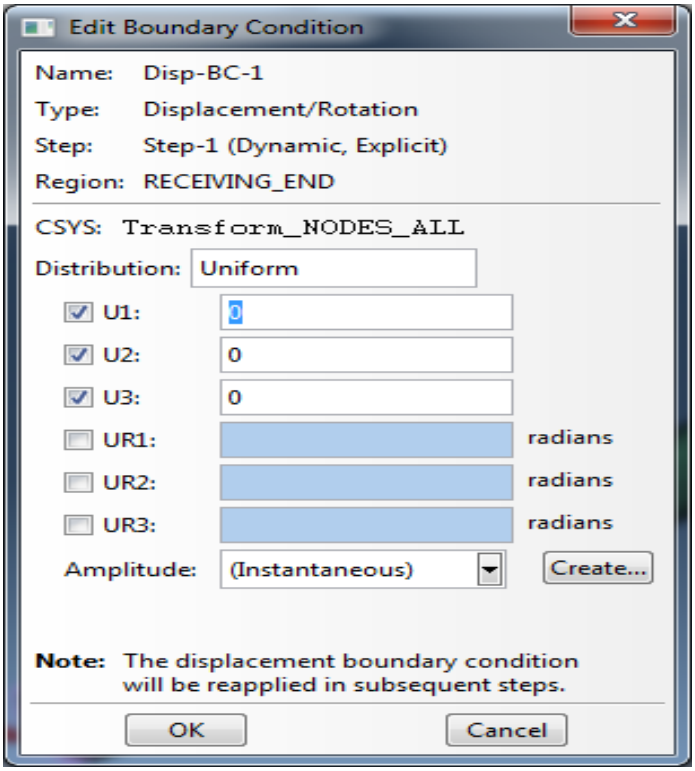

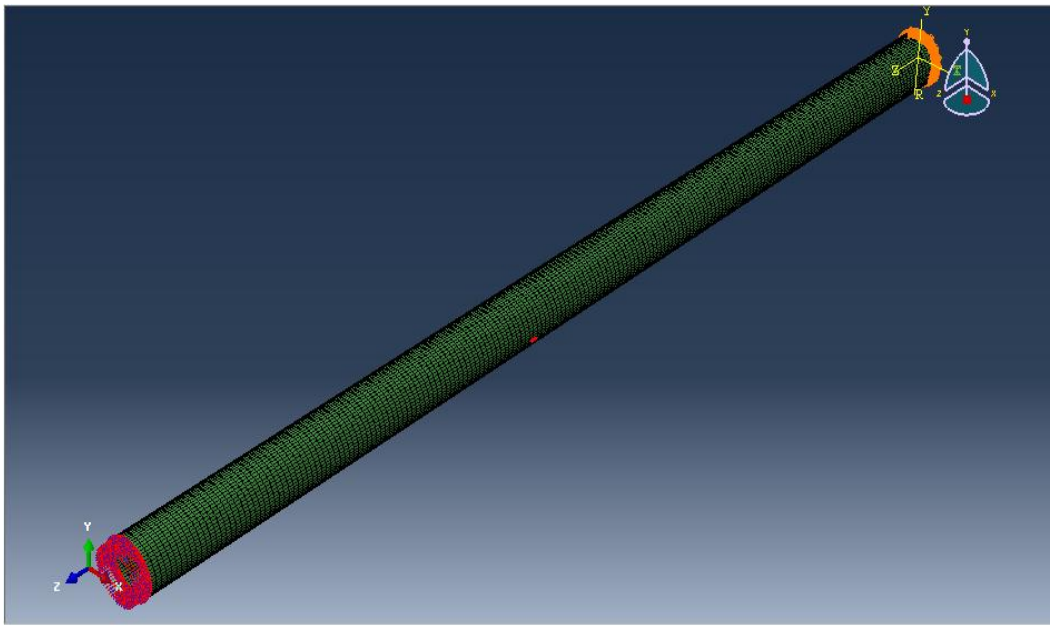

- Two field Output request set for Stresses, Strain, Displacement/Velocity/Acceleration, Force/Reaction and Contact at different interval

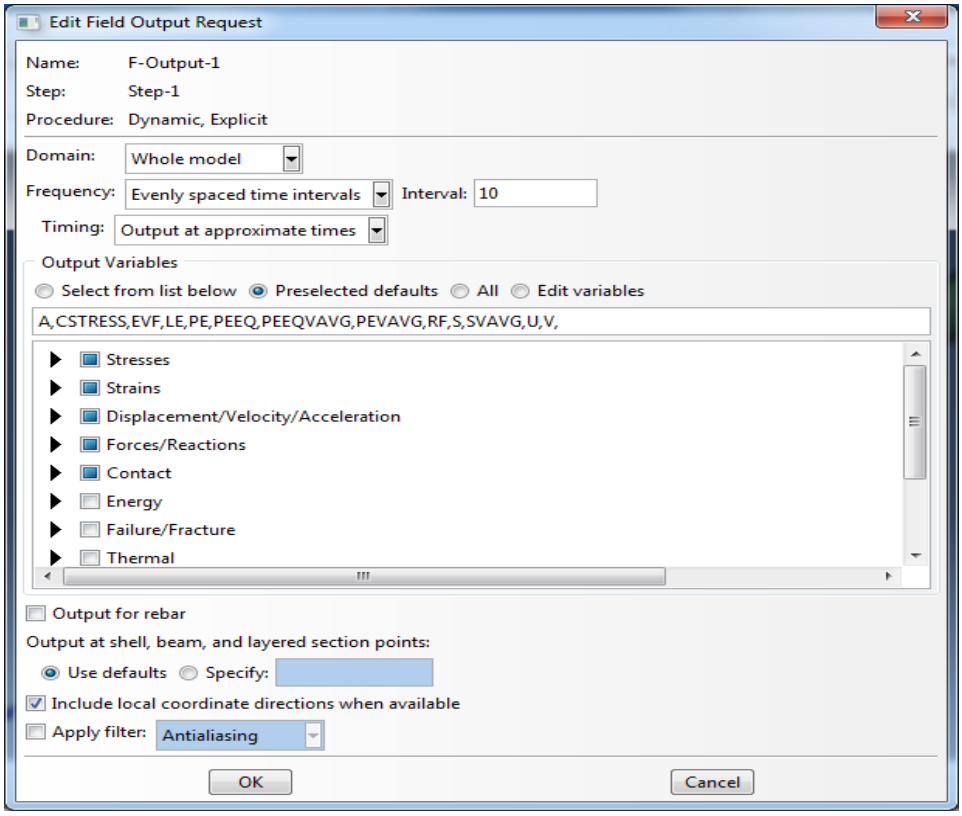
Edit Field Output Request
Name: F-Output-1
Step: Step-1
Procedure: Dynamic, Explicit
Domain: Whole model
Frequency: Evenly spaced time intervals
Interval: 10
Timing: Output at approximate times
Output Variables
Select from list below
Preselected defaults
All
Edit variables
A,CSTRESS,EVF,LE,PE,PEEQ,PEEQVAVG,PEVAVG,RF,S,SVAVG,U,V,
Stresses
Strains
Displacement/Velocity/Acceleration
Forces/Reactions
Contact
Energy
Failure/Fracture
Thermal
Output for rebar
Output at shell, beam, and layered section points:
Use defaults
Specify:
Include local coordinate directions when available
Apply filter:
Antialiasing
OK
Cancel

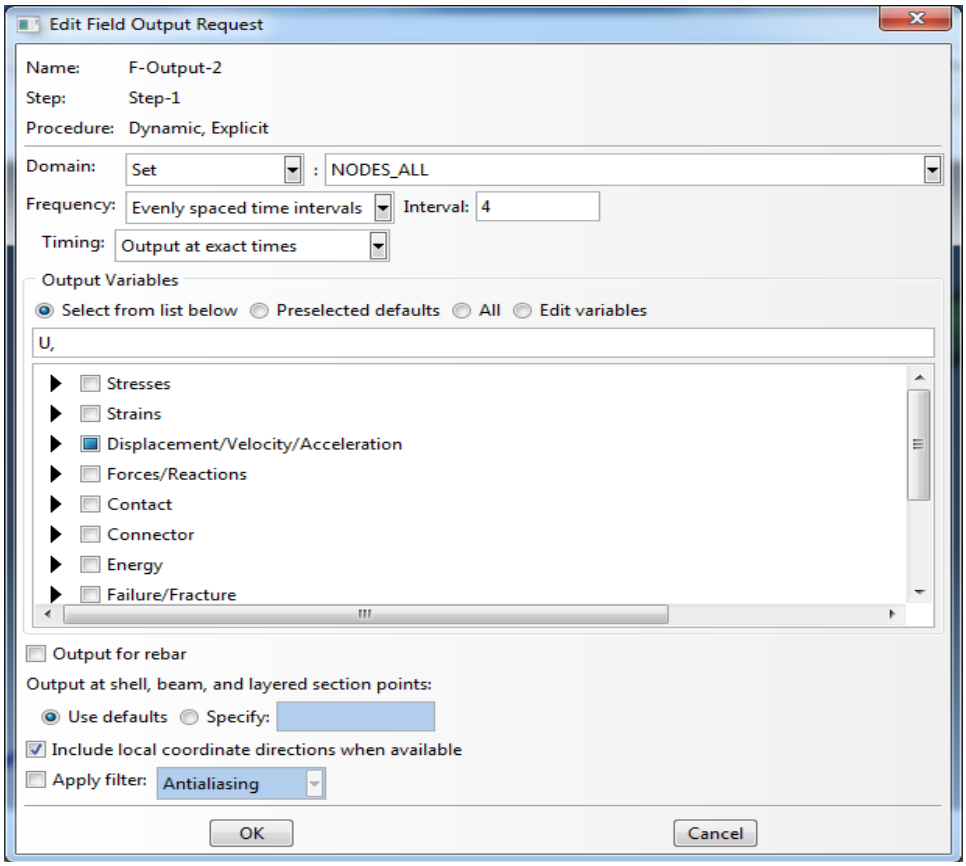
Edit Field Output Request
Name: F-Output-2
Step: Step-1
Procedure: Dynamic, Explicit
Domain: Set
NODES_ALL
Frequency: Evenly spaced time intervals
Interval: 4
Timing: Output at exact times
Output Variables
Select from list below
Preselected defaults
All
Edit variables
U,
Stresses
Strains
Displacement/Velocity/Acceleration
Forces/Reactions
Contact
Connector
Energy
Failure/Fracture
Output for rebar
Output at shell, beam, and layered section points:
Use defaults
Specify:
Include local coordinate directions when available
Apply filter:
Antialiasing
OK
Cancel

- Two-history output request set for Energy at different frequencies interval.

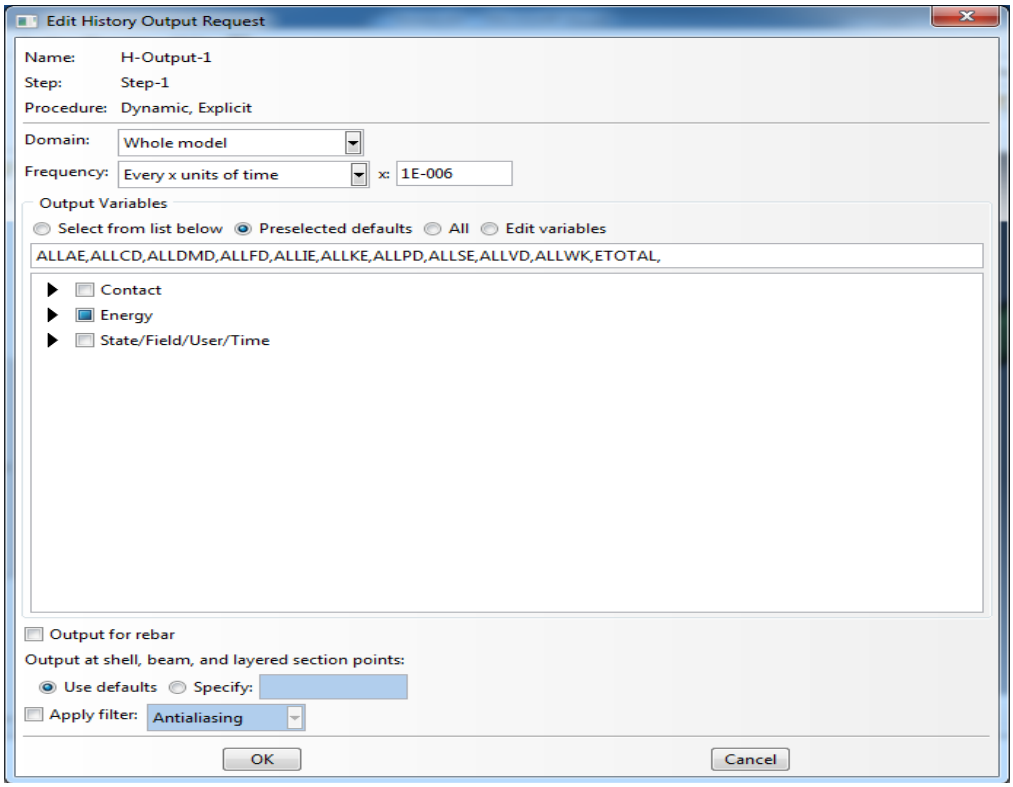

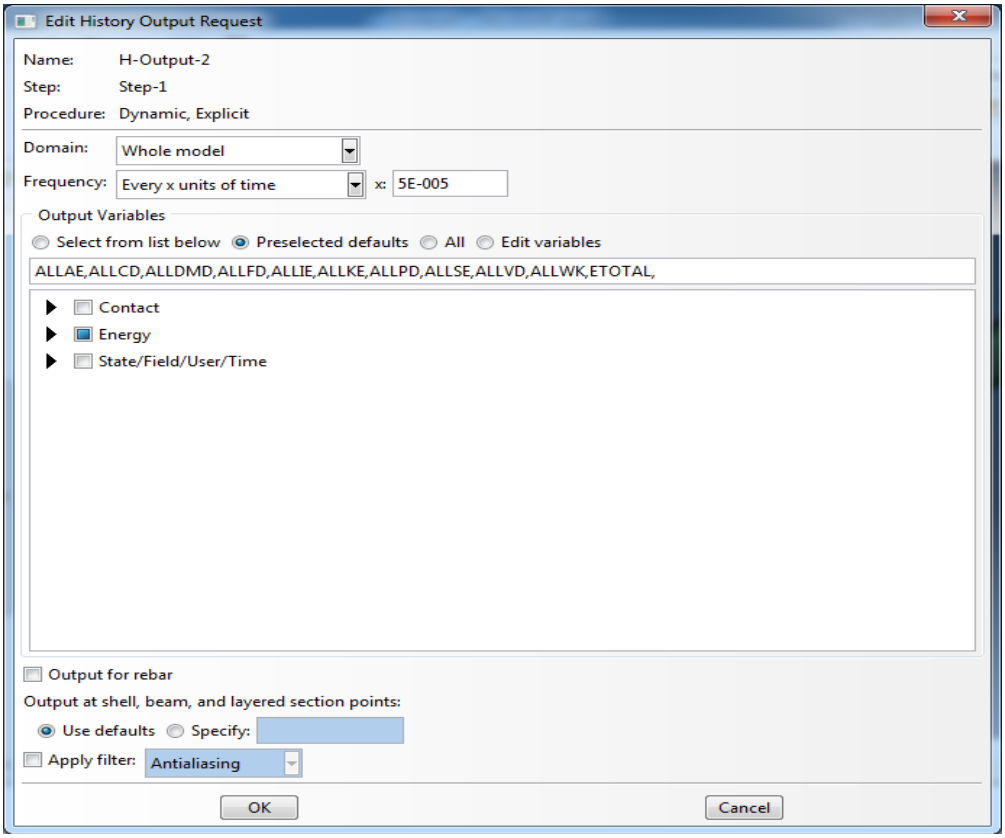

H. Load

- Pulse pressure load set at magnitude of 100000 for dynamic, explicit step.

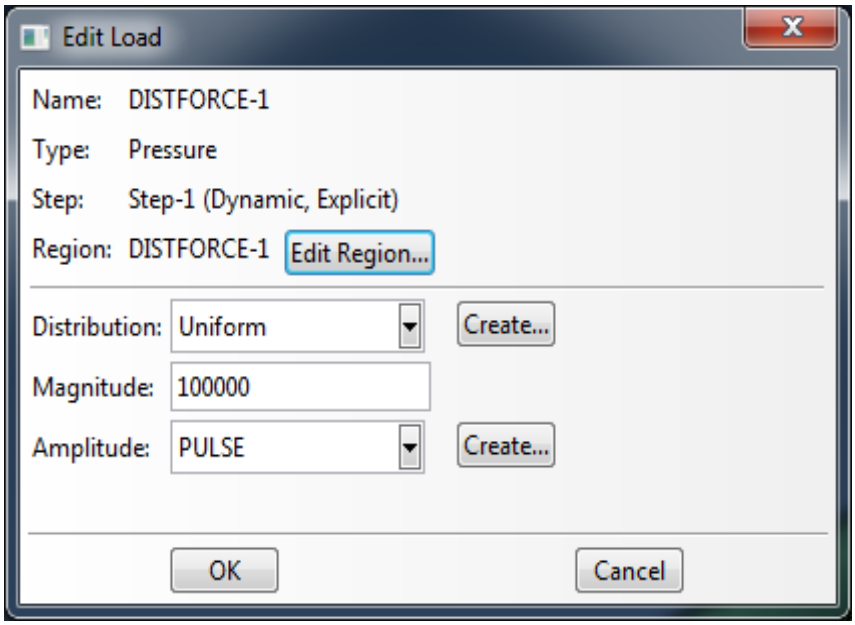

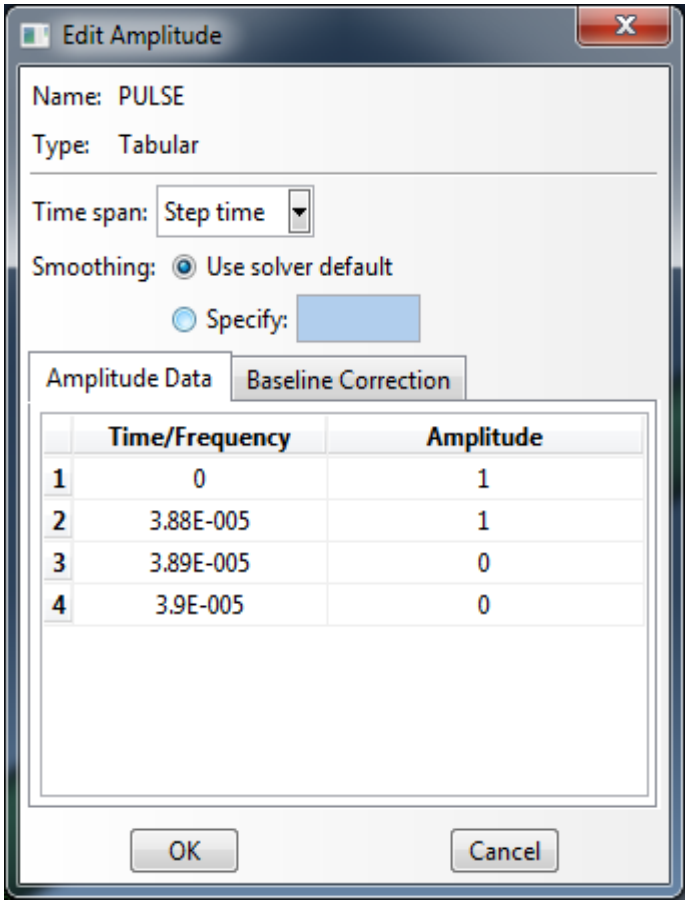

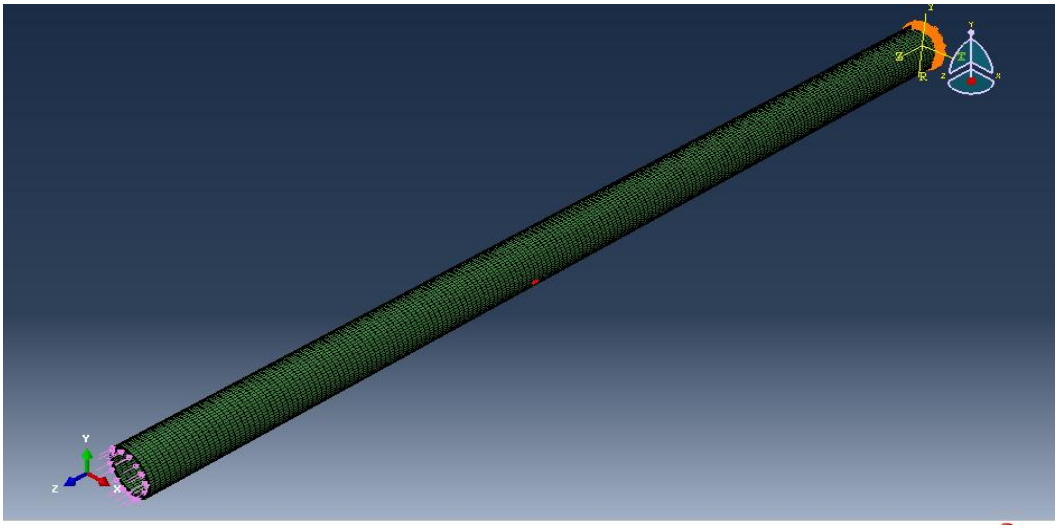

I. Job

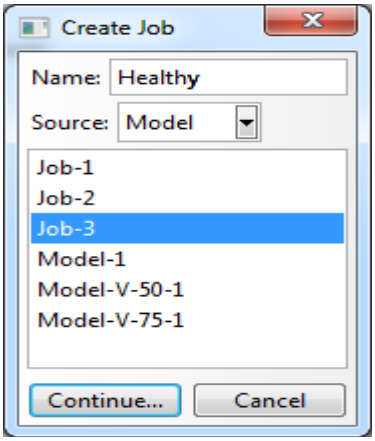
Create Job
Name: Healthy
Source: Model
Job-1
Job-2
Job-3
Model-1
Model-V-50-1
Model-V-75-1
Continue...
Cancel

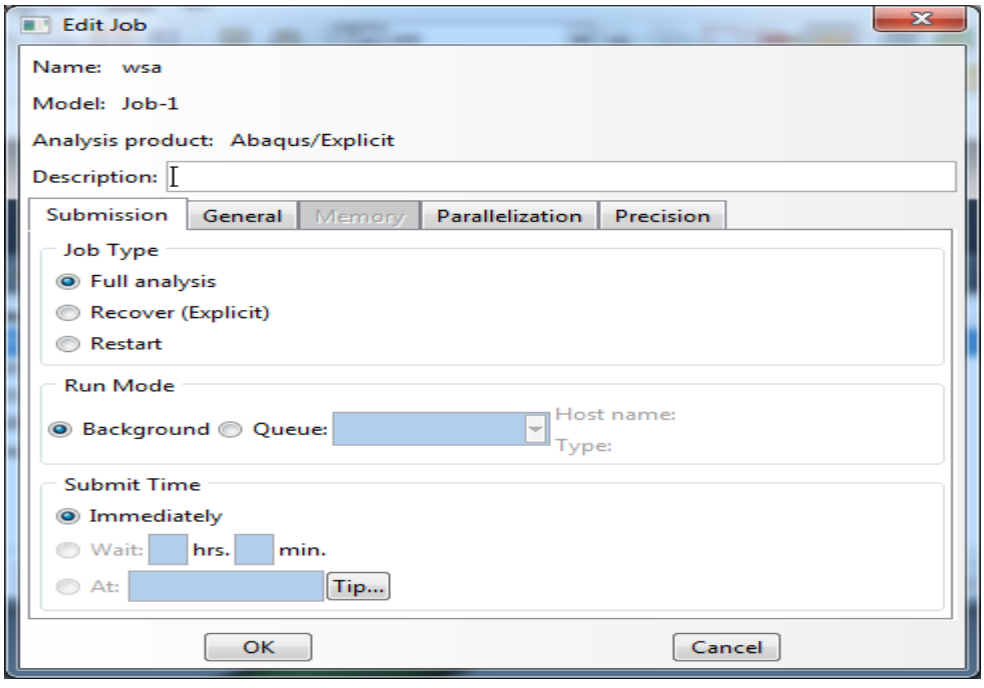
Edit Job
Name: wsa
Model: Job-1
Analysis product: Abaqus/Explicit
Description:
Submission
General
Memory
Parallelization
Precision
Job Type
Full analysis
Recover (Explicit)
Restart
Run Mode
Background
Queue:
Host name:
Type:
Submit Time
Immediately
Wait:
hrs.
min.
At:
Tip...
OK
Cancel

- Job manager window

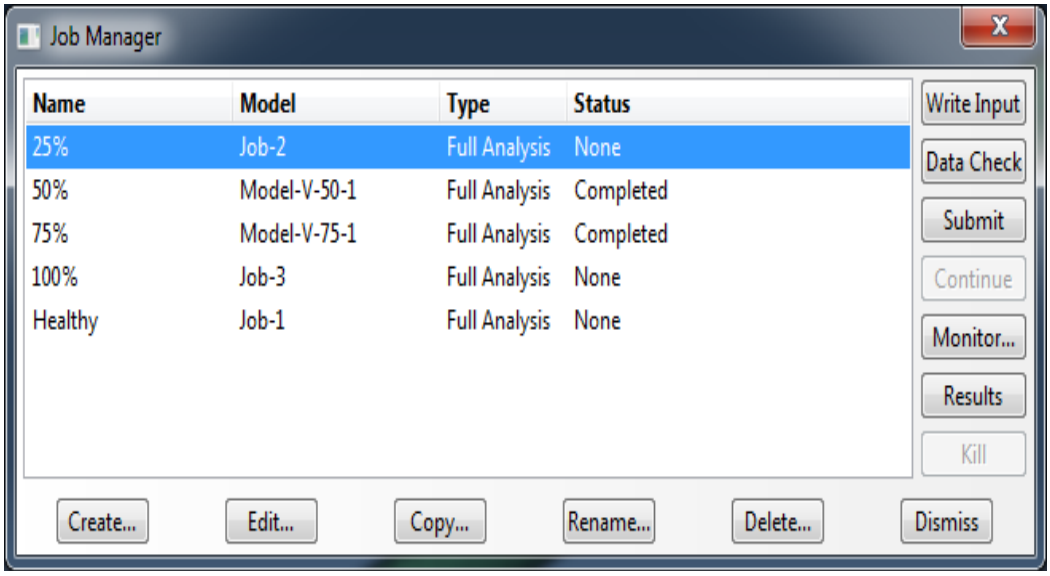

APPENDIX B: MAT LAB CWT CODE

```
clear all
CLOSE ALL
clc

for kf=1:5,
%% Faults variaion Effects
  if kf==2,load H_90 ,data = H_90(:,1); end
  if kf==1,load F1_90,data =F1_90(:,1);end
  if kf==3,load F2_90 ,data = F2_90(:,1);end
  if kf==4,load F3_90,data =F3_90(:,1);end
  if kf==5,load F4_90 ,data = F4_90(:,1);end

%      if kf==1,load H_50 ,data = H_50(:,1); end
%    if kf==2,load F1_50,data =F1_50(:,1);end
%   if kf==3,load F2_50 ,data = F2_50(:,1);end
%   if kf==4,load F3_50,data =F3_50(:,1);end
%   if kf==5,load F4_50 ,data = F4_50(:,1);end

%      if kf==1,load H_10 ,data = H_10(:,1); end
%    if kf==2,load F1_10,data =F1_10(:,1);end
%   if kf==3,load F2_10 ,data = F2_10(:,1);end
%   if kf==4,load F3_10,data =F3_10(:,1);end
%   if kf==5,load F4_10 ,data = F4_10(:,1);end
  a = 0.07;
  b = 0.19;
  Fs = 943000;
%Fs =  5.0000e+008;
 t=(0:length(data)-1)/Fs;
 x = detrend(data);
NFFT = 2^(nextpow2(length(x)));
FFTX = fft(x,NFFT);
NumUniquePts = ceil((NFFT+1)/2);
FFTX = FFTX(1:NumUniquePts);
MXs = abs(FFTX);
MXs = MXs/length(x);
MXs = MXs.^2;
MXs = MXs*2;
MXs(1) = MXs(1)/2;
  if ~rem(NFFT,2)
    MXs(end) = MXs(end)/2;
end
f = (0:NumUniquePts-1)*Fs/NFFT;
%%%%%%%%%%%%%%%%%%%%%%
AF=MXs';
  data=ftfilter(data,a,b);
figure(1)
   subplot(5,1,kf)
plot(t*1000,data);
grid
ylim([-10.1 10.1])
xlim([0 10])
 ylabel('Amplitude(V)','fontsize',12),xlabel('Time(ms)','fontsize',12);

figure(2)
   subplot(5,1,kf)
plot(t*1000,data);
```

```
gr

ylim([-10.1 10.1])
xlim([3.8 5])
 ylabel('Amplitude(V)','fontsize',12),xlabel('Time(ms)','fontsize',12);
figure(3)
   subplot(5,1,kf)
plot(f/1000,AF);
grid
ylim([0 .05])
xlim([40 300])
ylabel('Amplitude(V)','fontsize',12),xlabel('Frquency(KHz)','fontsize',12);
figure(4)
   subplot(5,1,kf)
plot(f/1000,20*log(AF));
grid
ylim([-350 0])

xlim([40 300])
ylabel('Amplitude(dB)','fontsize',12),xlabel('Frquency(KHz)','fontsize',12);

% figure(2)
%    subplot(5,1,kf)
% plot(f/1000,20*log10(AF));
% grid
% ylim([-200 10])
% xlim([0.004 470])
clear all
end
 break
clc
for kf=1:5,
%% Faults variaion Effects
   if kf==1,load H_50 ,data = H_50(:,1); end
    if kf==2,load F1_50,data =F1_50(:,1);end
   if kf==3,load F2_50 ,data = F2_50(:,1);end
   if kf==4,load F3_50,data =F3_50(:,1);end
   if kf==5,load F4_50 ,data = F4_50(:,1);end
   Fs = 943000;
%Fs =  5.0000e+008;
 t=(0:length(data)-1)/Fs;
 x = detrend(data);
NFFT = 2^(nextpow2(length(x)));
FFTX = fft(x,NFFT);
NumUniquePts = ceil((NFFT+1)/2);
FFTX = FFTX(1:NumUniquePts);
MXs = abs(FFTX);
MXs = MXs/length(x);
MXs = MXs.^2;
MXs = MXs*2;
MXs(1) = MXs(1)/2;
  if ~rem(NFFT,2)
    MXs(end) = MXs(end)/2;
end
f = (0:NumUniquePts-1)*Fs/NFFT;
%%%%%%%%%%%%%%%%%%%%%%%
AF=MXs';
 data=ftfilter(data(:,1),a,b);
figure(3)
   subplot(5,1,kf)
plot(t,data);
```

```
grid
ylim([-9.7 9.7])
xlim([0.0041 0.0047])
figure(4)
   subplot(5,1,kf)
plot(f/1000,20*log10(AF));
grid
ylim([-200 10])
xlim([0.004 470])
clear data
end
clc
for kf=1:5,
%% Faults variaion Effects
   if kf==1,load H_10 ,data = H_10(:,1); end
    if kf==2,load F1_10,data =F1_10(:,1);end
   if kf==3,load F2_10 ,data = F2_10(:,1);end
   if kf==4,load F3_10,data =F3_10(:,1);end
   if kf==5,load F4_10 ,data = F4_10(:,1);end
   Fs = 943000;
%Fs =  5.0000e+008;
 t=(0:length(data)-1)/Fs;
 x = detrend(data);
NFFT = 2^(nextpow2(length(x)));
FFTX = fft(x,NFFT);
NumUniquePts = ceil((NFFT+1)/2);
FFTX = FFTX(1:NumUniquePts);
MXs = abs(FFTX);
MXs = MXs/length(x);
MXs = MXs.^2;
MXs = MXs*2;
MXs(1) = MXs(1)/2;
  if ~rem(NFFT,2)
    MXs(end) = MXs(end)/2;
end
f = (0:NumUniquePts-1)*Fs/NFFT;
%%%%%%%%%%%%%%%%%%%%%
AF=MXs';
 data=ftfilter(data(:,1),a,b);
figure(5)
   subplot(5,1,kf)
plot(t,data);
grid
ylim([-9.7 9.7])
xlim([0.0041 0.0047])
figure(6)
   subplot(5,1,kf)
plot(f/1000,20*log10(AF));
grid
ylim([-200 10])
xlim([0.004 470])
clear data
end
```

APPENDIX C: AIR ULTRASONIC CERAMIC TRANSDUCERS

Air Ultrasonic Ceramic Transducers **235AC130**

Dimensions: dimensions are in mm

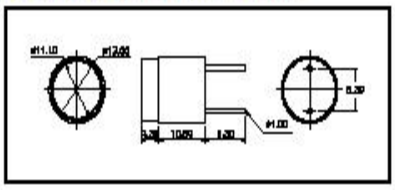

Impedance/Phase Angle vs. Frequency
Tested under 1Vrms Oscillation Level

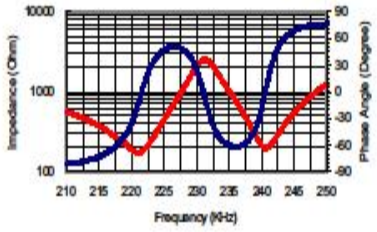

Specification

235AC130	Transceiver
Center Frequency	235.0±10Khz
Transmitting Sensitivity 0dB re 1μbar/1Vrms @ 30cm	15 dB
Receiving Sensitivity 0dB = 1Vrms/μbar	-73 dB
Figure of Merit (TS + RS)	-55 dB
Bandwidth (FOM)	10KHz
Nominal Impedance (Ohm)	1000
Capacitance at 1Khz ±20%	530 pF
Max. Driving Voltage (Pulse)	50Vpp 10% duty cycle
Total Beam Angle -6dB	15° typical
Matching Window	Silicone Rubber
Operation Temperature	-20 to 60°C
Storage Temperature	-30 to 70°C

All specification taken typical at 25°C
Closer frequency tolerance, shorter ringing and wider bandwidth models can be supplied upon request.
Model available:

1	235AC130	Aluminum Housing

Receiving/Transmitting Sensitivity & Figure of Merit (RS + TS)
Tested under 10Vrms @30cm

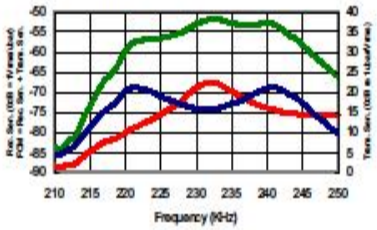

Beam Angle: Tested at 235.0Khz frequency

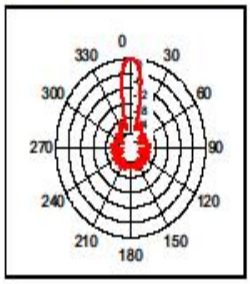

Products List Home

PUBLISHED PAPERS

PAPER 1

Engineering, 2013, 5, 551-555
doi:10.4236/eng.2013.56066 Published Online June 2013 (http://www.scirp.org/journal/eng)

Scientific Research

Oil Transmission Pipelines Condition Monitoring Using Wavelet Analysis and Ultrasonic Techniques

Waheed Sami Abushanab
School of Engineering, Manchester Metropolitan University, Manchester, UK
Email: wsabushanab@gmail.com

Received February 19, 2013; revised March 21, 2013; accepted March 30, 2013

ABSTRACT

In this paper, a reliable and sensitive diagnostic method for oil pipelines based on wavelet analysis and ultrasonic technique. This will be achieved by the use of 3-D finite element modeling software (Abaqus CAE 6.10) combined with a power full wavelet based signal processing technique will be used to collect the empirical ultrasonic data to validate the developed diagnostic method. The affect known seeded faults *i.e.*, 1 mm hole at 25%, 50%, 75% and 100% depth in pipe wall were investigated using FEM techniques. A developed acoustic transceiver (Air Ultrasonic Ceramic Transducer 235AC130) will be used to collect the empirical ultrasonic data to validate the developed diagnostic method. The amplitudes and frequency spectra of the ultrasonic signals were measured and the predicted results were found to be in good agreement with the measured data, and that to confirm that this method can provide important information on pipe defects.

Keywords: Ultrasonic; Abaqus; Continuous Wavelet Transform (CWT)

1. Introduction

Diagnosis of damage in pipelines requires the identification of the location and the type of damage and quantification of the degree of damage. Most of the recent damage detection methods rely on visual inspection or on localized measurements such as acoustic or ultrasound methods, magnetic field methods, radiography, eddy-current methods and thermal field method which requires that the vicinity of the damage area is known a priori and that the portion of the structure being inspected is readily accessible [1]. Those methods can detect damage on or near the surface of the structure [2]. Piezoelectric ultrasonic has been utilized for wall thickness measurements and crack detection. These tools work well in liquid filled pipelines since the fluid being transported is coupling the pressure wave generated by the piezoelectric transducers to the pipe wall. However, in natural gas pipelines this coupling mechanism does not work since nearly all of the acoustical energy generated by the transducer in the gaseous product is reflected by the pipe wall and does not travel into the pipe wall [3]. The ultrasonic sensor generates ultrasonic waves inside the pipe wall itself through a combination of Lorentz forces and magnetostriction, no matter what medium is present in the pipe [4]. The material being inspected is its own transducer, eliminating the need for a liquid coupling as required in traditional ultrasonic transducer methods [4]. Hu *et al.* [5] carried out a case study that shows the application of harmonic wavelet analysis to the problems of pipeline small leak detection with time-frequency domain analysis. A comparison was made between leak detection results of harmonic wavelet and Daubechies wavelet and it was found that harmonic wavelet based small leak detection approach performed better. Meurer *et al.* [6] used Lamb wave propagation in the wall of a pipe generated in a standoff manner for defect detection and found that this approach is accurate measurement of wall thickness on all kinds of materials and size only at the point of physical contact and not along the circumference of the pipe. Sun *et al.* [7] used the ultrasonic techniques based sensing network for underground pipeline monitoring by jointly utilizing the measurements of different types of sensors that are located both inside and around the underground pipelines. The magnetic induction-based sensor detects and localizes leakage throughout the pipeline network and reported to the administration center in real-time-guided waves and was not affected significantly by the presence of insulation. In the research mentioned above, it was noted that no rigorous analysis on ultrasonic techniques technology was carried

out and its capabilities are not yet fully investigated. The research proposed here focuses on developing finite element model to understand ultrasonic techniques advantages and limitations and pave the path for developing reliable oil pipes diagnosing systems.

2. Numerical Simulation

The elastic-plastic brick elements in Abaqus are intended to provide inexpensive solutions for problems involving part-through surface cracks in shell structures loaded predominantly in Mode I by combined membrane and bending action in cases where it is important to include the effects of inelastic deformation. When the brick element model reaches theoretical limitations, the shell-to-solid sub modeling technique is utilized to provide accurate J-integral results. The energy domain integral is used to evaluate the J-integral for this case.

3. Geometry and Model

The pipe has an inside radius of 2.15 mm, wall thickness of 3.5 mm, and 1m long. The mesh is shown in **Figure 1**. Four of flaws have ratios of 0.25 (a shallow crack), 0.5 and 0.75 (a deep crack) and it's refined around the crack by using multi-point constraints (MPCs). The shell elements type is C3D8R in the symmetric of 8-node linear brick along the crack. Five different flaws are studied. All have the semi-elliptic geometry and in all cases.

4. Material

The pipe is made of an elastic-plastic metal (Carbon Steel Pipe), with a Young's modulus of 2 GPa, a Poisson's ratio of 0.3, an initial yield stress of 482.5 MPa, and constant work hardening to an ultimate stress of 689.4 MPa at 10% plastic strain, with perfectly plastic behavior at higher strains.

5. Loading

The loading consists of uniform internal pressure applied to all of the shell elements, with edge loads applied to the far end of the pipe to provide the axial stress corresponding to a closed-end condition. Even though the flaw is on the inside surface of the pipe, the pressure is not applied on the exposed crack face. Since pressure loads on the flaw surface of brick elements are implemented using linear superposition in Abaqus, there is no theoretical basis for applying these loads when nonlinearities are present. I assume that this is not a large effect in this problem. For consistency with the brick element models, pressure loading of the crack face is not applied to the shell-to-solid sub-model.

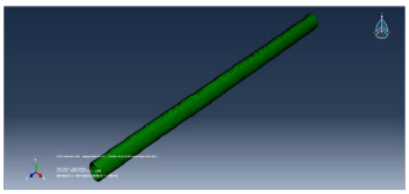

Figure 1. Pipe meshing.

6. Modelling Results

The brick elements provide J-integral values directly. **Figures 2** and **3** show the J-integral values and the strain at the whole model as functions of applied pressure for the four flaws and healthy. In the input data the maximum time increment size has been limited so that adequately smooth graphs can be obtained. **Figures 2** and **3** shows the displacement of specific node at the end edge of pipe for the half-thickness crack (3_a/t = 0.5), at pressure levels. The results are agreed closely to experimental results.

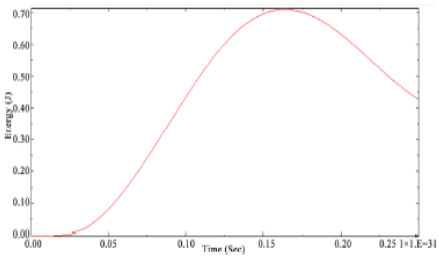

Figure 2. Healthy pipe strain energy, whole model.

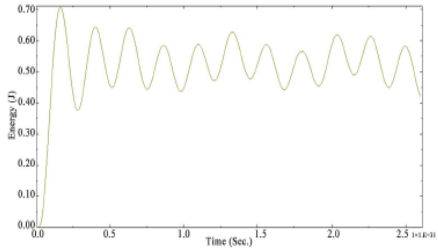

Figure 3. 50% Whole model strain energy.

Figure 4. Shows the aluminium stand and sensor set angle of 70˚.

7. Experimental Procedures

Series of experiments were carried out to investigate the propagation of ultrasound wave signal from a real 1 meter length healthy carbon steel and other real four 1 meter length carbon steel pipes with seeded 1mm hole at vary depth in each pipe and sources to an array of sensors. The overall purpose was to evaluate the potential of ultrasound monitoring to be used in real piping systems, acknowledging the effects of external (support, burial) environments may have on the propagation of the waves. To this end, five sets of experiments were carried out where the nature of the source and the environment were varied in a systematic way.

Five carbon steel pipes were used in research experiments. All pipe are from the same materials and has the same diameters that shown in **Table 1** below.

Five sets of experiments were carried out with the pipes suspended on aluminium stands in order to obtain a preliminary indication of the type of propagation behaviour shown by a wave generated from a simulated source. Sensor was mounted from one end of the pipe at 70˚ angle which is the best angle that shows clear result, whilst the other sensor was incrementally moved axially along the pipe to the other end at the same angle as shown at **Figure 4**.

8. Experiments Results

A time domain signatures of oscilloscope results for the five experimental sets (healthy, 1mm hole at 25% 50% 5% and 100% in depth) was recorded by Mat lab software and shows no clear differences as shown in **Figures 5** and **6** (zoom in) respectively.

Based on the results of time domain signatures above, A frequency domain signatures of oscilloscope results for the five experimental sets (healthy, 1mm hole at 25% 50% 75% and 100% in depth) was recorded by Mat lab software and shows no clear differences as shown in **Figure 7**.

As a result, a continuous wavelet transform (CWT) is used to divide a continuous function into wavelets, which shows clear differences in **Figure 8**.

9. Summary of Experiments

The frequency and angle of a specific Lamb wave mode was selected based on two aspects; first, incident angle for mode is equal to transducer frequency multiplied by material thickness and second is that ultrasonic and longitudinal velocities in the steel pipe and Lucite wedge which measured by be found that 70˚ degree present the best signal with transducer with an oscilloscope and ultrasonic pulsar/receiver frequency of 235 KHz.

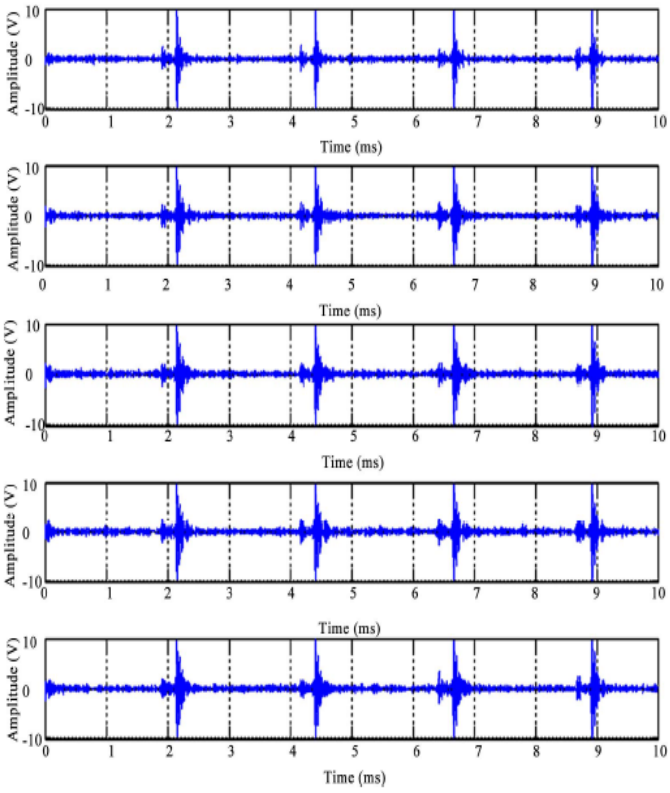

Figure 5. Time domain signatures for the five set of research experimental results.

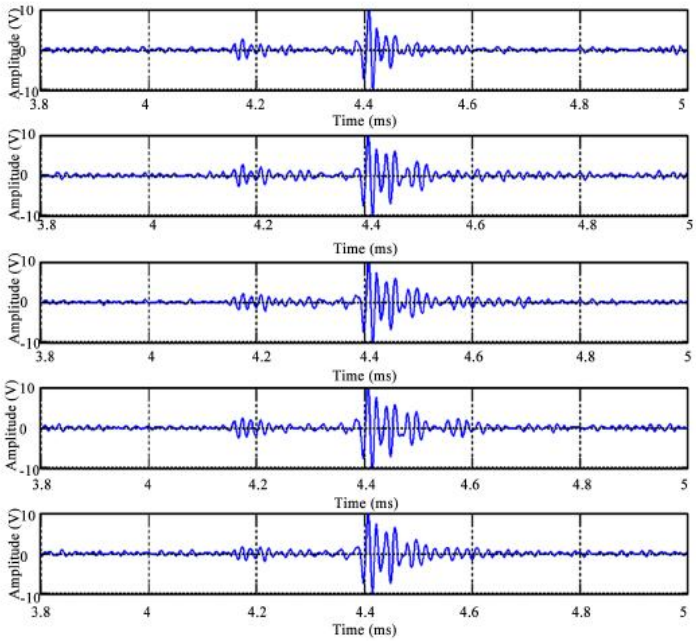

Figure 6. Time domain signatures for the five set of research experimental results (zoomed).

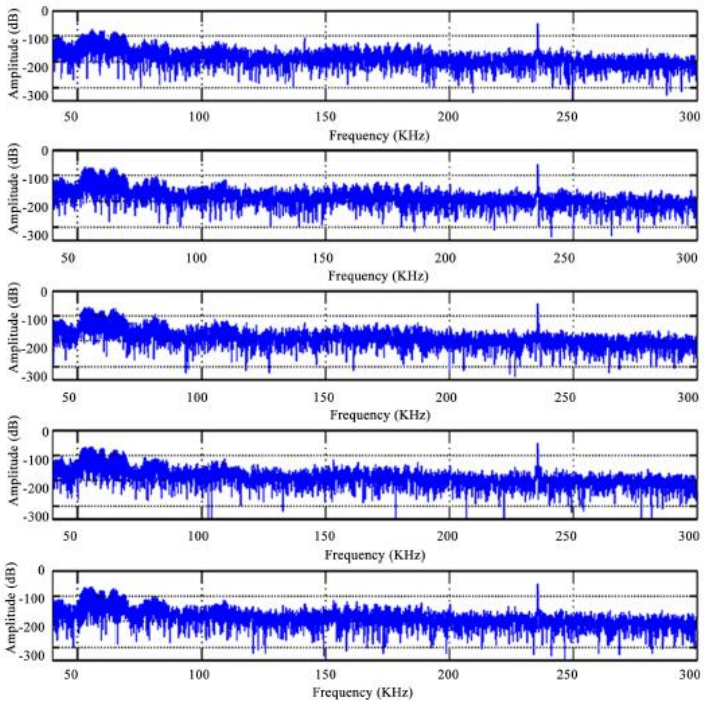

Figure 7. Frequency domain signatures for the five set of research experimental results.

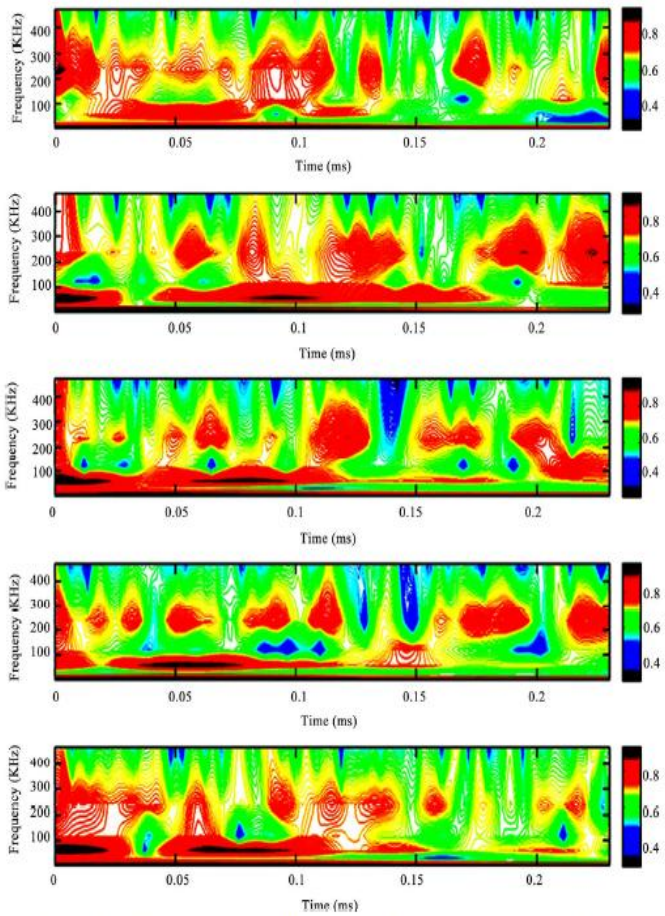

Figure 8. CWT signatures for the five set of research experimental results.

Table 1. Experimental five sets of pipes diameters.

Length	Diameter	Thickness	Material
1 m	2.5 cm	3.5 mm	Carbon Steel

The Time/Frequency domain are insufficient analyses as shown in **Figures 5-7** for since all signatures doesn't shows any differences between each cases, while CWT signature (**Figure 8**) is to be considered a sufficient analyses and the novelty of the research since red colour density that present the energy is increase in directly proportional to the increase of the depth of the hole.

REFERENCES

[1] A. Carvalho, J. Rebello, M. Souza, L Sagrilo and S. Soares, "Reliability of Non-Destructive Test Techniques in the Inspection of Pipelines Used in the Oil Industry," *International Journal of Pressure Vessels and Piping*, Vol. 85, No. 11, 2008, pp. 745-751. doi:10.1016/j.ijpvp.2008.05.001

[2] J. Laibin and Z. Wei, "Detection of Small Leakage from Long Transportation Pipeline with Complex Noise," *Journal of Loss Prevention in the Process Industries*, Vol. 24, No. 4, 2011, pp. 449-457.

[3] D. Sinha, "Acoustic Sensor for Pipeline Monitoring," Los Alamos National Laboratory, 2005. http://www.netl.doe.gov/technologies/oil-gas/publications/td/FWP 02FE05_0705Report.pdf

[4] M. klann and T. Beuker, "Pipeline Inspection with the High Resolution Ultrasonic Ili-Tool: Report on Field Experience," *Proceedings of the 6th International Pipeline Conference*, Calgary, 25-29 September 2006.

[5] C. R. Fuller and F. J. Fahy, "Characteristics of Wave Propagation and Energy Distribution in Cylindrical Elastic Shells Filled with Fluid," *Journal of Sound and Vibration*, Vol. 81, No. 4, 1982, pp. 501-518.

[6] T. Meurer, J. Qu and L. Jacobs, "Wave Propagation in Nonlinear and Hysteretic Media—A Numerical Study," *International Journal of Solids and Structures*, Vol. 39, No. 21-22, 2002, pp. 5585-5614. doi:10.1016/S0020-7683(02)00366-9

[7] Z. Sun, P. Wang, C. Mehmet, M. Al-Rodhaan and A. Al-Dhelaan, "Magnetic Induction-Based Wireless Sensor Networks for Underground Pipeline Monitoring," *AD Hoc Networks*, Vol. 9, No. 3, 2010, pp. 218-227.

PAPER 2

Engineering, 2013, 5, 337-343
doi:10.4236/eng.2013.54046 Published Online April 2013 (http://www.scirp.org/journal/eng)

Inexpensive Pipelines Health Evaluation Techniques Based on Resonance Determination, Numerical Simulation and Experimental Testing

Waheed Sami Abushanab
School of Engineering, Manchester Metropolitan University, Manchester, UK
Email: wsabushanab@gmail.com

Received February 19, 2013; revised March 20, 2013; accepted March 27, 2013

ABSTRACT

In this paper, a non-destructive, reliable, and inexpensive vibration-based technique for evaluating Carbon steel pipes structure integrity. The proposed techniques allow a quick assessment of pipes structures at final pipe manufacturing stages and/or just before installation. A finite element modelling (FEM) using ABAQUS software was developed to determine the resonance mode of healthy Carbon steel pipe and a series of experiments were conducted to verify the outcomes of the modelling work. Consequently, the effects of quantified seeded faults, *i.e.*, a 1 mm, 2 mm, 3 mm, and 4 mm diameter holes in the pipe wall on these resonance modes were determined using modelling work. A number of common used vibration analysis techniques were applied to detect and to evaluate the severity of those quantified faults. The amplitudes and frequencies of vibration signals were measured and compared. There were found to be in good agreement with the modelling work and provide important information on pipe construction condition and fault severity.

Keywords: Vibration Analysis's; Condition Monitoring; ABAQUS CAE

1. Introduction

The Maintenance of pipelines is of a great concern for oil companies. A proper and sensitive pipeline condition monitoring is desirable to predict leakage and other failure modes e.g. flaws, cracks, etc. Since pipeline passes through varied terrain, its condition will vary accordingly and inspecting the entire pipeline, using a specific methodology or tool, may not detect problems over its entire length. Most of the recent damage detection methods are relies on visual inspection or on localized measurements. Therefore, required that the vicinity of the damage is known a priori and that the portion of the structure being inspected is readily accessible thus subjected to these limitations, these experimental methods can detect damage on or near the surface of the structure.

Current damage detection methods are either visual or l Current damage detection methods are either visual or localized experimental methods, such as acoustic or ultrasound methods, magnetic field methods, radiography, eddy-current methods and thermal field methods. The diagnosis of damage in structural systems requires the identification of the location and type of damage and the quantification of the degree of damage.

Hu, Zhang and Liang [1] study case shows "small leak sensitive characteristics are recognized and the negative pressure wave inflexions are extracted by harmonic wavelet analysis, expressed in terms of harmonic wavelet time-frequency mesh map, time-frequency contour map". Also, comparison was made between leak detection results of harmonic wavelet and Daubechies wavelet, and it was found that harmonic wavelet based small leak detection approach performed better. Sinha [2] used Lamb wave propagation in the wall of a pipe generated in a standoff manner for defect detection and found that this approach is accurate measurement of wall thickness on all kinds of materials and size only at the point of physical contact and not along the circumference of the pipe. Khulief, Khalifa, Ben Mansour and Habib [3] presented an experimental investigation to address the feasibility and potential of in pipe acoustic measurements for detection. They constructed a test rig for simulation purpose. It used to simulate a water transmission pipeline and permit different leak siaes, pressure and flow rates. They stated that the feasibility and limitations of invoking in-pipe

measurements for leak detection were addressed. Hao, Yang, Shijiu and Zhoumo [4] proposed the principle of the distributed optical fiber pipeline leakage detecting and pre-warning system and the method to eliminate the desensitization. Moreover, they established the optical polarization model of oil and gas pipeline fiber warning system to analysis the desensitization that considered as a common problem of the fiber optic sensor. They stated that the experiment that the solution can solve the problem preferably and improve the locating accuracy and the sensitivity of the system. Jin, Yume and Ping [5] proposed new feature extraction and leak identification method to identify leaking in the presence of non-leak acoustic sources using autocorrelation analysis and approximate entropy algorithm. Moreover, they stated that a new method based on neural-network has been developed.

It is known from dynamic systems that a structure temporarily excited by an external force will vibrate at a frequency defined as the natural frequency. The natural frequency is characteristic of the entire structure and its boundary conditions. An external excitation applied to the structure at the same frequency as the structure's natural frequency will result in resonance. At resonance, the structure will vibrate at higher than normal amplitude levels. Depending upon the overall system design, the amplitude of vibration at resonance can cause unwanted operating conditions as well as a catastrophic failure. Determining the structure's natural frequency and maintaining the overall system at an operating condition that will not induce resonance can avoid this type of system failure. The natural frequencies of a structure can be determined by measuring frequency response. One means of measuring the frequency response is to impact test the structure. Impact testing is a measurement of the ratio of the structure's transient response to the excitation impulse versus frequency.

2. Modal Dynamic Analysis

The modal dynamic procedure provides a time-history analysis of linear systems. The excitation is given as a function of time, and it is assumed that the amplitude curve is specified so that the magnitude of the excitation varies linearly within each increment. When the model is projected onto the Eigen modes used for its dynamic representation, we obtain the following set of equations at time t:

$$\ddot{q}\beta + c\beta\alpha\dot{q} + \omega^2 q\beta = (f_t)\beta = f_{t-\Delta t} + \frac{\Delta f}{\Delta t}\Delta \qquad (1)$$

where the α and β indices span the Eigen space; $c_{\beta\alpha}$ is the projected viscous damping matrix; q_β is the "generalized coordinate" of mode β (the amplitude of the response in this mode); $\omega_\beta = \sqrt{k_\beta / m_\beta}$ is the natural frequency of the undammed mode β (obtained as the square root of the eigenvalue in the Eigen frequency step that precedes the modal dynamic time history analysis); $(f_t)_\beta$ is the magnitude of the loading projected onto this mode (the "generalized load" for the mode); and Δf is the change in f over the time increment, Δt. If the projected damping matrix is diagonal, Equation (1) becomes the following uncoupled set of equations:

$$\ddot{q}_\beta 2\xi_{\beta\omega\beta q\beta} + \omega_\beta^2 q\beta = (f_t)\beta\overline{q}\beta 2\xi_{\beta\omega\beta\overline{q}}\beta(f_t)\beta \qquad (2)$$

where ξ_β is the critical damping ratio given by the following relationship:

$$2\xi_{\beta\omega\beta} = \frac{c_\beta}{m_\beta}, \qquad (3)$$

where c_β is the modal viscous damping coefficient, and m_β is the modal mass in mode β.

3. Simulation Work

A finite element model of pipe was created using ABAQUS software program. The structure modelled in this analysis is carbon steel pipe **Figure 1** subjected to free suspension, which is hereafter called the basic model (a tube with no defects). The structural parameters of the model are the length L = 100 cm, the diameter D = 10 cm and the pipe thickness T = 0.35 cm, respectively. In addition, the model was simplified to 3-D, definable, homogeneous, plane-shell-revolution analysis with the assumption that the planned force is on the top surface at 15 cm from the edge of the tube. Different faults were seeded in the pipe with diameter 1 mm, 2 mm, 3 mm and 4 mm.

In the basic model, uniform tensile stresses were applied on the top surface at 15 cm from the edge of the tube by surface traction of 500 kN, as shown in **Figures 2-4** respectively.

The reliability of the results of FEA depends on how accurately the problem is modeled and analyzed. The accuracy of the model depends on including relevant geometrical details, assigning appropriate material properties, and specifying correct boundary conditions. The boundary conditions are included in the model to relate it

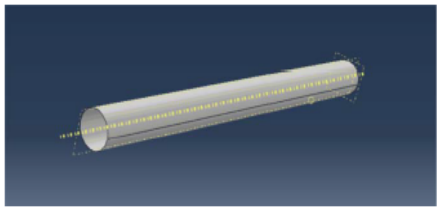

Figure 1. Abaqus Basic Pipe Model Simulation.

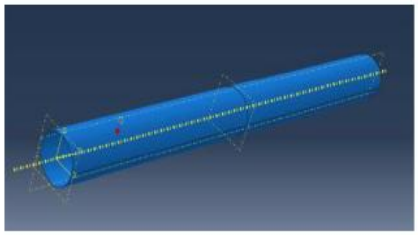

Figure 2. Abaqus Load Demonstration.

to reality by constraining the structural response to the applied load and a fixed constraint at a certain location. Therefore, there is a rigorous requirement that the correct boundary conditions be specified before conducting the analysis. The material properties used in the modeling are elastic and isotropic properties, in terms of stiffness and strength and the defect parameter, where (x) represents the distance the hole is from the end of the tube, and $\varnothing$ represents the diameter of the hole. The outputs of the model are acceleration, displacement, and velocity in the time domain. Collected data was analyzed and compared with experimental results.

4. Experimental Setup

An experiment to detect the hole in the carbon steel pipe was conducted in the laboratory. The experimental consists of carbon steel pipe, a hummer, charger amplifier, data acquisition and Accelerometer. The experimental setup, shown in **Figure 5** included a carbon steel tube with a wall thickness of 0.35 cm, a diameter of 10 cm, and a length of 100 cm.

5. Analysis Techniques

Statistical methods included kurtosis, (ku), standard deviation (sd) are a time-domain analysis techniques and Fourier analysis method (FFT) is a frequency domain analysis technique. They are commonly used to analyze vibration signals or acoustic and to assess the severity of any damage.

5.1. Variance

The variance technique was used as shown in **Figure 6**. The equation of Variances is:

Figure 3. Basic Model Load Conditions.

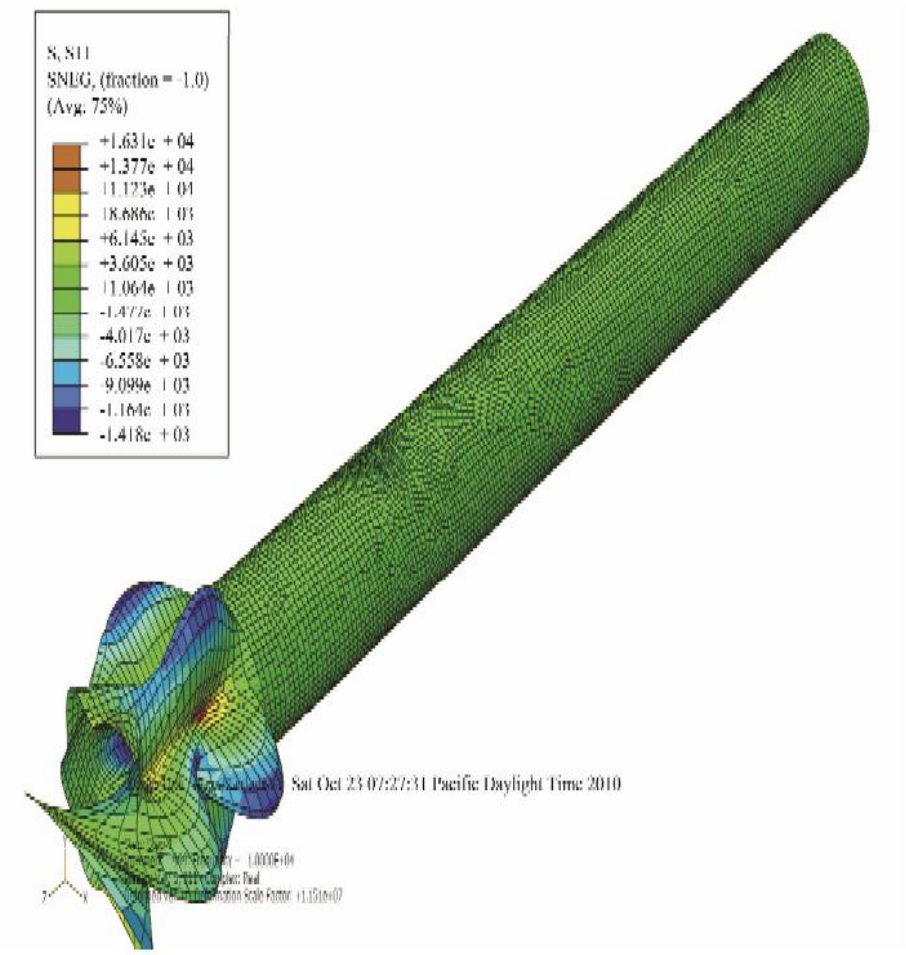

Figure 4. Load and Boundary Conditions Definitions of the Basic Model.

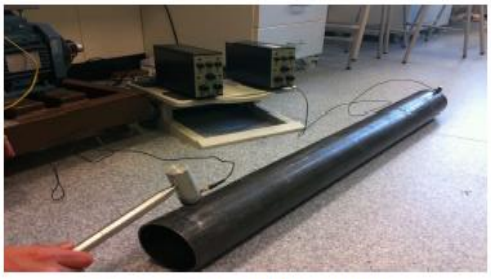

Figure 5. Carbon steel pipe specimen.

$$\sigma^2 = \frac{\sum_{i=1}^{n}(X_i - \mu)^2}{N} \quad (4)$$

The value of variance remains constant for healthy and faulty (1 mm hole), after that, it increases up to (0.2254) and then decreases up to (0.0005) that is mean, variance parameter is not suitable to predict the fault.

5.2. Standard Deviation

The *SD* is the square root of the variance. It indicates the spread of the data, the larger the *SD* the more widely the data are spread out. Although influenced by extreme values, the *SD* is important in many tests of statistical significance:

$$SD = \sqrt{\frac{\sum_{i=1}^{N}(x_i - \bar{x})^2}{N}} \quad (5)$$

where x_i a set of samples, N is the total number of samples, and $\bar{x}$ is the mean value of the samples.

5.3. Fast Fourier Transform (FFT)

This is a technique for transforming the signal from time-domain to the frequency-domain. The mathematical formula is:

$$X(f) = \int_{-\infty}^{\infty} x(t) e^{-2\pi i f t} dt \quad (6)$$

where $x(t)$ is a continuous signal in time domain, $X(f)$ is its Fourier transform and f is the frequency variable.

Simulation and experimental data collected and methods based on time and frequency techniques have applied for healthy and faulty cases of tested pipe for fault detecting.

6. Results and Discussions

The aim of this study is to detect and diagnose the faults in the pipe. The time-domain vibration signals collected from pipe as analyzed using variances and standard deviation as shown in **Figures 6** and **7**. As can be seen from figures there are fluctuations with the change of pipe condition between healthy and faulty signals. These fluctuations may lead to an incorrect decision for pipe condition and cannot be used to diagnose system defects.

The time domain methods results of the experimental and simulation vibration signals have shown that such measures are not suitable for detecting faults in carbon steel pipe. Therefore, frequency domain (FFT) is employed to determine its effectiveness in detecting faults.

Frequency response measurements are a type of model testing which can be used to determine the resonant frequencies of a structure. Frequency response testing is accomplished by exciting a system with a known input and simultaneously measuring the corresponding output response.

Fast Fourier Transform (FFT) was applied for healthy and faulty collected data then plotted to determine the resonance amplitude. The "Healthy" pipe accelerometer results records of the vibration signatures in the frequency domain are shown in **Figure 8**. It shows the signature of a "healthy" pipe's resonance frequency in the first mode of 500 Hz.

Experimental signal in healthy case was compared with simulation signal generated using ABAQUS software program. The result shows a good agreement between simulation and experimental signals using FFT method.

Fast Fourier Transform method was applied on simulation signals collected under different condition of the pipe (1 mm hole, 2 mm hole, 3 mm hole and 4 mm hole). The results are shown on **Figures 9-13**. **Figure 9** demonstrates the modeling simulation of (a) time domain and

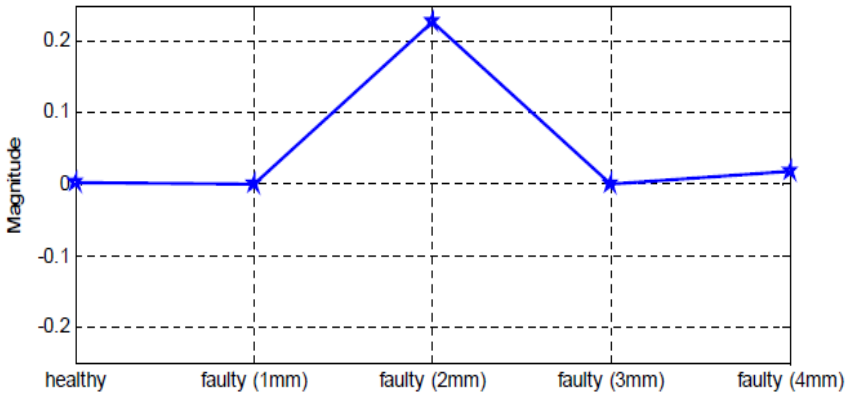

Figure 6. Statistical analysis-variance.

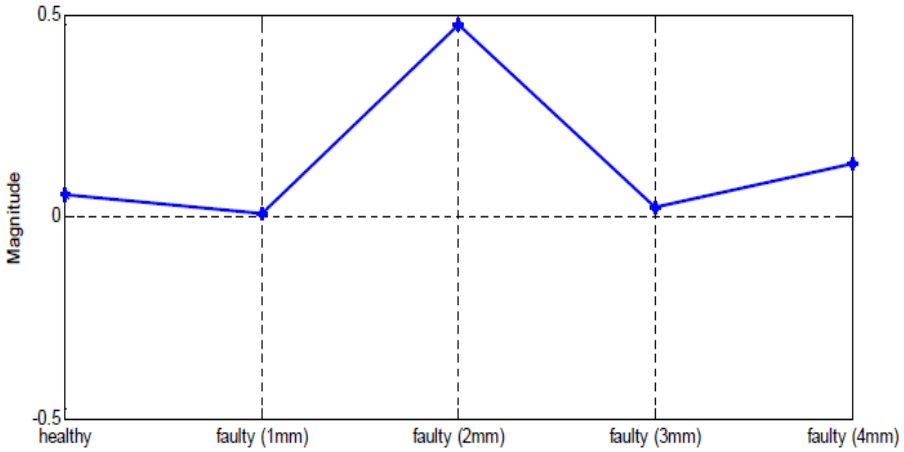

Figure 7. Statistical analysis-standard deviation.

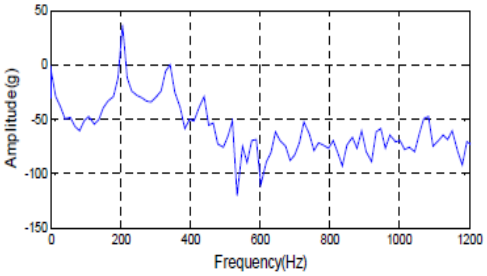

Figure 8. Experimental result-healthy.

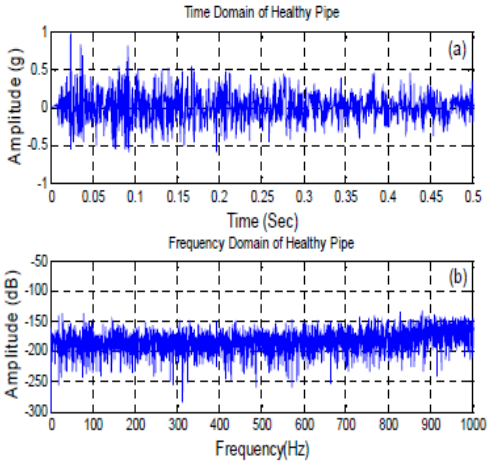

Figure 9. Vibration data for healthy pipe, (a) time domain, (b) frequency domain.

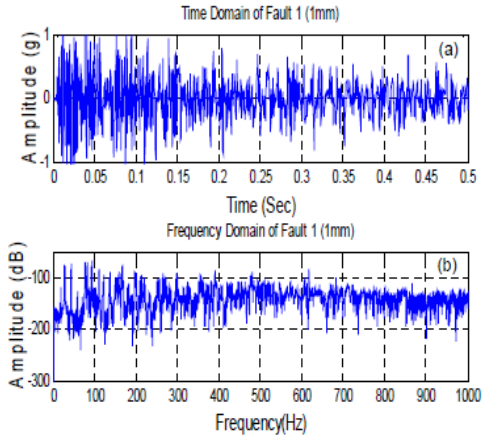

Figure 10. Vibration data for fault 1, (a) time domain, (b) frequency domain.

(b) frequency domain for the healthy pipe. At 500 Hz, which is "healthy" pipe's first resonance frequency mode, notice that the amplitude is (−155 dB) that means it is 92% matching the experimental results (−143 dB). Therefore, it is feasible to build on that agreement to simulate more defects.

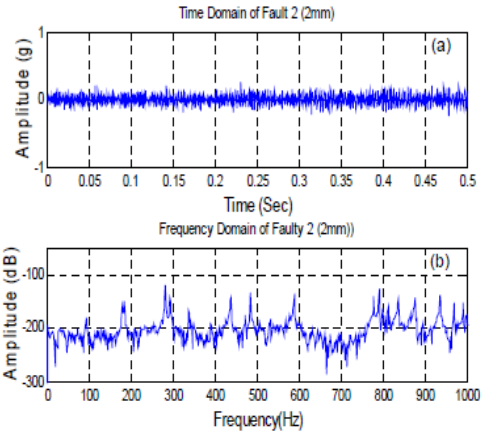

Figure 11. Vibration data for healthy pipe, (a) time domain, (b) frequency domain.

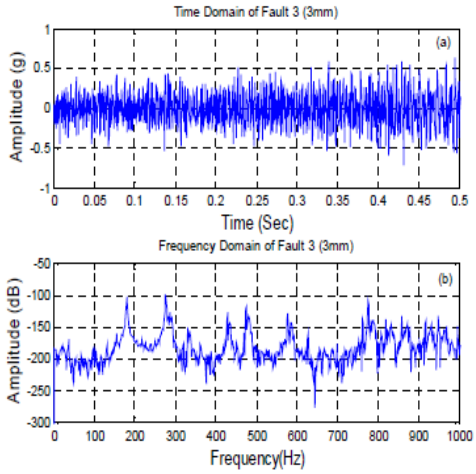

Figure 12. Vibration data for fault 3, (a) time domain, (b) frequency domain.

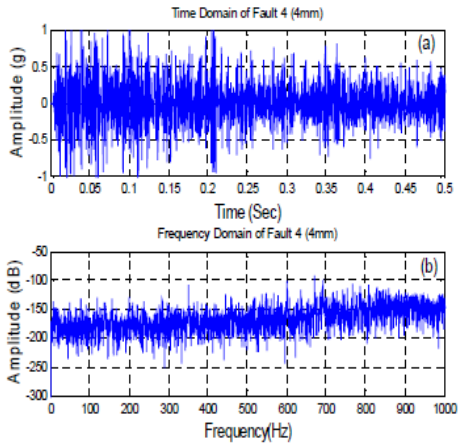

Figure 13. Vibration data for fault 4, (a) time domain, (b) frequency domain.

Figure 10 is vibration data for fault 1 mm, (a) Time domain, (b) Frequency domain. At 500 Hz, the frequency domain amplitude decrease (−25 dB) to become (−170 dB).

Figure 11 is vibration data for fault 2 mm, (a) Time domain, (b) Frequency domain At 500 Hz, the frequency domain amplitude decrease (−45 dB) to become (−200 dB).

Figure 12 is vibration data for fault 3 mm, (a) Time domain, (b) Frequency domain At 500 Hz, the frequency domain amplitude decrease (−65 dB) to become (−220 dB).

Figure 13 is vibration data for fault 4 mm, (a) Time domain, (b) Frequency domain At 500 Hz, the frequency domain amplitude decrease (−85 dB) to become (−240 dB).

Finally, the experimental and Abaqus modeling results were compared to examine the degree of agreement between the laboratory results and the theoretical results. Consequently, the results were assessed to determine whether it was reasonable and defensible to conclude that the size of the hole could be accurately predicted by conducting such a simple test of the pipe.

Based on results shown above there is a clear difference in the graphs based on pipe condition (healthy or damage) and graphs changes as per the nature of the tube defects situation. The greater the aperture size, the more significant the change in the shape of the graph is.

7. Conclusion

The main aim of this research was to study the natural response at different pipe conditions and to develop an inexpensive, reliable NDT method to diagnose faults related to carbon steel pipe. From the result it has been shown that the conventional techniques are not sufficient to reliably detect different types of faults in early stages and given detail information about their conditions as proven above by three different conventional techniques, whilst FFT is suitable method for analysing collected data. The proposed condition monitoring approach is based only on analyzing frequency response and does not require or depend on physical inspections. Also, it can be used to identify defective piping system supports, incurrectly placed supports, and the locations of maximum deflection requiring additional supports. The propose technique offers significant advantages such as avoidance of intrusive techniques and operator dependency and ability to measure the actual changes in the pipe hole and general applicability for any geometry or wall thickness. The experimental devices and modeling software used in this study achieved the main research objectives.

REFERENCES

[1] J. Hu, L. Zhang and W. Liang, "Detection of Small Leakage from Long Transportation Pipeline with Complex Noise," *Journal of Loss Prevention in the Process Industries*, Vol. 24, pp. 449-457. doi:10.1016/j.jlp.2011.04.003

[2] D. N. Sinha, "Acoustic Sensor for Pipeline Monitoring," Technical Report, Gas Technology Management Division Strategic Center for Natural Gas and Oil National Energy Technology Laboratory, Morgantown, 2005.

[3] Y. Khulief, A. Khalifa, R. Mansour and M. Habib, "Acoustic Detection of Leaks in Water Pipelines Using Measurements inside Pipe," *Journal of Pipeline Systems Engineering and Practice*, Vol. 3, No. 2, 2012, pp. 47-54.

[4] F. Hao, A. Yang, J. Shijiu and Z. Zhoumo, "Desensitization Elimination in Pipeline Leakage Detection and Pre-Warning System Based on the Modeling Using Jones Matrix," 2010 *IEEE on Sensors Applications Symposium* (*SAS*), Tianjin, 23-25 February 2010, pp. 101-104.

[5] Y. Jin, W. Yumei and L. Ping, "Information Processing for Leak Detection on Underground Water Supply Pipelines," 2010 *Third International Workshop on Advanced Computational Intelligence* (*IWACI*), Chongqing, 25-27 August 2010, pp. 623-629.

